Systematic investigations on the protein corona of different nanocarriers and its role in cellular uptake

Inaugural-Dissertation
to obtain the academic degree
Doctor rerum naturalium (Dr. rer. nat.)

submitted to the Department of Biology, Chemistry, Pharmacy
of Freie Universität Berlin

by

Tony Bewersdorff

2022

"The end of learning is the beginning of death."

(Eramir an Oriathan scholar, Path of Exile 2019)

This thesis was carried out at the German Federal Institute for Risk Assessment (BfR) in Berlin from September 2013 to August 2019 under the supervision of PD. Dr. Andrea Haase.

    1st reviewer: PD. Dr. Andrea Haase

    2nd reviewer: Prof. Dr. Rainer Haag

Date of defense: 21.03.2023

Selbstständigkeitserklärung

Hiermit versichere ich, die vorliegende Arbeit mit dem Titel „Systematic investigations on the protein corona of different nanocarriers and its role in cellular uptake" ohne Benutzung anderer als der zugelassenen Hilfsmittel selbstständig angefertigt zu haben. Alle angeführten Zitate sind als solche kenntlich gemacht. Die vorliegende Arbeit wurde in keinem früheren Promotionsverfahren angenommen oder als ungenügend beurteilt.

Ebenso versichere ich, dass ich an keiner anderen Stelle ein Prüfungsverfahren beantragt bzw. die Dissertation in dieser oder anderer Form an keiner anderen Fakultät als Dissertation vorgelegt habe.

Berlin, 15.07.2022

Tony Bewersdorff

Die Dissertation ist in englischer Sprache verfasst.

Danksagung

Als Erstes bedanke ich mich beim Bundesinstitut für Risikobewertung und Herrn Prof. Dr. Dr. Luch als Leiter der Abteilung Chemikalien und Produktsicherheit für die Möglichkeit, meine Laborarbeiten unter guten wissenschaftlichen Bedingungen durchführen zu können.

Frau Prof. Dr. Monika Schäfer-Korting bringe ich meine Wertschätzung für die anfängliche Übernahme meiner Betreuung entgegen.

Herrn Prof. Dr. Haag spreche ich meine Anerkennung für sein Interesse an meinem Projekt und das Fungieren als Zweitgutachter aus.

Für die Zusammenarbeit in verschiedenen Projekten und den gemeinsamen Veröffentlichungen gilt meine Hochachtung im Folgenden Herrn Prof. Dr. Haag und Dr. Jonathan Vonnemann, Prof. Dr. Klinger und Alexandra Gruber sowie Herrn Prof. Dr. Calderón und Dr. Emanuel Adriano Glitscher.

Der Abteilung 7 des BfR und all ihren Mitarbeitern danke ich für die Hilfe und Anregungen während meiner Promotionszeit.

Frau PD Dr. Haase drücke ich an dieser Stelle im Besonderen meine Dankbarkeit aus. Ohne sie wäre das Projekt der Doktorarbeit nicht möglich gewesen. Nicht nur, dass sie das Projekt initiiert hat, sondern sie stand nahezu zu jeder Zeit für Diskussionen und Input zur Verfügung. Bemerkenswert waren ihre Geduld und Hilfe bei der Erstellung wissenschaftlicher Texte und meiner Veröffentlichungen. Danke für die Möglichkeiten, eigene Ideen verwirklichen und verschiedene kleinere Projekte (auch abseits des eigentlichen Promotionsprojektes) realisieren zu können.

Natürlich geht eine Promotionszeit nicht spurlos an einem vorbei und das eine oder andere Mal müssen auch schon mal ein paar Haare daran glauben, weil manches vielleicht nicht so klappt wie gedacht. Für meine dennoch vorhandene Haarpracht danke ich dem einzigartigen Großraumbüro. Vielleicht gab es ein paar blaue Flecken an diversen Schienbeinen und sicherlich war nicht jeder mit dem Losglück geschmacklich annehmbarer Jelly Beans gesegnet. Dennoch gab es immer einen Panikknopf, der gedrückt werden konnte und man wurde geerdet. Dieses Paradies mit einzigartigen Menschen und ihren Charakteren ließ mich im wortwörtlichen Sinne das eine oder andere Mal ein misslungenes Experiment oder etwaige Nachtschichten vergessen.

Neben diesen wunderbaren Kolleg*innen gibt es auch außerhalb des BfR Menschen, denen ich meinen Dank ausspreche.

Da wäre zum Ersten Franziska, die sich den Gefahren der Nacht durch meine Schreibschichten alleine stellen musste. Trotz aller Entbehrungen unterstützte sie mich in allen Belangen und ermöglichte mir stets den erforderlichen Freiraum zum Schreiben. Dafür gebührt ihr mein außerordentlicher Dank.

Meinen Eltern möchte ich dafür Danke sagen, dass ich bei ihnen immer die nötige Unterstützung bekam. In allen Höhen und Tiefen standen sie immer hinter mir und boten mir stets eine helfende Hand. Ohne ihre moralische Unterstützung wäre dieser Abschnitt sicherlich nicht machbar gewesen.

Zum Schluss möchte ich mich noch bei zwei besonderen Menschen bedanken. Omas unvergleichbarer Streuselkuchen erleichterte mir in der Zeit des Studiums der Biologie manch eine Auswendiglernsession. Sicherlich wären ohne diesen die eine oder andere Klausur nicht bestanden worden.

Die Leidenschaft für die Naturwissenschaften und im Besonderen für die Biologie geht eindeutig auf den „Pupsgeist", eine Erfindung meines Opas, zurück. Im Kindesalter wollte er mir aufsteigende Faulgase aus dem Seeschlamm als mystisches Wesen verkaufen. Danke Oma und Opa! Ich wünschte, ihr wäret auf meinem Weg nicht nur im Geiste dabei.

Zusammenfassung

Im Bereich der Nanomedizin gewinnen Nanomaterialien als Nanotransporter mehr und mehr an Wichtigkeit, z.B. um Wirkstoffe besser zu formulieren, vor Abbau zu schützen und zielgerichtet zu transportieren. Allerdings interagieren Nanopartikel, sobald diese einer komplexen biologischen Umgebung (beispielsweise Blut) ausgesetzt sind, mit diversen Biomolekülen und binden diese als Korona. Die Proteinkorona ist der Schlüsselfaktor, welcher maßgeblich sowohl die biologische Halbwertszeit als auch den Transport und die Aufnahme von Nanopartikeln *in vivo* beeinflusst. Um das Verhalten von Nanopartikeln *in vivo* besser zu verstehen und gegebenenfalls auch vorhersagen zu können, ist es von zentraler Bedeutung, die Interaktion von Nanopartikeln und Proteinen zu entschlüsseln.

Im Rahmen dieser Arbeit untersuchte ich den Einfluss verschiedener physiko-chemischer Eigenschaften (Größe, Oberflächenladung, Struktur und Hydrophobizität) von Nanopartikeln auf die Bildung einer Proteinkorona. In Hinblick auf die spätere Anwendung als Nanocarrier wurde zudem der Zusammenhang zwischen Proteinkorona und der zellulären Aufnahme genauer analysiert. Dabei sollten Interaktionspartner, d.h. Andockungsstellen, für Koronaproteine an die Zellmembran und damit mögliche zelluläre Aufnahmewege identifiziert werden.

Die von mir verwendeten Nanopartikel wurden betreffend ihrer physiko-chemischen Eigenschaften umfangreich charakterisiert. Im Anschluss erfolgte die Bestimmung der Proteinkorona in humanem Serum mittels verschiedener Methoden wie z.B. 2D Gelektrophorese in Kombination mit MALDI TOF/TOF Massenspektrometrie. Die zelluläre Aufnahme der Nanopartikel in humane THP-1 Monozyten untersuchte ich mittels Durchflusszytometrie und Fluoreszenzmikroskopie. Zudem wurden zelluläre Interaktionspartner über Pull Down Versuche identifiziert.

Innerhalb dieser Arbeit konnte gezeigt werden, dass alle untersuchten physiko-chemischen Eigenschaften einen Einfluss auf die Bildung und Zusammensetzung der Proteinkorona haben. Den am stärksten ausgeprägten Einfluss hatten die Oberflächenladung sowie die Hydrophobizität. Deren Zunahme resultierte in einer erhöhten Bindung von Proteinen.

Ebenso bewirkte eine negative Ladung eine höhere Anzahl an gebundenen Proteinen im Vergleich zu einer positiv geladenen Nanopartikeloberfläche.

Für die ausgewählten Partikelsysteme erzeugten Veränderungen in der Zusammensetzung der Proteinkorona Unterschiede in der zellulären Aufnahme *in vitro*. So korrelierte die in humane THP-1 Monozyten aufgenommene Menge an Nanopartikeln mit Veränderungen der Zusammensetzung der Proteinkorona.

Zudem gelang es für die dendritischen Polyglycerole potentielle initiale Andockstellen auf humanen THP-1 Monozyten zu identifizieren und Hinweise auf einen möglichen Aufnahmemechanismus zu erhalten. So weist die Identifizierung von Serotransferin beispielsweise auf eine Clathrin-vermittelte Endozytose hin.

Die erzielten Ergebnisse bestätigen den relevanten Einfluss der Proteikorona auf die zelluläre Aufnahme. Bestimmte Proteine (Opsonine) können die Aufnahme der Nanopartikel durch das mononukleär-phagozytäre System vermitteln und so die biologische Halbwertszeit sowie die systemische Zirkulationszeit verkürzen. Diese Resultate liefern einen wichtigen Beitrag zum optimierten Design der zukünftigen Nanocarrier.

Abstract

In the field of nanomedicine, nanomaterials are becoming increasingly important as nanotransporters, e.g. to better formulate active substances, protect them from degradation and transport them in a targeted manner. However, as soon as nanoparticles are exposed to a complex biological environment (e.g. blood), they interact with various biomolecules and bind them as a corona. The protein corona is the key factor that significantly influences both the biological half-life as well as the transport and uptake of nanoparticles *in vivo*. In order to better understand and eventually predict the behaviour of nanoparticles *in vivo*, it is essential to decipher the interaction of nanoparticles and proteins.

In this work, the influence of different physicochemical properties (size, surface charge, structure and hydrophobicity) of nanoparticles on the formation of a protein corona was investigated. In terms of future utilization as nanocarriers, the connection between protein corona and cellular uptake was also analysed in more detail. The aim was to identify interaction partners, i.e. docking sites, for corona proteins on the cell membrane and thus possible cellular uptake pathways.

The nanoparticles used in this dissertation were extensively characterised with regard to their physicochemical properties. Subsequently, the protein corona in human serum was determined using various methods such as 2D electrophoresis in combination with MALDI TOF/TOF mass spectrometry. The cellular uptake of the nanoparticles into human THP-1 monocytes was investigated by flow cytometry and fluorescence microscopy. In addition, cellular interaction partners were identified via pull-down experiments.

Within this work it could be shown that all investigated physicochemical properties have an influence on the formation and composition of the protein corona. The most pronounced influence was exerted by the surface charge and the hydrophobicity. Increasing hydrophobicity led to the binding of more proteins. Similarly, a negative charge led to a higher number of bound proteins compared to a positively charged nanoparticle surface.

For the selected particle systems, changes in the composition of the protein corona led to differences in cellular uptake *in vitro*. Thus, the amount of nanoparticles taken up in human THP-1 monocytes correlated with changes in the composition of the protein corona.

In addition, for the dendritic polyglycerols it was possible to identify potential initial docking sites on human THP-1 monocytes and to obtain indications of a possible uptake mechanism. For example, the identification of serotransferin indicates clathrin-mediated endocytosis.

The results obtained confirm that the protein corona has a significant influence on cellular uptake. Certain proteins (opsonins) can mediate the uptake of nanoparticles by the mononuclear-phagocytic system and thus shorten the biological half-life and systemic circulation time. These results provide an important contribution to the optimised design of future nanocarriers.

Abbreviations

Au	gold
AuNCs	gold nanocubes
AuNP/AuNPs	gold nanoparticle/ gold nanoparticles
CDE	caveolae-dependent endocytosis
CME	clathrin-mediated endocytosis
DLS	dynamic light scattering
DNA	deoxyribonucleic acid
DOX	doxorubicin
dPGs	dendritic polyglycerols
EMA	European Medicines Agency
EPR	enhanced permeability and retention
FDA	Food and Drug Administration
HIV	human immunodeficiency virus
IND	Investigational New Drug
ISO	International Organization for Standardization
LC-MS/MS	liquid chromatography-tandem mass spectrometry
MPS	mononuclear phagocytic system
NDA	New Drug Application
NM/NMs	nanomaterial/nanomaterials
NP/NPs	nanoparticle/nanoparticles
NG/NGs	nanogel/nanogels
2D – PAGE	two-dimensional polyacrylamide gel electrophoresis
PEG	poly(ethylene glycol)
RES	reticuloendothelial system
RNA	ribonucleic acid
SPARC	secreted protein, acidic and rich in cysteine
SPR	surface plasmon resonance
THP-1	human monocytic like cell line
rhTNFα	recombinant human tumour necrosis factor alpha

Table of contents

1 Introduction

1.1 What are nanoparticles?

Nanomaterials (NMs) were used even before the concept of nanotechnology existed. With the progressive development of various NMs, the regulation of terminology became more and more important.

According to the International Organization for Standardization (ISO), all materials with at least one dimension in the nanoscale range or structures in the order of 1-100 nm are to be considered as NMs. The definition of the ISO differentiates between (i) nanostructured materials and three mayor types of (ii) nano-objects. These are the (i) nanoplates, (ii) nanofibers and (iii) nanoparticles (NPs) with one, two or three dimensions between 1-100 nm (Figure 1).
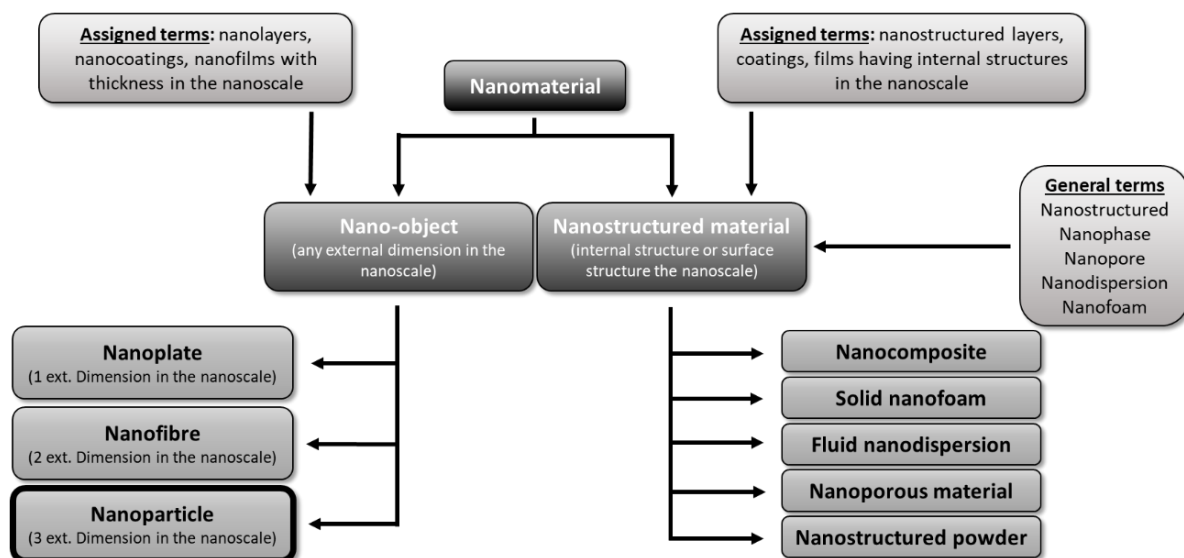
Figure 1 Illustration of the definition of nanomaterials according to ISO/TS 8004 of the International Organization for Standardization.

In addition to a categorization based on dimensional sizes, NMs can be classified based on their chemical composition. In detail, NPs can be made from (i) carbon, (ii) inorganic or (iii) organic substances or (iv) composites. Inorganic materials include metal and metal oxides like gold (Au) which can be synthesized into AuNPs.[1] Polyglycerols, for example, can be used as the basis for organic NPs.[2] NPs can originate from (i) natural, (ii) unintended or an

(iii) intended (synthetic) process. Nature itself is providing us with a wide range of particles including NPs which are emitted from volcanoes or mineral springs, for instance.[1, 3] Moreover, NPs are also emitted during anthropogenic combustion processes. However, in nanoscience we typically focus on intentionally synthesized NPs, which can be produced via (i) Top-Down or (ii) Bottom-Up methods (Figure 2). Whereas the Top-Down methods include the grinding/ milling of bulk materials, the Bottom-Up approaches use chemical synthesis methods to form nanoscaled structures de novo.[4-6]
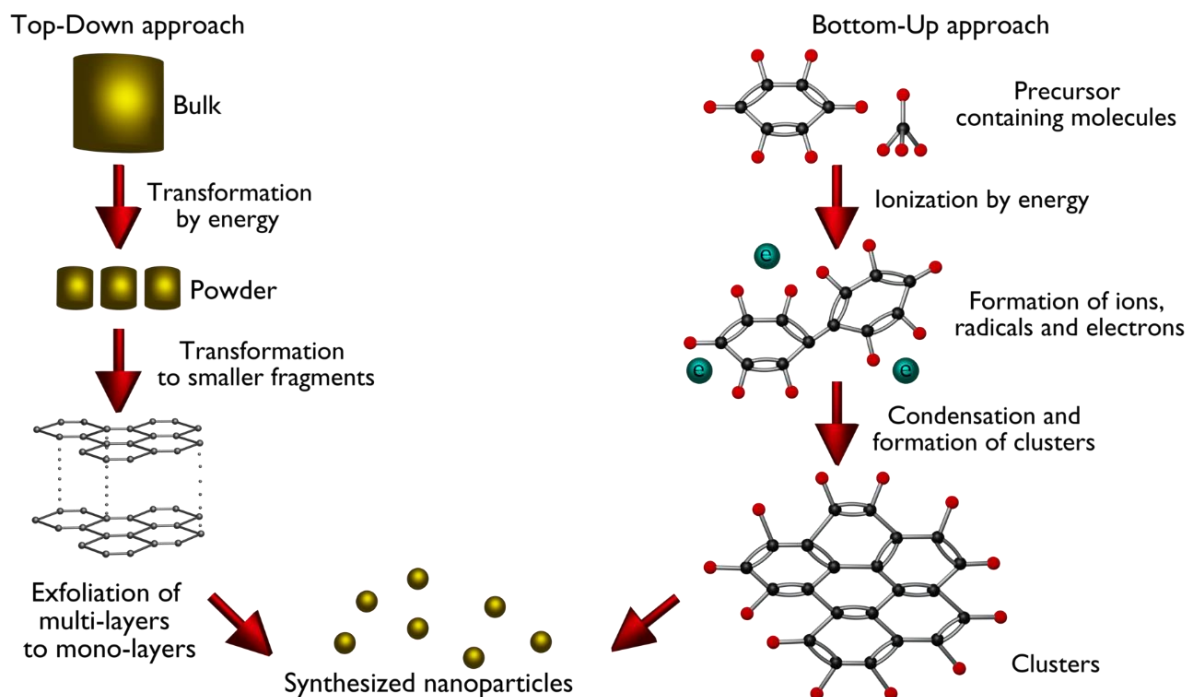
Figure 2 Synthesis of nanoparticles using top-down or bottom-up methods. Modified from Habiba et al.[7]

Intentionally synthesized NPs are already widespread used, for instance, in building and construction, in cosmetic products, in packaging or in textiles.[8, 9] However, in particular the applications in medicine are receiving more and more attention.[10] Possible applications are inter alia as nanosensors and nanoparticular contrast agents for diagnostic purposes, as a nanoscale coating for better compatibility of implants, in tumour therapy or as a carrier system of drugs.[11] Nanocarriers should be small enough to overcome physiological boundaries or penetrate target cells, but large enough to deliver a certain amount of medical substance to the desired site of action.[12] In this context it is important to note, that the smaller size of the NPs compared to the starting (bulk) material leads to altered physical and chemical characteristics and can therefore cause specific physical, chemical or biological

effects. One of the main factors influencing this significantly changed behaviour is the surface to volume ratio (specific surface) of NPs.[13]

In addition, surface modifications can offer possibilities to increase the effectiveness of NPs. Thus, NPs functionalized with poly(ethylene glycol) (PEG) showed less aggregation than untreated NPs.[14] Even an increased biocompatibility or an improved cellular internalization can be achieved by functionalization of the NP surface. Using different molecules like PEG, dextran or chitosan the biocompatibility could be drastically improved in comparison to the non-functionalized NPs.[15] A number of other advantages result from the modification of the surface of NPs, such as enabling specific interactions between NPs and cells, or even ensure directed transport or specific accumulatio in targeted organs. Furthermore, they can also drastically prolong the retention time of NPs in the blood by preventing detection and removal by the mononuclear phagocytic system (MPS), also known as reticuloendothelial system (RES).[16-18]

Immune cells (e.g. macrophages) of the RES are able to eliminate NPs from the bloodstream in a matter of seconds after intravenous application, which will prevent them from fulfilling their capacity as site-specific transport vesicles.[19] However, macrophages and other phagocytic cells are not able to directly identify the NPs themselves, but they recognize specific proteins, i.e. opsonins, associated with the surface.[20] An opsonin is any molecule that functions as a marker for phagocytosis, but complement system proteins such as complement C3, C4 and C5 as well as immunoglobulins are the most frequently occurring. By means of various functionalizations (e.g PEG), the binding of opsonins can be prevented or at least reduced, thus increasing the retention time of the NPs in the blood.[21] Opsonins are not the only ones that influence the behaviour of NPs in biological systems. Characteristics of most NPs differ greatly from their purely intrinsic (i.e. physical or chemical) properties after entering a biological system. In contact with a biological milieu the surface of NPs is in a dynamic exchange with ions, small molecules, proteins and lipids.[22, 23] Plasma proteins play a special role in the formation of nano-bio interfaces. They are able to attach to the surface of NPs and form a protein corona, which can subsequently drastically change the NP behaviour (see 1.4).[24] In the end it is the protein corona which is "expressed" at the surface of the NPs that is "read" by the living cells within the cell-NM interaction.[25] Precisely this protein corona forms on almost every NP. However, it varies depending on the nature of the NP, despite exposure to the same biological environment.[26-28] The physico-chemical

properties of a NP determine the composition of the protein corona. But the knowledge of exactly how these physico-chemical properties of the NP (e.g. size, shape, surface charge and coating etc.) influencing the protein corona, as well as the biological functions of the corona is not yet fully complete.

1.2   Nanoparticles for medical applications

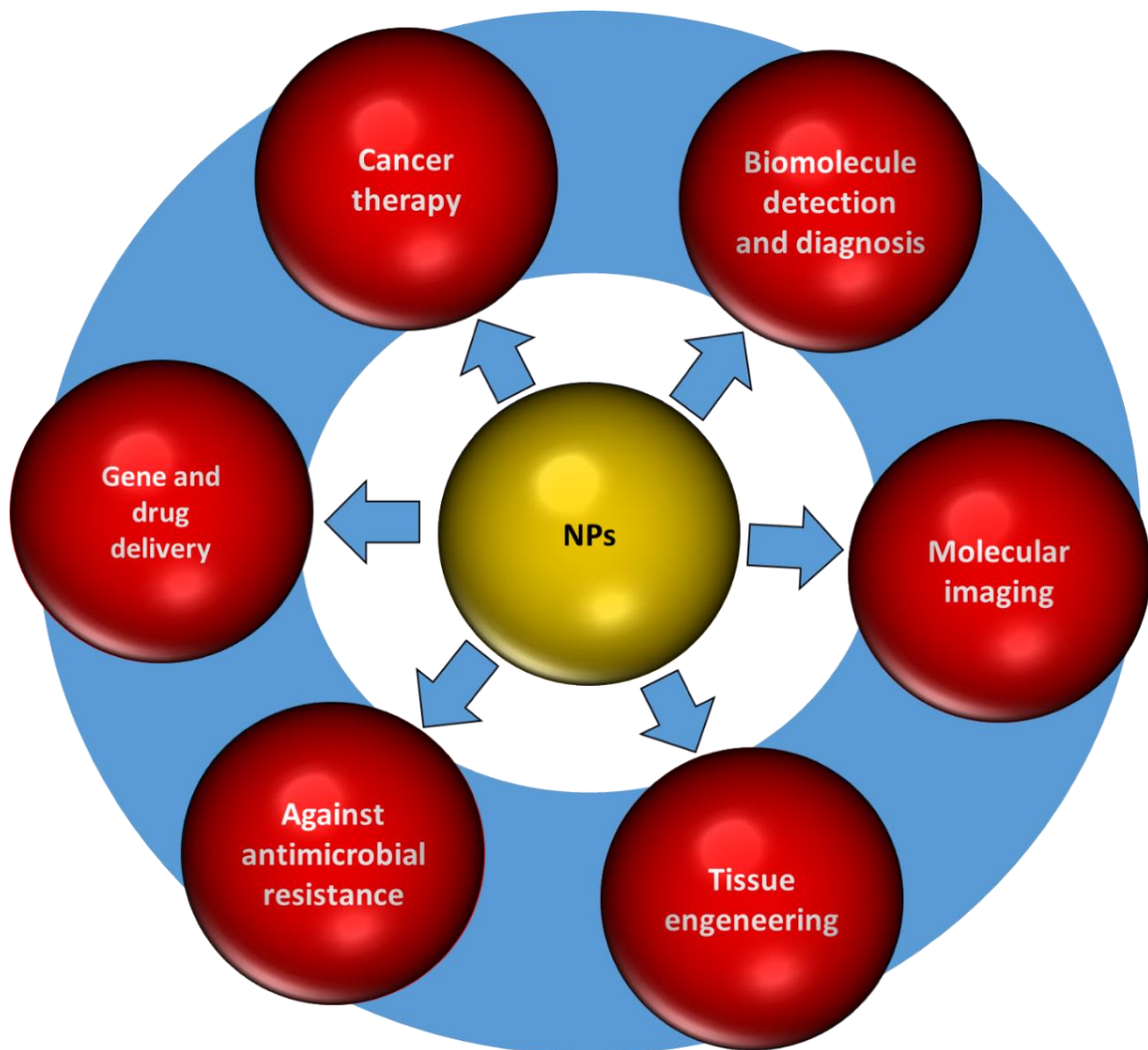**Figure 3 Possible applications of nanoparticles in the field of medicine.** Nanoparticles have a broad spectrum of possible applications and some selected ones are shown here.

The use of NPs in medical applications such as molecular imaging, diagnosis, treatment and control of diseases is referred to as "nanomedicine". In this field, NPs exhibit a broad spectrum of possible applications (Figure 3).

Even if it seems as if this is a newly emerging field of medicine, the basics are already several decades old. For instance, the first versions of lipid vesicles (which later became known as liposomes) were described in 1965.[29] 11 years later, in 1976, the first controlled release polymer system of macromolecules[30] and in 1994, the first long circulating stealth polymeric NP was introduced.[19]

One year later, in 1995, liposomal doxorubicin (Doxil^{TM} / Caelyx^{TM}) becomes the first nanomedicine approved by the U.S. Food and Drug Administration (FDA).[31, 32] In the time passed, a variety of NP-based therapeutic and diagnostic pharmaceuticals has been developed inter alia for the treatment of cancer, diabetes and allergy.[33, 34] With the condition that nanomedicines are defined as therapeutic or imaging agents that contain NPs to control biological distribution, increase efficacy or reduce toxicity. In 2019 a total of 29 FDA-and European Medicines Agency (EMA) approved and 47 nanomedicines in clinical trials can be found.[35] Even if NPs are widely used in nanomedicine, it is their function as drug transporters to which we have focused our attention in this work. Some of the main advantages of the NPs as carriers are that they offer time-controlled, site-specific delivery, an increase in efficiency and safety of the drug due to enhanced stability and improved bioavailability as well as an extended effect of the drug in the tissue.[36, 37] In addition, they can deliver a wide variations of substances like deoxyribonucleic acid (DNA), ribonucleic acid (RNA), proteins and drugs.[38, 39] To be more specific, the poor water solubility of many existing and novel bioactive drugs is one of the biggest challenges that pharmaceutical industry is facing. Many potential candidates fail in preclinical studies due to limited solubility, stability and toxicity closely associated with the hydrophobic character of the concerned substances. As a result, many nanocarriers has been developed to counteract this problem.

In general, there are two major ways to transport substances: (i) covalent binding or (ii) encapsulation. In the end, the substance should be able to unfold its effect at the desired location. For the covalent binding this involves the cleavage of the bond via an external trigger. Using encapsulation as transport mechanism, theoretically, the carrier can be used with a wide range of different substances.[2]

As previously mentioned, the physico-chemical properties of NPs are usually different from the original (bulk) material. This gives NPs unique physico-chemical properties, depending on the type of material.[40] They may have a larger surface area, a controllable particle size, an increased catalytic activity or fluorescence, a unique biocompatibility, surface plasmon

resonance (SPR) and easy surface functionalization and bio-conjugation.[41, 42] When designing drug delivery via NPs, one of the major issues is their targeting specificity. Accumulation in a tumour can rely on passive or active processes.

The passive transport of NPs to tumour tissues is based on the enhanced permeability and retention (EPR) effect. In general, NPs of certain sizes tend to accumulate to a greater extent in tissues of tumours than in healthy tissues.[43] An explanation for this phenomenon of the EPR effect is that, in order for tumour cells to grow quickly, they are depending on a sufficient blood supply for their need of nutrients and oxygen. To ensure this they must stimulate the production of blood vessels. These newly formed vessels are usually abnormal in form and architecture. They may have poor alignment and possess wide fenestrations. Precisely this enables NPs circulating in the blood to penetrate the tumour tissue (permeation). Removal of these NPs is more difficult due to the usually deficient lymphatic system in tumour tissues (retention). The increased permeability and retention capacity of tumour tissue can be used for tumour-targeted therapies.[43, 44] Addressing NPs for enhanced drug delivery due to the EPR effect, some aspects should be considered. These include, but are not restricted to a long blood half-life and minimal nonspecific delivery.[45]

Active delivery depends on substances coated to the surface of the NPs, which possess a high affinity for overexpressed receptors in tumours or their microenvironment. Among them are compounds such as peptides, small organic or synthetic molecules, antibodies, variant types of RNA as well as DNA and oligosaccharides.[46-52] Some of these ligands are able to promote the intracellular accumulation of NPs in cancer cells.[53] Transferrin receptors, for example, are overexpressed in many solid tumours compared to normal cells and can therefore be used for active targeting with transferrin-conjugated NPs.[54] Addressing folate receptors using folate-conjugated NPs is also an option, as the alpha isoform is present in about 40% of all human cancers.[55] In summary, this form of administration can be used to provide NPs with a specificity for different tumour types.

However, the efficient and controlled trafficking into cells remains a major challenge for the nanomedicine. A deeper insight and better understanding of the uptake mechanisms is crucial in designing safe nanocarriers.

In the following chapters, the NPs that have been examined in my thesis should be introduced by briefly describing their structure and providing examples for possible medical applications.

1.2.1 Dendritic polyglycerols

Dendrimers are highly branched, monodisperse macromolecules with a well-defined structure. This structure has a great impact concerning their physical-chemical properties.[56] Compared to linear polymers of the same or at least similar molecular weight, the "treelike" spherical structure of these molecules leads to a number of interesting characteristics.[57, 58] In contrast to linear polymers, well-designed high-branched dendrimers have a pronounced "interior" which is sterically isolated in the dendrimer and facilitates their usage as nanocarriers.[56] Due to their high biocompatibility, dendritic polyglycerols (dPGs) have a broad application spectrum in medicine and pharmacology. The following small section describes some current trends for therapeutic purposes, such as for improved solubility of hydrophobic compounds and the transport of active substances across biological barriers.

Due to the possibility to chemically modify either the core (increase hydrophobicity) or the shell (increase hydrophilicity) of dPGs, the solubility profile of these nanocarriers can be tailored. Park and co-workers could show that the solubility of the poorly water-soluble cancer chemotherapy drug paclitaxel is enhanced depending on the generation and concentration of the dPGs.[59]

Dendritic systems are influenced by three main factors concerning their transport properties: (i) the core, determining the shape of the carrier; (ii) the internal structure, regulating the interactions between transported substance and the carrier; and (iii) the outer shell, defining the solubility properties as well as influencing the loading and release properties.[2, 60] The relatively simple modification of the dPGs provides, apart from the broad transport possibility, an excellent platform for the attachment of cell-specific targeting groups, solubility modifiers and stealth moieties.[61] As a result, dendrimers are found in a wide range of biomedical applications[62, 63], such as drug [64] and gene delivery [65]. Their flexibility in terms of size, shape and surface charge can be used for bypassing the cellular membrane.[66, 67] Some dendrimer products are already available on the medical market, for example VivaGel$^®$, which is used for the treatment of bacterial vaginosis and as protection against the human immunodeficiency virus (HIV).[68]

1.2.2 Nanogels

These three-dimensional delivery systems consists of hydrogel particles within the sub-micron size range [69] and can be formed by physical and/or chemical intercrossing of different kinds of polymer chains.[70, 71] These bonds can either be covalent or non-covalent. Nanogels (NGs) can possess some unique characteristics such as biocompatibility, adjustable size, high stability and the ability to respond to external stimuli like temperature, light or pH.[71-73] Accompanying this NGs are emerging as versatile drug carriers, being interesting for many applications ranging from cancer therapy to nanoantibiotics.[74-81] Precisely because of their enormous versatility, there are many different types of nanogels. A potential classification based on their properties is shown in Figure 4.
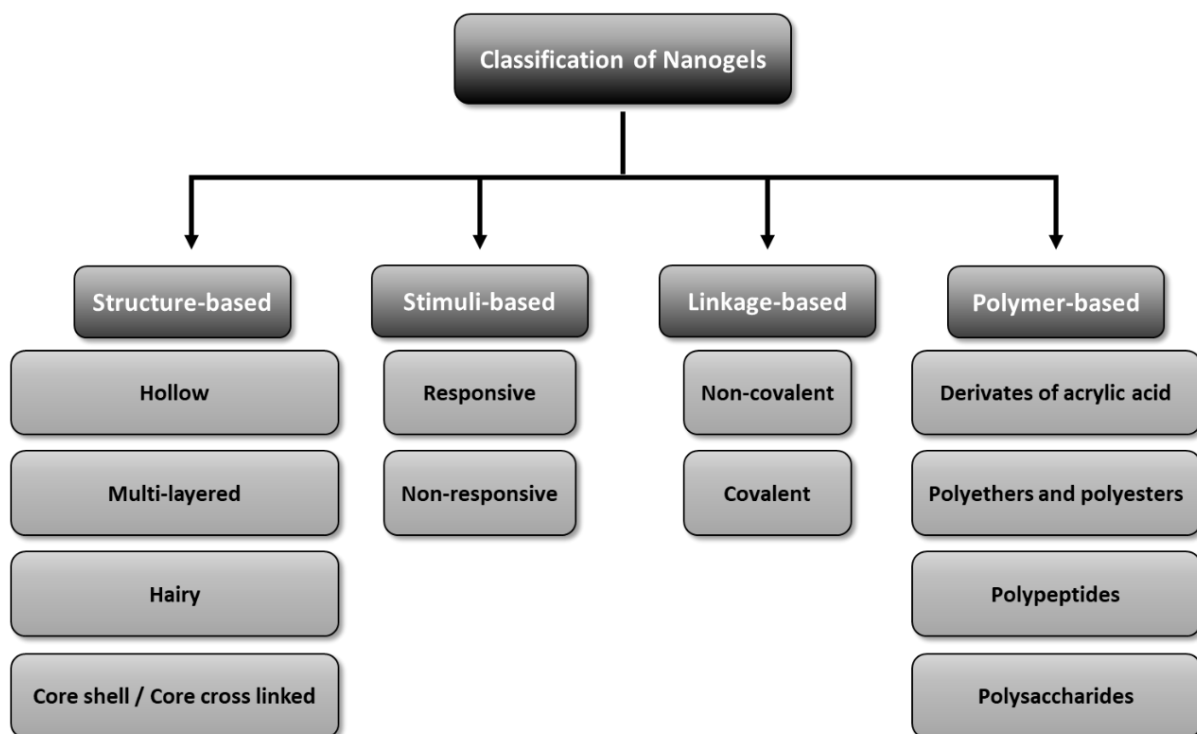
Figure 4 Classification of nanogel formulations. NGs can be classified into four different groups regarding their structure, their response to stimuli, if they require cross-linking agents and which type of polymer is used. Modified from Shah et al.[82]

Depending on the structure, a distinction can be made between hallow or multi-layered NGs, to name only a selection. Hollow NGs have a hollow cavity within their gel matrix, giving them a significantly larger surface area compared to conventional NGs. A greater surface area may result in an increased drug loading capacity as well as in an enhanced drug release.[83, 84] Multi-layered NGs consist of multiple layers of either a single or multiple polymers.

The selection of these polymers plays an important role concerning the site specificity as well as in the drug release profile of the NGs. Drugs which are highly toxic or sensitive to the body fluids, peptides, oligopeptides and nucleotides are only a few examples that can be transported using multi-layered NGs.[84, 85]

The capability to respond to stimuli, offers a further possibility to differentiate NGs. Thus, a distinction is made between responsive and non-responsive. Responsive NGs change some of their properties depending on their local environment, which ultimately leads to a release of their cargo, while non-responsive NGs release the drug independently.[84] Such stimuli include inter alia temperature susceptibility[86], photosensitivity[87, 88] and pH-sensitivity[89, 90].

Unfortunately, there is one major drawback: the overall hydrophilicity of conventional NGs limits their application for hydrophobic drugs. This problem can be bypassed using a combination of different polymers. For example, amphiphilic NGs can be created by forming a hydrophilic polymer network with randomly distributed hydrophobic groups. The amphiphilic character of these NGs allows the encapsulation of hydrophobic drugs.[91, 92] The potential of NGs is already used for a wide range of disorders.

Concerning disorders in the central nervous system for example, NGs already showed promising results in the treatment of glioblastoma due to targeted delivering of doxorubicin (DOX)[93] and in the treating of intra-cranial glioma via cisplatin loaded NGs[94]. A pH responsive system composed of chitosan for temozolamide delivery for aggressive skin papilloma was prepared and superior antitumour efficacy *in vivo* compared to plain drug was noticed. Furthermore, the pH responsive system accelerated the drug release in the acidic tumour environment.[95] Taken all together, NGs are one of the most tuneable delivery systems. Their capabilities can be utilized to enhance the potency of several drugs that are incorporated within them.[84]

1.2.3 Gold nanoparticles

Because of their special properties, metal NPs, especially AuNPs, have generated enormous attention within a variety of scientific fields. To mention only a few special features: ease of synthetic manipulation, enabling precise control over the particle's physicochemical properties[96], unique tuneable optical[97] and distinct electronic properties[98].

Many efforts have been made to adapt the properties of AuNPs to specific biological applications, for instance in bio-imaging, gene diagnostics, analytical sensing and targeted delivery of biomolecular cargos. The properties of AuNPs such as the morphology, solubility, size, surface functionality and stability can be designed via different synthetic routes, including the Turkevich, the Brust and the Perrault method.[99-108] While Turkevich's method was predominantly used to produce spherical NPs, a wide variety of shapes can be achieved today. Among others, it includes rod-[109], cage-[110] and star-shaped[111] AuNPs. Based on the features of AuNPs, some of the leading biomedical applications are associated with imaging (e.g. computed tomography), administration of drugs and therapeutic strategies like radiosensitization and photothermal therapy.[112-114] However, due to their compatibility and simplicity of modification AuNPs have proven to be excellent drug carriers.[115] To control inter alia their stability, solubility and the interaction with the biological environment, the coating of AuNPs can be altered.[116] These surface modifications with polymeric materials are able to increase the circulation time, stability and furthermore reduce nanotoxicity of the AuNPs.[117-119] Several studies already highlighted the potential of AuNPs to provide drugs for cancer treatment.[120, 121] And indeed there is already an example of a nanostructured drug carried via an AuNPs is Aurimune^{TM} (CYT-6091). This gold-based tumour-targeting nanomedicine consists of a 27 nm PEGylated colloidal AuNP on whose surface recombinant human tumour necrosis factor alpha (rhTNFα) and thiolyated PEG are bound. The approach of a systemic delivery of the rhTNFα into the cancer cells has already been used in Phase I clinical studies, and Phase II is currently being performed.[119, 122, 123] Aurimune^{TM} is supposed to carry rhTNFα into the tumours and destroy their blood vessels. If followed by chemotherapy, it is possible to induce increased cancer cell death.[122]

1.3   Drug development and approval

Approval by the EMA can be roughly divided into three phases.[124] The entire process of development and approval of a new drug can normally take easily 10 to 15 years and approximately 1 billion dollars.[125]

The first phase in this process is the research and development phase in which the initial identification of new therapeutic candidates, the testing of their effectiveness and first toxicity studies take place. Discoveries of new small molecule drug candidates are made by a number of different approaches. In some instances, candidates can be predicted in silico or can be found by screening libraries of small molecule drugs against known targets.[126, 127] Generally speaking, nanoparticulate platforms require functionalisation to achieve the desired drug effect.[128] Therefore, nanotherapeutics are built on mature, well-characterised nanoparticle platforms whose synthesis and surface and/or internal modification are well known and can be easily controlled.[129] Regarding the safety of the new drugs, preclinical testing focusing in particular on the interaction with biological systems. In cell culture, it is essential to demonstrate the mechanism of action of the therapeutic agent and, most importantly, that the observable effect is a result of the therapeutically active component and not the nanoparticle platform itself. After evaluation *in vitro*, the next step is the assessment of safety in animals. After discovering, characterization, demonstration of efficacy and safety *in vitro* and *in vivo* the new drug can be submitted as Investigational New Drug (IND) to the EMA. After the successful application of the IND, the clinical phase follows. In Phase I trials the main goal is to provide initial information regarding dosing, acute toxicity and drug excretion in humans. Increased numbers of patients, further evaluation of the safety and efficacy of the IND in a group of patients who suffer from the disease to be treated heralds the second clinical phase (Phase II). Phase III is even larger containing randomized. placebo-controlled trials. These studies are used to compare the IND to the eventually existing "gold-standard" and to demonstrate further safety and efficacy. After this a New Drug Application (NDA) can be filed with the EMA requesting approval for marketing purposes. At request of the EMA postmarketing studies (Phase IV) are undertaken after the NDA has been approved. These may be desired to study long-term effects of the drug or the efficacy of the drug in additional indications.[125, 130]

1.4 Biological environment and NPs -the protein corona

A key aspect in preclinical testing of new medicines is the study of their behaviour in biological environments. It must be ensured that the effect originates from the therapeutically active component and not only from the NP platform itself. The importance of these investigations is illustrated in the following.

Ideally, the NPs would be injected into a patient's blood, where they circulate until they reach the targeted tissue. Then the ligand on the NP would recognise its specific receptor and the drug could be delivered in a regulated manner. Unfortunately, it is not always that straightforward.

As soon as the NPs enter a biological system (e.g. blood stream), they are exposed to ions, small molecules, proteins and lipids.[22, 23] Due to their large surface-to-volume ratio NPs have a very active surface chemistry compared to the bulk variant. Therefore, unless they have been designed to do otherwise, in a physiological environment NPs will always try to reduce their surface energy by adsorbing biomolecules.[25, 131] Exactly this newly formed corona will influence the interaction between biological entities like cells or tissues and the NPs. [132] After all, this complex formed by NPs and the corona instead of the bare NP is the first thing a biological entity sees first (Figure 5).[133] The so-called protein corona is primarily composed of proteins, although the presence of other biomolecules is assumed but has not been investigated in detail.[134, 135] Understanding the formation of the protein corona in biological environments is crucial for the application of NPs as drug carriers. It is known, that the protein corona formation depends on several physico-chemical properties of NPs such as size, shape, surface charge, or hydrophobicity and can influence cellular uptake *in vitro*.[133, 136-142]
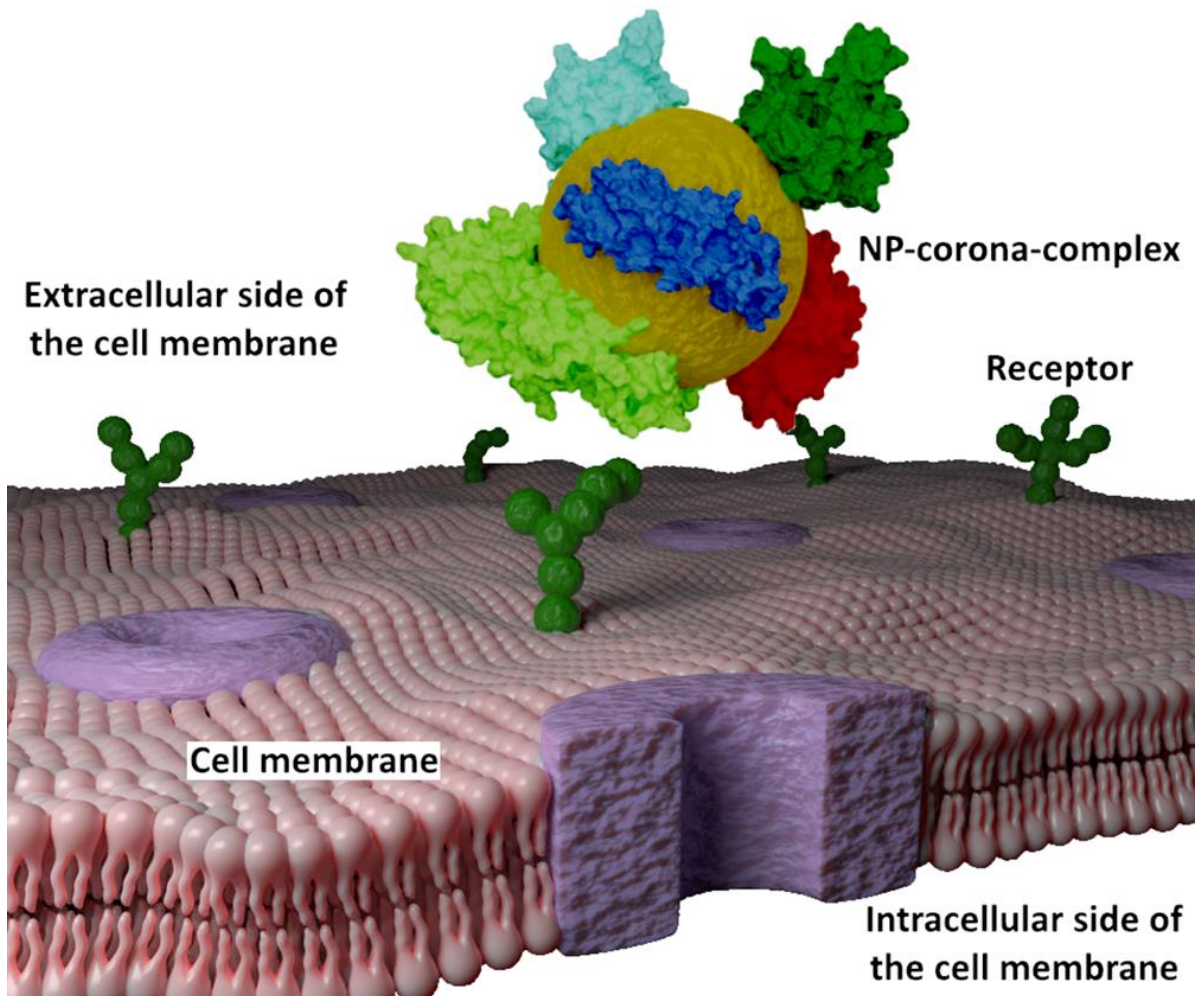
Figure 5 The NP-corona-complex in a biological environment. The NP-corona-complex, rather the bare NP, is the first thing the cell sees. Depicted is a NP with different proteins bound to the surface. Adapted from Monopoli et al.[131]

The variability of the corona is determined not only by the NPs themselves, but also by various properties of the proteins. Thus, (i) the wide range of binding affinities and equilibrium constants, (ii) variations in the association/dissociation rate and (iii) differences of the protein profile in biological fluids have a significant impact on the dynamics of the protein corona.[132]

When proteins are adsorbed from solutions containing many different types of proteins (e.g. blood plasma), the combination of the concentration and size of the protein determines its diffusion flux. As a result, the kinetics of its adsorption are also determined.[143] In a biological environment, proteins that are present in large quantities, have higher kinetics and will be initially adsorb on the surface of the NPs. Subsequently, a critical equilibrium between the kinetics and thermodynamics of all proteins controls the corona formation on the NPs. Thermodynamically, a protein will spontaneously adsorb on a surface if that results in a

reduction of the total system's energy.[144] Due to kinetic interactions, proteins that have a higher affinity to the material surface and thus contribute more to lowering the free energy, reach the NP surface at a later point in time. There, they displace the originally adsorbed proteins. This process is long known as the Vroman effect.[145, 146]

Regarding the affinity of the proteins towards the NP surface, the protein corona can be classified as hard or soft. In contradiction to the hard corona, where proteins with a low dissociation (k_{off}) constant and high affinity to the NP surface are commonly observed, the soft corona contains proteins with a high dissociation (k_{off}) constant and low affinity (Figure 6).[147]
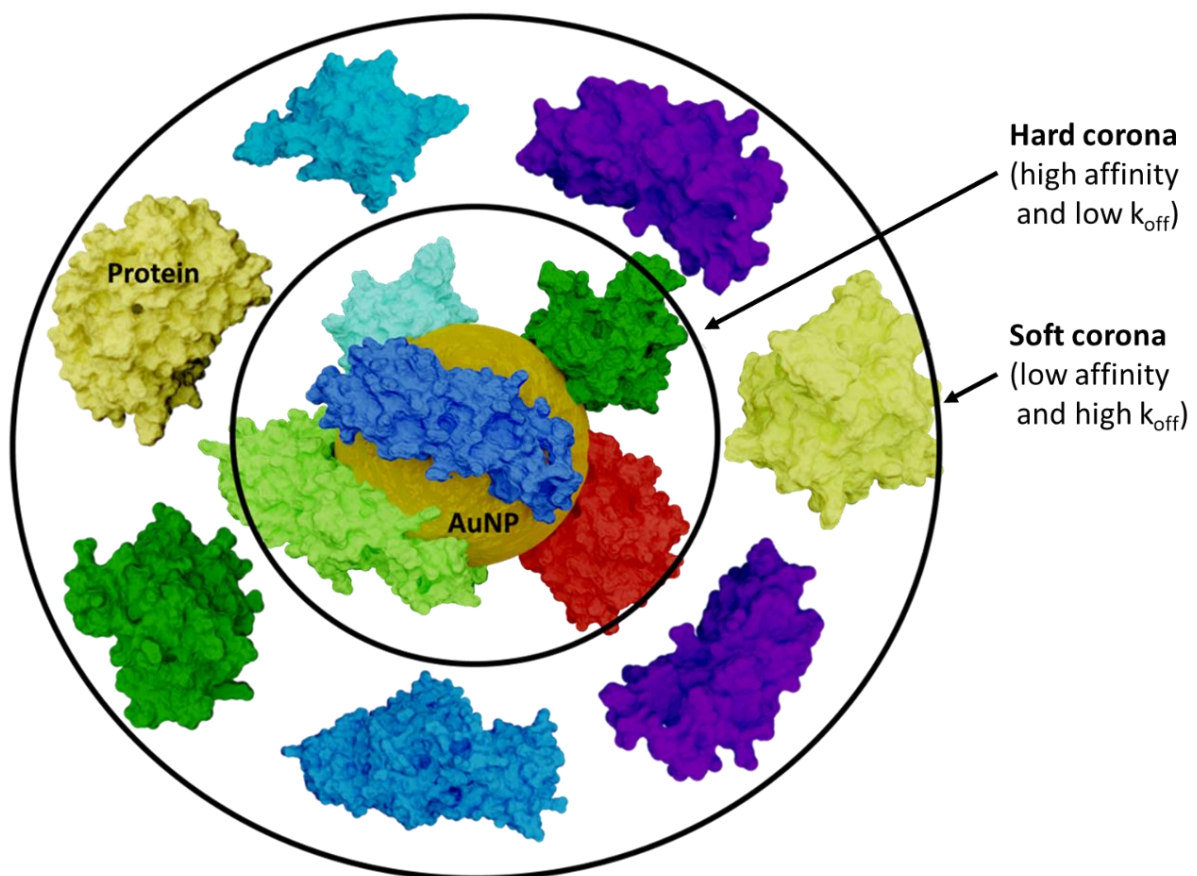
Figure 6 Schematic illustration of a protein corona. Modified from Fleischer et al.[147]

Investigation of the NP-protein corona complex usually results in the examination of the hard corona, as this is the only part of the corona that can be isolated and studied. Loosely bound proteins, either to the NPs or the proteins of the protein corona, are referred as the soft corona. This part is experimentally practically inaccessible, since the soft corona desorbs during isolation. However, even though the proteins of the hard corona possess a high affinity, its composition is still variable. If the NP-protein corona-complex is trafficking

through different environments (e.g. uptake into cells or tissues) the hard corona will change and evolve due to adsorbing of environment specific proteins.[148] The adsorption of proteins is a dynamic process consisting of a steady adsorption/desorption equilibrium of proteins on and off the NP surface (Figure 7). The kinetics of this time dependent process are given by the association (k_{on}) and dissociation (k_{off}) constants. K_{on} depends on the frequency of contact between NP and protein, whereas the binding energy of the NP-protein complex determines k_{off}. The balance of these two values, defines the affinity of a protein for the NP and is referred to as the dissociation constant k_{d}.[132]
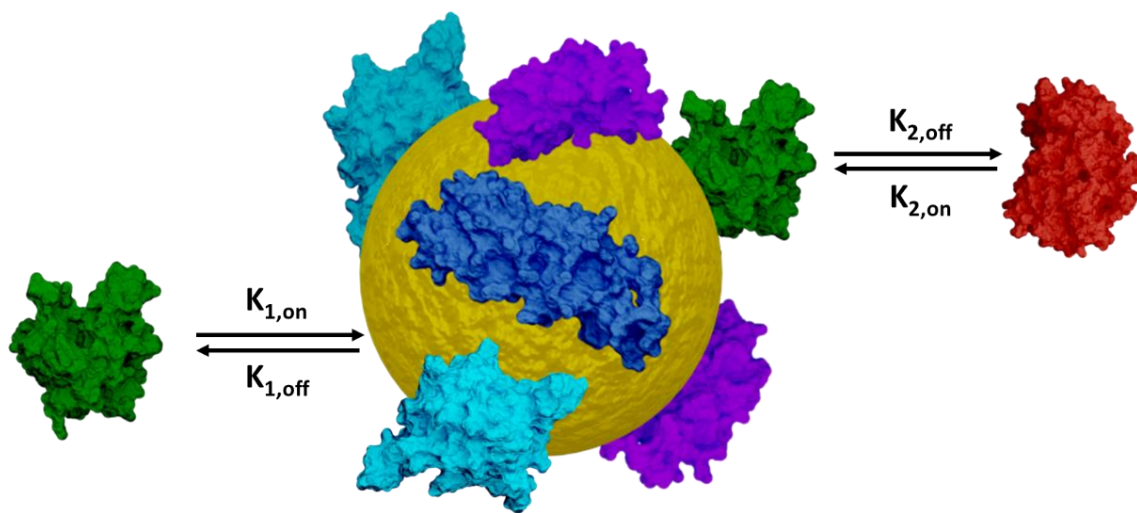
Figure 7 Adsorption and desorption - interactions between NPs and proteins. A section of relevant processes for the interaction of proteins with a NP is depicted. Biomolecules in the surroundings adsorb on the naked NP surface (k_1) and form a firmly bound layer, the hard corona. Other biomolecules, namely the soft corona, display a lower residual affinity to the NP-hard-corona complex, so that these molecules are in rapid exchange with the environment (k_2). Modified from Monopoli et al.[131]

1.5 Cell membrane interactions and NP cellular uptake pathways

Reaching the exterior membrane of a cell, NPs will interact with the components of the plasma membrane or extracellular matrix. To achieve cellular uptake, NPs need to overcome the cell plasma membrane. This involves highly regulated mechanisms with complex biomolecular interactions. It is important to know how NPs enter cells, as the underlying uptake pathway will determine the function and intracellular fate of the NP.[149] To cross the cell membrane, several pathways of entry are available for NPs. These pathways can generally

be divided into two different groups: (i) endocytosis-based (Figure 8) and (ii) direct cellular entry like direct translocation, lipid fusion, electroporation or microinjection.[150]
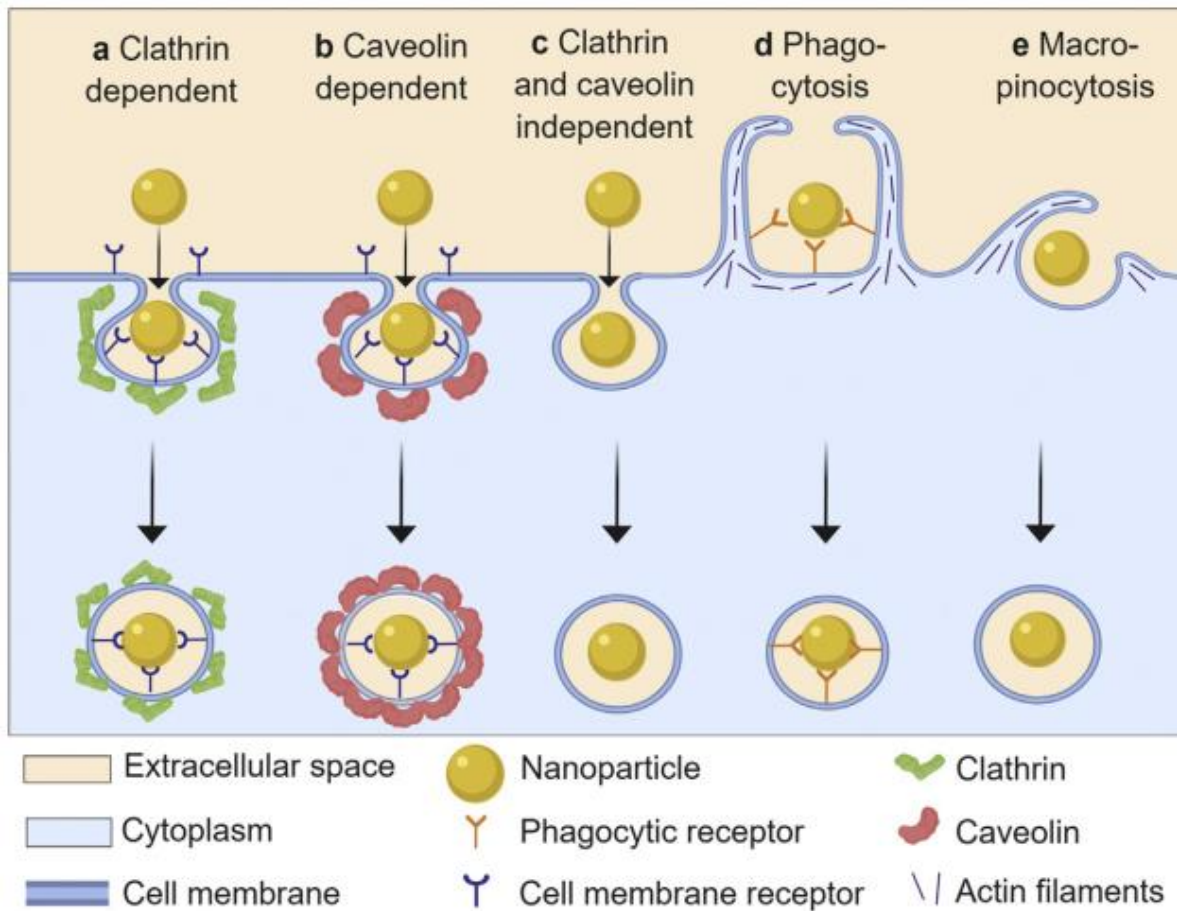
Figure 8 Schematic overview of NP uptake pathways via endocytosis. The figure was used from Nathan D. Donahue et al.: "Concepts of nanoparticle cellular uptake, intracellular trafficking, and kinetics in nanomedicine"; Advanced Drug Delivery Reviews 2019 [150]

The term endocytosis is used to summarize different pathways and mechanisms. Generally, there are five mechanistically different endocytosis pathways for NPs to enter the cell (Figure 8). In biomolecular terms, these pathways are highly controlled and driven by various types of lipids and transport proteins (e.g. lipid rafts, clathrin and caveolin). After endocytosis, NPs are typically trapped in intracellular vesicles such as endosomes, phagosomes or macropinosomes. Therefore, they do not have immediate access to the cytoplasm or the cell organelles.[150]

Since not many NPs are documented to utilize the other three variants (Figure 8 c,d,e), only two (Figure 8 a,b) are described briefly in the following.

1.5.1 Clathrin-mediated endocytosis

Clathrin-mediated endocytosis (CME) (Figure 8 a) is the main pathway by which cells are provided with nutrients and plasma membrane components. This is achieved either via receptor-specific uptake or via non-specific adsorptive uptake, also known as receptor-independent CME.[151] CME takes place in a clathrin-rich area of the plasma membrane. Such areas cover about 0.5-2 % of the cell surface.[152] Together with other proteins, the clathrin is responsible for the assembly of a complex structure that will ultimately create the curvature of the membrane and then the budding vesicle. Following a cascade of protein interactions, dynamin, a membrane cleaving protein, finally binds to the neck of the budding vesicle, releasing the vesicle into the cytoplasm.[153, 154]

CME is considered as the major pathway for NP cellular entry and is mediated by interaction of NP surface ligands and cell membrane receptors.[155, 156] After pinching off the membrane the NP is transported via the vesicle to the endosomes. Endosomes are either recycled or fuse with lysosomes leading to the breakdown of the engulfed payloads. Therefore, CME is a possibility for NPs to reach the cell's endolysosomal system. Benyettou and co-workers were able to exploit this pathway. As reported, they were able to deliver anticancer therapeutics to HeLa cancer cells *in vitro*. After lsysosomal entrapment the NPs released their payloads in response to the low pH of lysosomes, resulting in an increased anti-cancer activity.[157]

1.5.2 Caveolin-dependent endocytosis

Caveolae-dependent endocytosis (CDE) (Figure 8 b) plays a crucial role in numerous biological processes. These include, for instance, cell signalling, transcytosis and the regulation of membrane proteins and membrane tension. Furthermore, CDE seems to play a part in multiple diseases such as cancer, diabetes and viral infections.[158-161]

Caveolae are membrane invaginations present in epithelial and non-epithelial cells. They are interspersed between regions of dense bodies that anchor the cytoskeleton. Caveolin, a dimeric protein that lines the caveolae and is involved in the formation of their characteristic flask shape.[159]

This signalling pathway has aroused great interest in nanomedicine. This is related to the fact that the CDE has the ability to bypass lysosomes. Lysosomes possess hydrolytic enzymes that contribute to the degradation of biomolecules. If the lysosomes are bypassed by means of the CDE, the premature degradation of NPs could also be prevented and may result in a more efficacious efficiency.[162] Several pathogens exploit this fact to prevent lysosomal degradation.[163] Maybe it could also be beneficial for the cellular transport of proteins and DNA.[164] However, among others, the nanotherapeutic Abraxane® was already found to be taken up by cancer cells via the CDE. This albumin-bound form of paclitaxel binds to gp60, the albumin receptor in the caveolae of endothelial cells, entering the interstitial spaces of the tumour and is captured by SPARC (secreted protein, acidic and rich in cysteine). SPARC is selectively secreted by the tumours. The complex of NP and SPARC is taken up in tumour cells resulting in selective cytotoxicity.[165]

2 Aim of the work

The interaction between the biological environment and NPs is of major relevance for the biological half-life, the cellular uptake and the associated efficacy as well as the general behaviour of NPs in medical applications.

Therefore, the overarching objective of my research was to systematically investigate the influence of physico-chemical properties of NPs on the formation of a protein corona. In this context, different NPs, representing promising nanocarrier systems have been selected and their physico-chemical properties were systemically altered. For dPGs the influence of the size and surface charge on the protein corona formation has been investigated (see chapter 3.1). Amphiphilic NGs have been examined with respect to the impact of hydrophobicity (see chapter 3.2). Furthermore, for AuNPs the effect of shape and surface charge (see chapter 3.3) on protein corona formation has been studied. An overview is given in Figure 9. For the selected NPs the formation and the composition of the protein corona has been investigated using different proteomic methods such as two-dimensional polyacrylamide gel electrophoresis (2D PAGE) analysis in combination with mass spectrometry.

Furthermore, the influence of the protein-corona on cellular uptake was a second objective of my thesis. These investigations have been undertaken in differentiated THP-1 cells as a cellular model for the mononuclear phagocytic system. The cellular uptake of selected NPs was assessed by flow cytometry and fluorescence microscopy.

In addition, ligand-receptor interactions were investigated to understand the initial docking step on the cell membrane. For this purpose, pull-down experiments have been performed.

Figure 9 Nanoparticles used in this thesis are grouped into their respective examination criteria. From top to bottom these are the dendritic polyglycerols (chapter 3.1), the amphiphilic nanogels (chapter 3.2) and the gold nanoparticles (chapter 3.3).

3   Publications

3.1   The influence of surface charge on serum protein interaction and cellular uptake: studies with dendritic polyglycerols and dendritic polyglycerol-coated gold nanoparticles

Tony Bewersdorff, Jonathan Vonnemann, Asiye Kanik, Rainer Haag, Andrea Haase

The supplementary material to the publication embedded on the following pages is contained in Annex I.

The authors contribution:

Sample preparation for characterization, protein corona analysis and NP uptake studies

Data analysis

Analysis of proteomic results (2D-SDS-PAGE and MALDI-TOF/TOF)

Cell culture

Investigation of the cellular uptake by flow cytometry

Discussion and evaluation of the results (with other authors)

Preparation of the manuscript (with other authors)

Open Access Full Text Article

ORIGINAL RESEARCH

The influence of surface charge on serum protein interaction and cellular uptake: studies with dendritic polyglycerols and dendritic polyglycerol-coated gold nanoparticles

Tony Bewersdorff[1]
Jonathan Vonnemann[2]
Asiye Kanik[1]
Rainer Haag[2]
Andrea Haase[1]

[1]Department of Chemical and Product Safety, German Federal Institute for Risk Assessment (BfR), Berlin, Germany; [2]Institute of Chemistry and Biochemistry, Freie Universität Berlin, Berlin, Germany

Correspondence: Andrea Haase
Department of Chemical and Product Safety, German Federal Institute for Risk Assessment, Max-Dohrn-Strasse 8–10, 10589 Berlin, Germany
Tel +49 30 18412 3423
Fax +49 30 18412 6 3423
Email andrea.haase@bfr.bund.de

Abstract: Nanoparticles (NPs) have gained huge interest in the medical field, in particular for drug delivery purposes. However, binding of proteins often leads to fast NP uptake and rapid clearance, thereby hampering medical applications. Thus, it is essential to determine and control the bio–nano interface. This study investigated the serum protein interactions of dendritic polyglycerols (dPGs), which are promising drug delivery candidates by means of two dimensional gel electrophoresis (2DE) in combination with mass spectrometry. In order to investigate the influence of surface charge, sulfated (sulfated dendritic polyglycerol [dPGS]) and non-sulfated (dPGOH) surfaces were applied, which were synthesized on a gold core allowing for easier separation from unbound biomolecules through centrifugation. Furthermore, two different sizes for dPGS were included. Although size had only a minor influence, considerable differences were detected in protein affinity for dPGS versus dPGOH surfaces, with dPGOH binding much less proteins. Cellular uptake into human CD14+ monocytes was analyzed by flow cytometry, and dPGOH was taken up to a much lower extent compared to dPGS. By using a pull-down approach, possible cellular interaction partners of serum pre-incubated dPGS-Au20 NPs from the membrane fraction of THP-1 cells could be identified such as for instance the transferrin receptor or an integrin. Clathrin-mediated endocytosis was further investigated using chlorpromazine as an inhibitor, which resulted in a 50% decrease of the cellular uptake of dPGS. This study could confirm the influence of surface charge on protein interactions and cellular uptake of dPGS. Furthermore, the approach allowed for the identification of possible uptake receptors and insights into the uptake mechanism.

Keywords: sulfated dendritic polyglycerols, protein corona, cellular uptake, uptake receptors, clathrin-mediated endocytosis

Introduction

Nanotechnology is often regarded as one of the key enabling technologies of the century. Nanoparticles (NPs) are already used for various diverse purposes including medical applications such as drug delivery.[1] NP-based drug delivery systems offer several advantages. In particular, they are used with difficult-to-formulate chemicals, can protect drugs from degradation, enhance drug half-lives, and finally can enable drug targeting as NPs may reach and accumulate at specific sites in the body, where they may also be used as local drug depots. Thus, often for nano-formulated drugs, lower doses can be applied compared to conventional formulations leading to significantly reduced side effects.[2] Some NP drug carrier systems are already approved, mostly

for tumor therapy such as DaunoXome®, a liposome-based formulation of daunorubicin being used to treat human immunodeficiency virus-related Kaposi's sarcoma.[3] However, not only liposome-based formulations but also dendrimers seem to be useful candidates for drug delivery purposes. They allow packaging of larger molecules and are in particular useful to solubilize poorly water-soluble drugs.[4,5]

Often the use of NPs in medicine is hampered by the fast binding of plasma proteins to their surfaces (opsonization), leading to quick clearance of the circulating NPs by the reticuloendothelial system, which is also called the mononuclear phagocytic system.[6–8] This may decrease the injected dose by as much as 50% within a few hours.[9] Thus, for medical applications, it is often desired to synthesize NPs that are rather repellent to plasma protein interaction. Polyethylene glycol as a surface modifier for example was shown to enhance blood circulation and half-life of superparamagnetic iron oxide nanoparticles in vivo in mice fivefold.[10] On the other hand, in order to achieve site-specific targeting of a drug specific interactions of a NP with selected serum proteins may be desired. One example is poly(n-butyl-2-cyanoacrylate) NP, which upon coating with polysorbate 80 was able to mediate transport across the blood brain barrier in vivo.[11–13] This was shown to be dependent on recruiting apolipoprotein E from blood plasma onto the NP surface.[14,15] Thus, in nanomedicine, it is necessary to understand the behavior of NPs in physiological environments and to analyze the NP protein corona. The protein corona formation depends on several physicochemical properties of NPs such as size, shape, surface charge, or hydrophobicity and can influence cellular uptake in vitro.[16–23] Therefore, the protein corona can also influence NP functionality and their biological effects.[24,25] For example, transferrin coating was shown to enhance the endocytosis of lipid-coated NPs in A549 cells in vitro and furthermore to have the best inhibitory effect on tumor growth in vivo compared to the other used NPs.[26]

Within this study, we focused on dendritic polyglycerols (dPGs), which are interesting carrier systems for medical applications. They are highly biocompatible and can be synthesized with different functionalities on their surface offering a high variability and allowing modulation of the binding affinity.[27–29] Sulfated dendritic polyglycerol (dPGS) has been shown to possess anti-inflammatory properties in vivo and in vitro with the relevant cellular targets being L- and P-selectins.[28,30,31] The aim of this study was to investigate the influence of size and charge of dPGs on the interactions with serum proteins and to study the influence of the protein corona on cellular uptake in human CD14+ monocytes by flow cytometry. Furthermore, this study aimed to elucidate

cellular interaction partners being possibly involved in cellular uptake by using a pull-down approach with purified cell membrane proteins of THP-1 cells and to get first insights into the uptake mechanisms.

Materials and methods
Synthesis of the NPs
The synthesis of the native citrate-functionalized gold NPs as well as their functionalization with TA (thioctic acid)-dPGS-10 kDa and TA-PGOH-10 kDa is described in detail elsewhere.[32] Briefly, native citrate-functionalized gold NPs were synthesized by the reduction of tetrachloroauric acid at elevated temperatures in an aqueous solution.[33] Larger-sized gold NPs (50 nm) were obtained by a seed-mediated growth procedure according to a protocol established by Ziegler and Eychmüller.[34] The functionalization of the gold NPs with TA-PGOH-10 kDa and TA-dPGS-10 kDa, respectively, was performed according to an own established salt aging procedure to maximize the ligand packing on the NPs.[32] Briefly, the citrate-stabilized gold NPs were incubated with TA-dPGS-10 kDa and TA-PGOH-10 kDa, respectively, under rapid stirring. After 30 min, the ionic strength of the solution was increased from 0 to 1.5 M over 30 min by the drop-wise addition of a NaCl (5 M) stem solution. The particles were incubated for 1 h under rapid stirring with 2 s sonification every 20 min. For purification, the colloidal dispersion was purified 6 times by centrifugation (15,000× g, 20 min, room temperature [RT]) for the removal of the supernatant and redispersion of the pellet in water. The concentration of gold NPs in the solutions was calculated by the ratio of the mass concentration of gold in the colloidal solution as determined by atomic adsorption spectroscopy and the mass of one gold NP as calculated by the diameter obtained from dynamic light scattering (DLS) and the assumption of a perfect sphere.[32,35]

The syntheses of rhodamine B-labeled dendritic polyglycerol (dPGOH-RB) and rhodamine B-labeled dendritic polyglycerol sulfate (dPGS-RB) are explained and depicted schematically in Figures S1 and S2, complete details are described elsewhere.[36]

Characterization of the NPs
Transmission electron microscopy (TEM)
Droplets of the corresponding sample solutions (5 µL) were placed for 30 s on hydrophilized (60 s plasma treatment at 8 W using a BAL-TEC MED020 device [Leica Microsystems, Wetzlar, Germany]) carbon-coated copper grid. Excess fluid was removed with a filter paper, and the samples were analyzed in a CM-12 by FEITM with an accelerating voltage of 60 kV.

DLS and zeta potential measurement

NPs were diluted 1:200 either in ultra-pure water (Milli-Q [MQ] reference ultrapure water purification system; Merck Millipore, Darmstadt, Germany), phosphate-buffered saline (PBS; PAN Biotech GmbH, Aidenbach, Germany) or Dulbecco's Modified Eagle's Medium (DMEM, without phenol red and L-glutamine; PAN Biotech GmbH) containing 10% non-heat-inactivated fetal bovine serum (FBS gold, PAA Laboratories GmbH, Cölbe, Germany). The NPs (dPGOH-Au50 with a final concentration of 24.6 µg/mL, dPGS-Au50 with 20 µg/mL, and dPGS-Au20 with 10.08 µg/mL) were dispersed at RT under constant stirring (700 rounds per minute, rpm) with a magnetic stirring device (HMC Cyclone; HMC Europe, Tüssling, Germany). These concentrations are in line with the ones used for studying cellular uptake. After 120 min, samples were taken and measured using a Zetasizer Nano ZS (Malvern Instruments GmbH, Herrenberg, Germany) equipped with a red laser (He-Ne-Laser 633 nm, maximum 4 mW). Pre-equilibration time for the samples of 60 s was used before the measurement (5 runs with 10 measurement points [equals n=50] for each sample) at 25°C. The attenuator and voltage calibration were selected automatically during the automatic measurements.

In order to measure zeta potential, NP dispersions were measured at 1 mg/mL in 10 mM NaCl dissolved in ddH_2O (Merck Millipore) at 25°C using Zetasizer Nano ZS. A pre-equilibration time of 2 min was also used, attenuator and voltage were selected automatically, and three runs of 30 measurements were used.

Nanoparticle tracking analysis (NTA)

The NanoSight LM20 system (638 nm visible radiation, maximum output 40 mW, Malvern Instruments GmbH) was used for NTA. Sizes were calculated from videos (60 s, 30 frames per second, camera gain =1, and background extract on) by the NTA software (Version 2.3 Build 0033). Particles were diluted using filtrated MQ water (filtered through a 0.2 µm filter) to final concentrations of dPGOH-Au50 2.46 µg/mL, dPGS-Au50 2 µg/mL, and dPGS-Au20 1.008 µg/mL and measured at 25°C.

Dispersion of the NPs for protein corona analysis

For analysis of the protein corona, the concentrations of all NPs (dPGS-Au20, dPGS-Au50, and dPGOH-Au50) were adjusted such that protein to surface ratio was kept constant (total available NP surface was adjusted to approximately 66 cm^2. Ratio was kept at approximately 300 microgram protein/cm^2.). The total available surface for protein binding

was calculated by assuming a perfect spherical shape. NPs were dispersed in DMEM containing 10% FBS gold in a total volume of 5 mL in sterile glass vials containing magnetic stir bar by stirring (700 rpm for 2 h at RT) with a magnetic stirring device (HMC Cyclone; HMC Europe).

Protein elution and analysis of protein content in eluate

For the separation of the NPs with adsorbed corona from unbound proteins, the NP dispersions (5 mL) were loaded on top of 2 M sucrose (4.5 mL), and the NPs were pelleted through ultracentrifugation (17,900× g, 2.5 h at RT). DMEM with 10% FBS gold without NPs served as control and was treated similarly. Proteins in the NP pellets were eluted in 500 µL two dimensional (2D) lysis buffer containing 7 M urea, 2 M thiourea, 4% chaps, 2% pharmalyte pH 4–7, 1% dithiothreitol (DTT), and protease inhibitors for 2DE analysis while rotating for 1 h at RT. Samples for 2DE analysis were centrifuged (40,000× g for 1 h at 15°C) and total protein content was measured using the 2D Quant kit (GE Healthcare, Berlin, Germany) according to manufacturer's instructions.

2D-Polyacrylamide gel electrophoresis (PAGE) analysis of the protein corona

For the isoelectric focusing (IEF), samples (500 µL) were loaded on nonlinear IPG strips (24 cm Immobiline™ DrySrip pH 4–7 [NL]; GE Healthcare) and equilibrated in equilibration buffer EB1 containing 360 mg/mL urea (Carl Roth GmbH, Karlsruhe, Germany), 24 mg/mL sodium dodecyl sulfate (SDS; Carl Roth GmbH) and 50.4 mM/mL tris(hydroxymethyl)aminomethane-hydrogen chloride (Tris-HCl), pH 8.6 (Carl Roth GmbH) for 1 h. Active rehydration and focusing were performed (15 h at 30 V, 1.5 h at 200 V, 1 h at 500 V, 13.5 h gradient 500–1,000 V, 3 h gradient 1,000–8,000 V, and 6 h at 8,000 V) with the GE Ettan IPGphor 3 (GE Healthcare). After the IEF proteins were first reduced using DTT (1% DTT in EB1; Carl Roth GmbH) and then alkylated using iodacetamide (4% IAA in EB1; SERVA, Heidelberg, Germany) 15 min each. For the second dimension, strips were transferred onto 12.5% SDS-polyacrylamide gels. Electrophoresis was carried out with the GE Ettan DALTtwelve System Seperation Unit (GE Healthcare). Later, the gels were fixed using 30% ethanol (Sigma-Aldrich, Munich, Germany) and 10% acetic acid (Carl Roth GmbH) in water and thereafter stained with ruthenium II tris (bathophenanthroline disulfate) chelate (0.4 µM RU-II and 20% ET in MQ).[37] After scanning of the gels with the FLA 9,500 (GE Healthcare, excitation λ=473 nm and detection at λ=610 nm), they were analyzed with Delta2D

version 4.4 (Decodon, Greifswald, Germany). Each sample was analyzed in three independent replicates. Spots with an increased intensity compared with control gels without NPs (>1.5 fold increase, n=3, $p<0.05$) were further analyzed by mass spectrometry to identify the respective proteins.

Matrix-assisted laser desorption ionization (MALDI)-time of flight (TOF)/TOF

Spots of interest were excised using a spot picker (Proteome Factory, Berlin, Germany), destained in 200 mM ammonium bicarbonate (ABC; Sigma-Aldrich) containing 50% acetonitrile (ACN; Sigma-Aldrich) and digested overnight with trypsin using a standard protocol (50 mM ABC and 5% ACN, 1.2 ng/µL trypsin). Peptides were extracted from the gel piece with 60% ACN and then with 100% ACN. Collected and combined supernatants were dried using a speedvac. Dry peptide pellets were resuspended in 0.1% TFA and purified using a C18 ZipTip (Merck Millipore). Samples were spotted with an α-cyano-4-hydroxy-cinnamic acid (HCCA; Sigma-Aldrich) matrix on AnchorChip targets (383/800; Bruker, Bremen, Germany) and measured using a UltrafleXtreme MALDI-TOF/TOF (Bruker) device equipped with FlexControl (version 3.3) and FlexAnalysis (version 3.3) software packages. For analysis, ProteinScape (version 4.0) and MASCOT (version 2.3.02) were used based on search in Swissprot database (MS tolerance 50 ppm, MS/MS tolerance 0.8 Da, Carbamidomethyl [Cys] and Oxidation [Met] as variable modifications, 1 partial cleavage).

Cell culture THP-1 cells

The human monocytic cell line THP-1 was obtained from DSMZ (German Collection of Microorganisms and Cell Cultures, Germany) and was cultivated in RPMI-1640 complete medium containing 10% FBS, 2 mM L-glutamine, 100 mM 4-(2-hydroxyethyl)piperazine-1-ethanesulfonic acid, 100 units/mL penicillin, 0.1 mg/mL streptomycin in an incubator (37°C, 5% CO_2). Cell culture medium, FBS, and additives were obtained from PAN Biotech GmbH. Cell viability and quantity were determined through a cell counter Casy TTC (Roche Diagnostics GmbH, Mannheim, Germany).

Isolation of the CD14+ cells through CD14 MicroBeads

Primary human CD14+ monocytes were isolated from blood samples (buffy coats) obtained from Deutsche Rote Kreuz (Berlin, Germany). Samples were diluted with PBS, layered on Ficoll-Paque™ Plus (GE Healthcare) solution and centrifuged ($400\times g$ for 35 min at RT) to obtain peripheral

blood mononuclear cells (PBMCs). PBMCs were washed with PBS and finally dispersed in auto MACS™ Running buffer (Miltenyi Biotec GmbH, Bergisch Gladbach, Germany) (40 µL per 10^7 cells). CD14+ MicroBeads (Miltenyi Biotec GmbH) were added (10 µL per 10^7 cells). After 15 min of incubation, CD14+ cells were separated using positive selective LS columns (Miltenyi Biotec GmbH). Figure S3 depicts quality control through flow cytometry before and after CD14 MicroBeads purification. For analysis 1×10^5 cells (PBMC or CD14+ monocytes) were washed (300 g, 5 min) with buffer (PBS, 1% FBS and 2 mM ethylenediaminetetraacetate [EDTA]) and stained in 50 µL buffer with a-CD14-PE (TÜK4) as a marker for CD14+ monocytes, with a-DC-Sign-APC (DCN47.5) as a marker for dendritic cells and with a-CD86-Fitc (FM95) as an activation marker (all 1:50; Miltenyi Biotec GmbH) for 30 min at 4°C. After washing, the samples were measured using the BD FACSAria III with Diva 6.0 software (BD Biosciences, Heidelberg, Germany).

Investigation of the uptake of NPs through flow cytometry

CD14+ cells (10^5 cells per well in 1 mL RPMI-1640 medium containing 10% FBS) were seeded in 12-well plates (TPP, Trasadingen, Switzerland). After 24 h, the medium was replaced with either RPMI-1640 medium containing 10% FBS or cell culture RPMI-1640 medium containing 3 mg/mL bovine serum albumin (BSA) or RPMI-1640 medium without any proteins. Rhodamine B-labeled dPG NPs were diluted in the respective cell culture medium (final concentration dPGOH-RB 50 µg/mL and dPGS-RB 20 µg/mL) and pre-incubated for 1 h (at 37°C) such that a protein corona can form. Cell culture medium from the monocytes was then replaced with the respective cell culture medium containing the NPs and incubated for 1 or 6 h, respectively. Later, the cells were rinsed with PBS and detached using trypsin (PAN Biotech GmbH), washed again using PBS and fixed using 100 µL 1× CellFix solution (BD Biosciences). Uptake was analyzed using an FACS Aria III (BD Biosciences), equipped with a blue laser (488 nm) and fluorescence detector (585/42 nm) using a 70 µm nozzle.

Purification of cell membrane protein fraction
Biotinylation of the THP-1 cells
Prior to the treatment with sulfosuccinimidyl-2-(biotinamido) ethyl-1,3-dithiopropionate (Biotin; Antibodies-online GmbH, Aachen, Germany), THP-1 cells were washed three times with PBS (500 g for 10 min, 4°C). After incubation with Biotin for 10 min at RT (0.05 mg/mL biotin diluted in PBS

per 5×10^6 THP-1 cells) Tris-HCl (pH 7.5 with 50 mM) was added followed by incubation for another 10 min at RT. Thereafter cells were washed with PBS five times (4°C at 500 g for 10 min) and lyzed by 30 min incubation on ice in modified RIPA buffer (0.05 M Tris-HCl [pH 7.4], 0.15 M NaCl, 0.001% EDTA, 1% Igepal CA-630, 0.25% sodiumdeoxycholate) followed by centrifugation (14,000× g for 20 min at 4°C). All chemicals were obtained from Sigma-Aldrich. Total protein content was determined in supernatants using a Bradford assay (BioRad, Munich, Germany) according to the manufacturer's protocol.

Purification of the biotinylated membrane proteins through avidin-agarose beads

Biotinylated proteins were isolated using avidin-agarose beads (15 µL of a 50% w/w slurry per 25 mg lysate), which were incubated with the cell lysates (three runs, each 15 min incubation). After binding, beads were washed with PBS (five times) and proteins eluted by adding DTT (100 mM in PBS, 1 h at RT). Concentration of the eluate was determined by Bradford assay according to manufacturer instructions. In total, 615 µg of protein was obtained using this protocol from 250×10^6 cells.

Pull-down experiment with dPG NPs

The NPs dPGS-Au50 and dPGOH-Au50 (final concentrations 100 µg/mL) were washed with PBS three times and incubated for 2 h at RT with the relevant medium (RPMI-1640 medium ±10% FBS), later washed again with PBS three times. Then, NPs with or without serum pre-treatment were incubated (2 h at RT) with the purified membrane protein fraction (115 µg total protein per 100 µg NP) and later washed with PBS three times and pelleted by centrifugation. Proteins from NP pellets were eluted using Laemmli buffer (0.25 M Tris-HCL pH 6.8, 4% SDS, 20% glycerol [Sigma-Aldrich] with 10% ß-mercaptoethanol [Merck Millipore]) at 95°C for 10 min. Eluted proteins were separated through 10% SDS-PAGE and stained with Coomassie brilliant blue R 250 (AppliChem GmbH, Darmstadt, Germany). Each lane was cut into 10 bands, proteins were digested, peptides were eluted, dried, and redissolved in ACN/0.1% TFA (ratio 7:3). Peptides were then analyzed by nano high performance liquid chromatography (nanoHPLC) coupled offline with MALDI-MS/MS.

Analysis of pulled down proteins through nanoHPLC-MALDI-MS/MS

For the chromatographic separation of the samples, a reversed-phase HPLC UltiMate3000 (Thermo Scientific) with gradient elution was used. The nonpolar stationary phase (Acclaim® PepMap RSLC, 75 µm ×50 cm nano Viber, C18, 2 µm, 100 Å) consists of C18-modified silica. Equilibration was done with solvent A (0.1% TFA) for 5 min, and the separation of the samples was done by increasing the concentration of the nonpolar solvent B (0.08% TFA/80% TFA, reaching following concentrations at the given time points: 1 min 20%, 11 min 25%, 95 min 50%, 105 min 80%, and after 115 min 95% concentration of solvent B). Ultraviolet spectrum was measured at 214 nm. Eluates from nanoHPLC were automatically spotted with matrix solution (HCCA) at a target (AnchorChip 1536 TF, Bruker) and measured through an UltrafleXtreme MALDI-TOF/TOF (Bruker).

Investigation of possible uptake pathways of dPGS-RB in THP-1 cells

THP-1 cells were seeded in 96-well plates (TPP) at 75,000 cells per well in 100 µL cell culture medium (CCM, RPMI-1640 medium containing 10% FBS) 24 h before treatment. To investigate energy-dependent uptake, cells were then either transferred to 4°C or were kept at 37°C (control) for the rest of the treatment. After 4 h at the respective temperature conditions, 20 µg/mL of pre-incubated dPGS-RB NPs (2 h in CCM, RT) were added for another 2 or 4 h. To investigate endocytosis, cell culture medium was replaced with serum-free RPMI-1640 medium (control) or serum-free RPMI-1640 medium containing 5 or 10 µg/mL chlorpromazine (CP) to investigate clathrin-mediated endocytosis (Sigma-Aldrich) or 200 µM genistein (Sigma-Aldrich) and incubated for 2 h. Then, 20 µg/mL of pre-incubated dPGS-RB NPs (in CCM) were added for another 2 h. Thereafter in both cases, cells were washed twice with ice cold PBS (300× g, 5 min). Life/Dead Fixable Near-IR Dead cell Stain Kit (Thermo-Fisher Scientific, Darmstadt, Germany) diluted 1:1,000 in ice cold PBS was added for 30 min (constant shaking, 4°C). Samples were washed twice with PBS (300× g, 5 min) and fixed (2 h, 4°C) using 100 µL 1× CellFix solution (BD Biosciences). Uptake was analyzed using a FACS Aria III (BD Biosciences), equipped with a blue laser (488 nm) and fluorescence detector (585/42 nm) using a 70 µm nozzle.

Results
Characterization of the NPs

This study used gold NPs functionalized with either sulfated or non-sulfated dPGs with a molecular weight of 10 kDa, dPGS-10 kDa or dPGOH-10 kDa, respectively. Figure 1 schematically depicts the chemical structures of dPGS-10 kDa and dPGOH-10 kDa as well as the NPs used in this study.

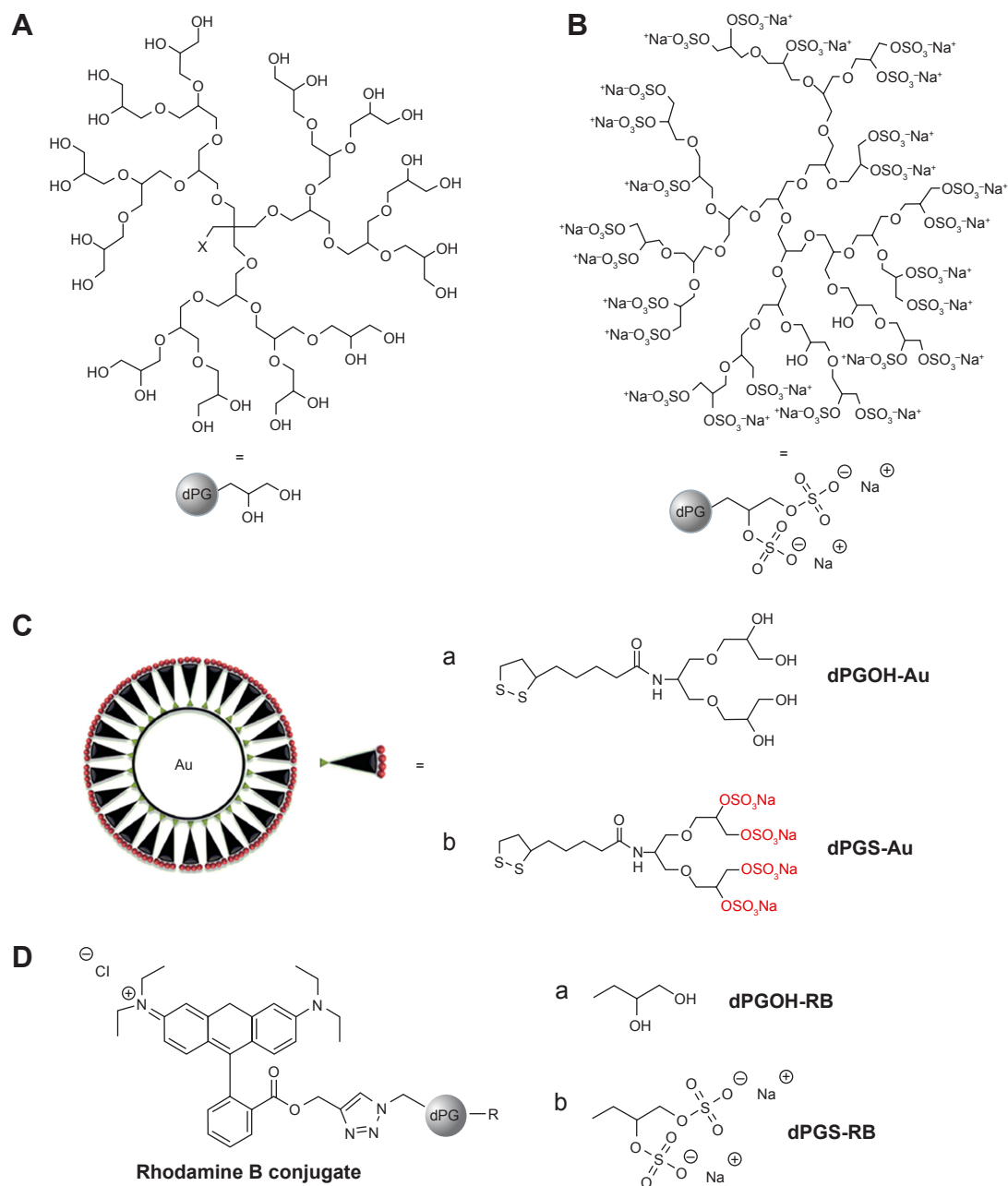Both, dPGS-10 kDa and dPGOH-10 kDa were functionalized with ~1 TA anchor moiety, resulting in TA-dPGS-10 kDa

Figure 1 Schematic structures of the dPGs.

Notes: The structures of dPGOH-10 kDa (**A**), dPGS-10 kDa (**B**), (a) TA-dPGOH-10 kDa, which was then attached to the Au surface; (b) TA-dPGS- 10 kDa, was was then attached to the Au surface (**C**), and the rhodamine-B-labeled NPs, dPGOH-RB and dPGS-RB (**D**) are depicted. The surface of the gold NPs (**C**) can be coated by using thioctic acid functionalized with either sulfated or non-sulfated PG. Depicted is the first generation non sulfated PG-dendron (**C**a), which would result in dPGOH-Au NPs and the first generation sulfated PG-dendron (**C**b), which would result in dPGS-Au NPs. The moieties of the Rhodamine-B-labeled dPGs (**D**) are either non-sulfated dPGs forming the dPGOH-RB NPs (**D**a) or sulfated dPGs resulting in the dPGS-RB NPs (**D**b).

Abbreviations: dPG, dendritic polyglycerol; NP, nanoparticle.

and TA-dPGOH-10 kDa, respectively, to permit the binding to the gold NP surface through stable sulfur–gold linkage.[38] The dPGOH- and dPGS-coated gold NPs (dPGS-Au and dPGOH-Au) were synthesized by ligand exchange from citrate-coated gold NPs according to a previously established salt-aging procedure, which permits a maximization of the ligand density on the NPs.[32] This leads to a slight increase in NP radii compared with the original citrate-coated gold NPs

(Figure 2). The dPGS-Au was synthesized in two different sizes, using 20 and 50 nm gold cores, herein referred to as dPGS-Au20 and dPGS-Au50, respectively. In the case of dPGOH-Au, a 50 nm gold core was used for the synthesis, resulting in dPGOH-Au50. NPs were fully characterized with respect to size and size distribution using TEM, DLS, and NTA. The DLS and NTA results are summarized in Table 1, and TEM images and DLS data are depicted in Figure 2.
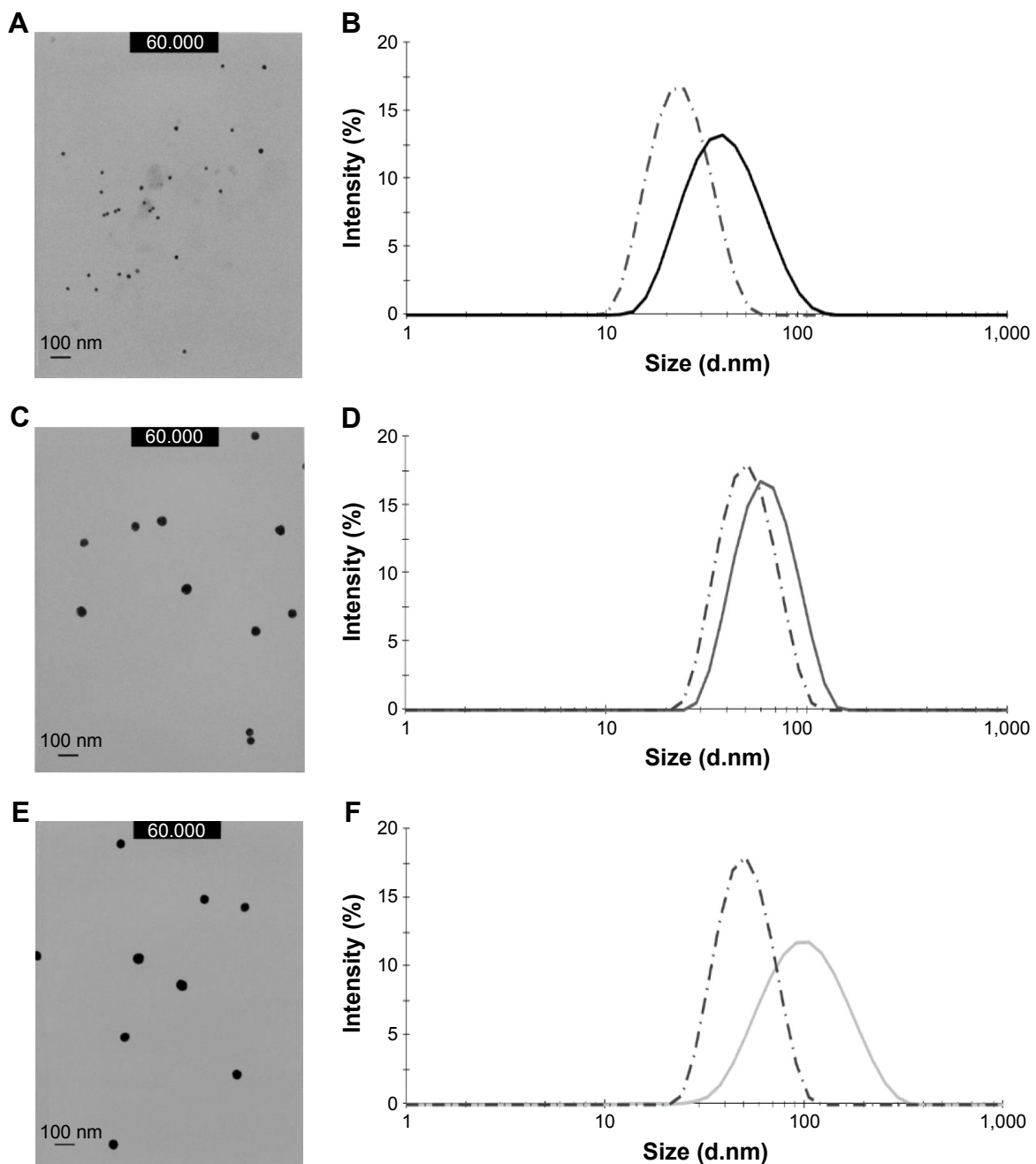
Figure 2 NP characterization by TEM and DLS.
Notes: TEM images of the dendrimer-coated NPs are depicted on the left panel and DLS data of the native gold citrate NPs (scattered lines) and dendrimer coated gold NPs (solid lines) on the right panel, with dPGS-Au20 (**A** and **B**), dPGS-Au50 (**C** and **D**), and dPGOH-Au50 (**E** and **F**). 60.000= 60 sec plasma treatment at 8 W using a BAL-TEC MED020 device.
Abbreviations: NP, nanoparticle; TEM, transmission election microscopy; DLS, dynamic light scattering.

NPs were dispersed in different biological dispersion media, that is, PBS or complete CCM, consisting of DMEM supplemented with 10% FBS. NPs seem to be stably dispersed in PBS and CCM over the time course of the experiment, that is, for up to 2 h. However, a shift in NP hydrodynamic radii was observed over time in the protein containing CCM dispersion medium compared with PBS, in particular for the dPGS-Au NPs. This may indicate the

formation of a protein corona (Table 1). For dPGS-Au50, the increase in hydrodynamic radius in CCM accounts for 25 nm, which is consistent with the reported changes that occurred because of the formation of a protein corona of ~50 nm NPs as reviewed in Walkey and Chan.[39] In addition, the zeta potential in 10 mM NaCl in MQ water was also determined for dPGS (−25.7 mV) and dPGOH (+12.1 mV) particles. For studying cellular uptake, rhodamine-labeled

Table 1 NP characterization of dPGS-Au and dPGOH-Au by DLS and NTA

NP	DLS					NTA		
	Incubation (min)	Medium	Z-average (d, nm)	SD (nm)	PDI	Average size (d, nm)	Mode (nm)	SD (nm)
dPGS-Au20	120	PBS	36	0.76	0.35	45	38	20
		MQ	40	5.53	0.26			
		CCM	48	6.27	0.47			
dPGS-Au50	120	PBS	51	0.33	0.11	56	51	18
		MQ	53	0.32	0.13			
		CCM	76	9.78	0.89			
dPGOH-Au50	120	PBS	52	0.53	0.11	85	65	30
		MQ	54	0.36	0.14			
		CCM	60	4.44	0.39			

Notes: NPs were dispersed in water, PBS or CCM, respectively. Analysis by DLS was performed after 120 min. NTA was performed in water only with freshly dispersed NPs.
Abbreviations: NP, nanoparticle; MQ, Milli-Q; DLS, dynamic light scattering; NTA, nanoparticle tracking analysis; PBS, phosphate-buffered saline; CCM, complete cell culture medium (DMEM containing 10% FBS); FBS, fetal bovine serum; SD, standard deviation; PDI, polydispersity index.

dPGS-RB and dPGOH-RB were used, which were also fully characterized (Table S1).

NP protein corona

The NPs were incubated in CCM for 2 h such that they could form a stable protein corona. As of course the total amount of bound protein would depend on available NP surface, the NP concentrations for this experiment were adjusted such that similar ratios of total protein to NP surface were obtained.

A detailed analysis of protein coronas was performed using 2D gel electrophoresis (2DE) in combination with MALDI-TOF/TOF. 2DE analysis revealed qualitative and quantitative differences between the coronas of all NPs. Each NP displayed an individual spot pattern. It becomes obvious that dPGOH surface binds considerable less protein compared with dPGS surfaces (Figure 3). Significant quantitative and qualitative differences were observed in protein coronas for the different surface functionalized NPs, that is, dPGOH-Au50 versus dPGS-Au50, whereas the differences for the two sizes of dPGS, that is, dPGS-Au20 versus dPGS-Au50, appeared marginal only (Figure S4).

In order to identify relevant proteins, spot patterns of all gels were analyzed and compared with control gels. Protein spots with significantly increased intensity compared with controls (ie, intensity increased >1.5, $p<0.05$, n=3) were excised and analyzed by MALDI-TOF/TOF (Figure S5).

Clearly, dPGS surfaces bind more proteins compared with dPGOH (ie, compare dPGS-Au50 versus dPGOH-Au50, Figure 3). The corona of dPGOH-Au50 consisted only of 36 protein spots, whereas 169 were detected on dPGS-Au50 and 114 on dPGS-Au20. Similarities and differences in the protein coronas are visualized in a Venn diagram based on the spot numbers (Figure 3C). Comparing the proteins in the different coronas as identified by mass spectroscopy, it was found that most proteins detected on dPGOH-Au50 were also found on dPGS-Au50 (for instance complement factor H and serum albumin). However, several of them such as for instance serotransferrin and vitronectin (VN) were unique for the dPGS NP coronas (Table 2).

Influence of the protein corona on cellular uptake

Next, the study aimed to analyze whether the differences in protein binding would correlate with differences in cellular uptake. For this analysis, we used rhodamine B-labeled dPGS and dPGOH NPs without a gold core, herein referred to as dPGS-RB and dPGOH-RB (refer to Figures S1 and S2 for a summary of their syntheses and to Table S1 for their physico-chemical characterization). The fluorescence label allowed for easy quantification of cellular uptake using flow cytometry. NPs were pre-incubated for 2 h in different biological media. DMEM cell culture medium was used without serum (ie, no proteins were present), CCM with serum such that a complete protein corona can form or cell culture medium containing BSA only, which was considered a rather unspecific binder with moderate affinity.

Figure 4 shows that dPGS-RB was taken up much more efficiently by primary human monocytes compared with dPGOH-RB, regardless of the kind of pre-incubation. Using confocal laser scanning microscopy, it could be confirmed that dPGS-RB NPs (Figure S6) and also dPGOH-RB NPs (Figure S7) were taken up into monocytes. However, amounts of dPGOH-RB taken up seemed to be very low.

Comparing different conditions of pre-incubation for dPGS, it was found that without any protein pre-incubation, dPGS was taken up most efficiently (Figures 4 and S6). Thus, clearly the presence or absence of a protein corona influences the cellular uptake of dPGS. In addition, the
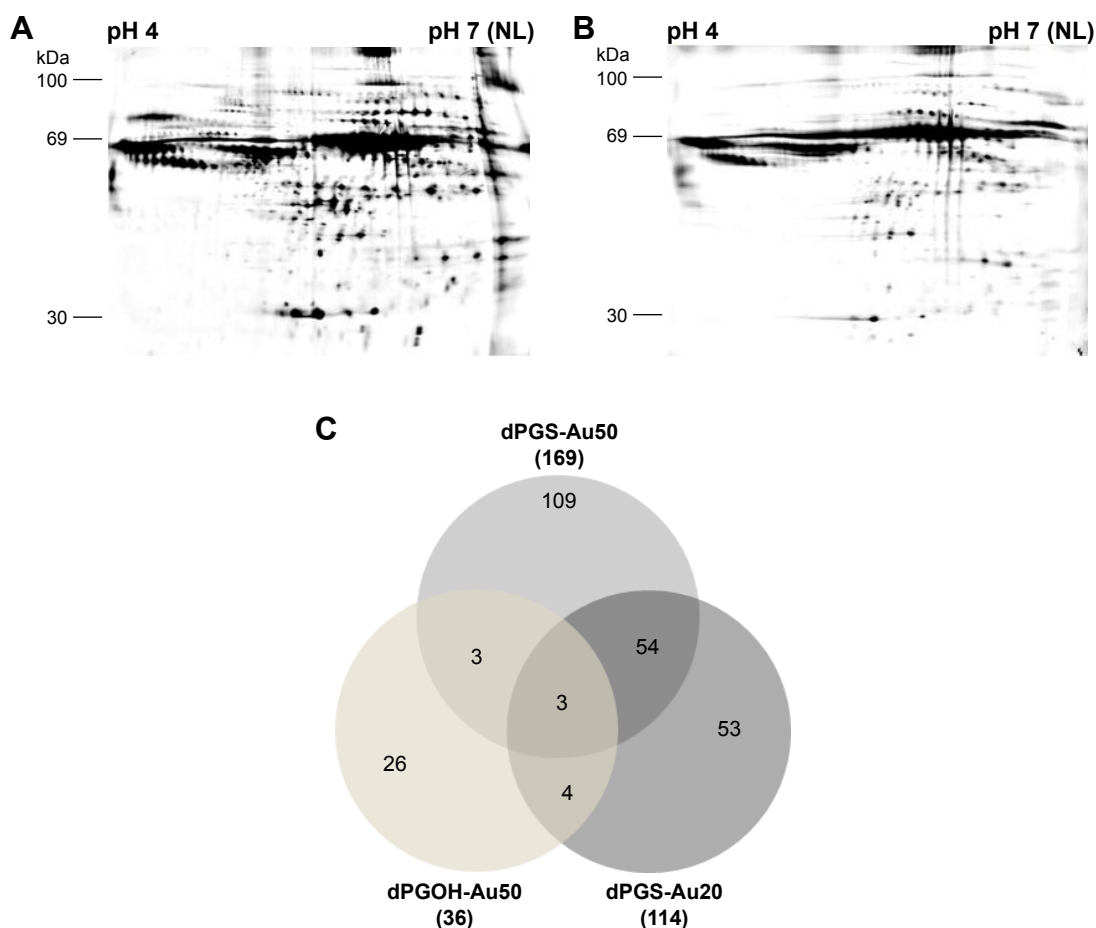
Figure 3 Analysis of the protein corona by 2DE.
Notes: 2D gels of dPGS-Au50 (**A**) and dPGOH-Au50 (**B**) are depicted. A Venn diagram was used to compare the corona composition of the different NPs based on the number of protein spots in their coronas as obtained from 2DE analysis (**C**). The total number of significant protein spots within the gels compared with controls is given within parentheses.
Abbreviation: 2DE, two-dimensional gel electrophoresis.

composition of the corona seems to affect cellular uptake as well (compare uptake in the presence of BSA alone, which is a rather unspecific binder compared to uptake in the presence of complete serum).

Identification of putative cellular interaction partners

This prompted us to further analyze the interactions between protein-coated NPs and cellular surfaces in more detail. For this purpose, the cell membrane proteins of THP-1 cells were purified after biotinylation by affinity chromatography. Purified membrane fraction was used in pull-down experiments with dPGS-Au50 (Figure 5A) and dPGOH-Au50 as control (Figure 5B), both of which have been pre-incubated in CCM. Later, pulled down proteins were identified using a nanoHPLC-MALDI-TOF/TOF approach.

A total of 138 proteins could be identified in the pull-down experiment with CCM-pre-incubated dPGS-Au50,

out of which 22 were membrane or membrane-associated proteins. A few selected identified membrane proteins, that is, those for which possible protein interaction partners may be suggested from the identified proteins in the protein corona of dPGS, are listed in Table 3, and all of them are listed in Table S2. In particular, transferrin receptor protein 1 and the integrin βII might be involved in cellular recognition of the dPGS.

Investigation of possible uptake pathways

In the pull-down experiment, the transferrin receptor was identified as a possible cellular interaction partner, which indicates that clathrin-mediated endocytosis is involved in the cellular uptake of dPGS as the transferrin receptor is internalized through this pathway.[40] To further look into this, this study first aimed to analyze whether the uptake process is energy dependent, which may be expected for endocytotic processes and then whether it may be inhibited by CP, which

Table 2 Identified proteins of the protein coronas of all NPs

Protein	Accession	MW (kDa)	PI	MS	UP	dPGOH-Au50	dPGS-Au50	dPGS-Au20
Actin, cytoplasmatic 1	ACTB_BOVIN	41.7	5.48	945	3	–	+	+
Alpha-1-antiproteinase	A1AT_BOVIN	46.1	6.1	109.5	2	+	+	–
Alpha-1B-glycoprotein	A1BG_BOVIN	53.5	5.3	419	8	+	+	–
Alpha-2-HS-glycoprotein	FETUA_BOVIN	38.4	5.3	84.8	2	+	–	–
Alpha-fetoprotein	FETA_BOVIN	68.5	5.9	170.2	4	–	–	+
Apolipoprotein A-I	APOA1_BOVIN	30.3	5.7	345.3	9	+	+	+
C4b-binding protein alpha chain	C4BPA_BOVIN	68.9	6.38	424	8	–	+	+
Coagulation factor XII	FA12_BOVIN	67.2	7.9	115	2	–	+	–
Collagen alpha-1(I) chain	CO1A1_BOVIN	138.9	5.78	124.6	2	+	+	+
Complement C3	CO3_BOVIN	187.1	6.4	173.7	4	–	+	+
Complement component C9	CO9_BOVIN	62	5.7	130	3	+	+	+
Complement factor B	CFAB_BOVIN	85.3	7.9	128.9	2	+	+	+
Complement factor H	CFAH_BOVIN	140.4	6.8	164	5	+	+	+
Factor XIIa inhibitor	F12AI_BOVIN	51.7	6.2	289	6	–	+	+
Gelsolin	GELS_BOVIN	80.7	5.5	156.6	3	–	+	+
Inter-alpha-trypsin inhibitor	ITIH1_BOVIN	101.2	7.2	349	10	–	+	+
Pigment epithelium-derived factor	PEDF_BOVIN	46.2	6.6	493.3	10	+	+	+
Plasma serine protease inhibitor	IPSP_BOVIN	45.3	9.36	141.2	4	–	–	+
Serotransferrin	TRFE_BOVIN	77.7	6.8	295.9	6	–	+	+
Serum albumin	ALBU_BOVIN	69.2	5.8	1,782.6	32	+	+	+
Tetranectin	TETN_BOVIN	22.1	5.5	238	3	+	+	+
Vitamin D binding protein	VTDB_BOVIN	53.3	5.52	184	4	+	+	–
Vitronectin	VTNC_PIG	53.3	5.6	81	1	–	+	+

Note: The labels "+" and "−" indicate whether the respective protein was present in the corona of the given nanoparticle.
Abbreviations: NP, nanoparticle; MW, molecule weight; PI, isoelectric point; MS, MASCOT score; UP, unique peptides.
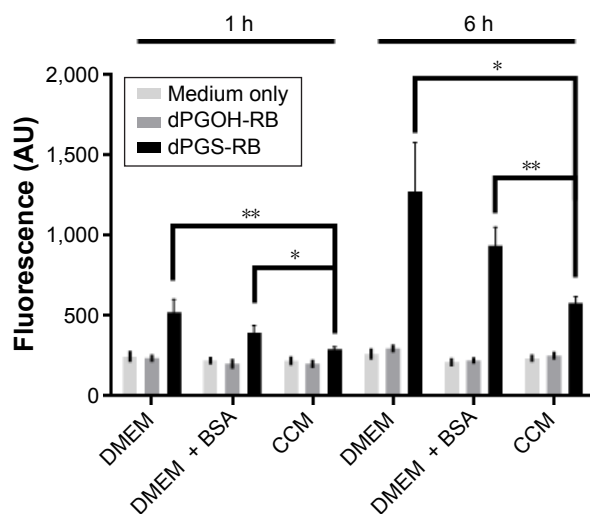

Figure 4 Uptake of dPGS-RB and dPGOH-RB in primary human monocytes analyzed by flow cytometry.
Notes: NPs were pre-incubated for 2 h with DMEM only, with DMEM containing BSA or with DMEM containing 10% FBS (CCM). Later, the NPs were incubated with monocytes for 1 or 6 h. Mean fluorescence values including SEM (n=8–10 biological repeats) as bars (with significance: **$P<0.01$ and *$P<0.05$) are depicted.
Abbreviations: DMEM, Dulbecco's Modified Eagle's Medium; BSA, bovine serum albumin; CCM, complete cell culture medium; FBS, fetal bovine serum; NP, nanoparticle; SEM, standard error of the mean.

is a known inhibitor for clathrin-mediated endocytosis.[41] When transferring the cells to 4°C and thereby blocking energy-dependent uptake processes, it could be shown that the uptake of dPGS-RB NPs is indeed significantly decreased, that is, ~79% after 2 h and ~66% after 4 h (Figure 6A). When pretreating THP-1 cells for 2 h with CP, the uptake was decreased by ~25% after 2 h using 5 µg/mL and by ~50% using 10 µg/mL (Figure 6B). Caveolin-mediated endocytosis was also considered, and cellular uptake could be blocked by ~20% after 2 h and by ~30% after 4 h incubation with genistein (Figure 6C). Therefore, it is concluded that clathrin-mediated endocytosis seems to be the major uptake pathway for dPGS particles. However, other pathways, in particular caveolin-mediated endocytosis also contribute but to a lesser extent. Also energy-independent processes seem to exist and can also contribute to cellular uptake of dPGS.

Discussion

The aim of this study was to investigate the influence of size and surface chemistry for dPGs on interactions with
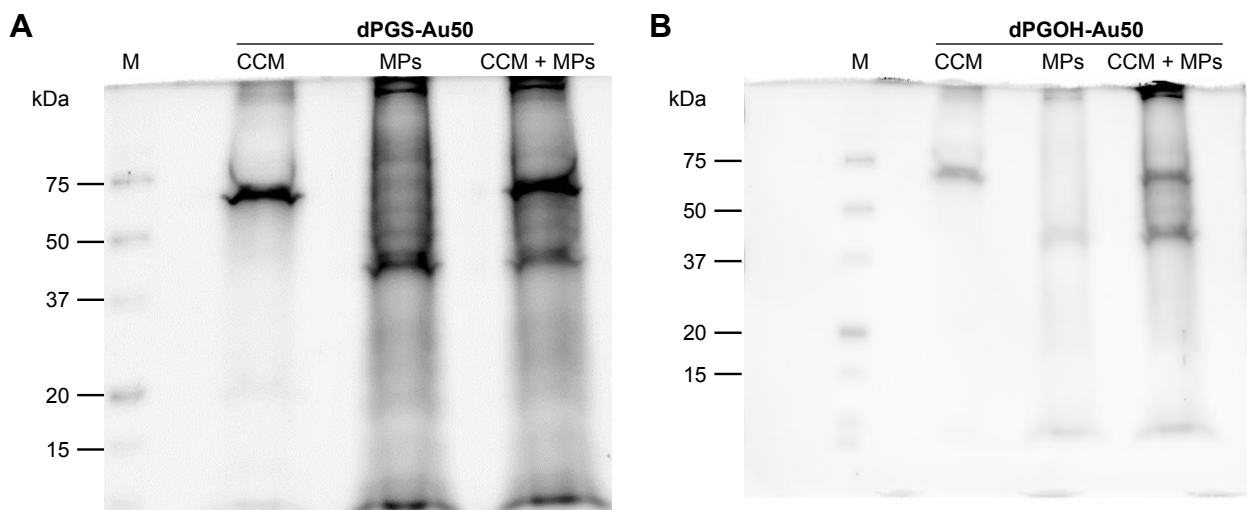
Figure 5 Pull-down experiment of serum pre-incubated dPGS-Au50 or dPGOH-Au50 with purified membrane fractions.
Notes: The dPGS-Au50 (**A**) and dPGOH-Au50 (**B**) NPs were incubated with RPMI-1640 medium serum containing 10% FBS (CCM), with isolated MPs or were first pre-incubated with RPMI-1640 medium containing 10% FBS and then incubated with MPs (CCM + MPs). Proteins were eluted from NP surfaces using Laemmli buffer and analyzed by SDS-PAGE. Eluted proteins were visualized by Coomassie and the identified by nanoHPLC coupled with MALDI-TOF/TOF.
Abbreviations: NP, nanoparticle; FBS, fetal bovine serum; MPs, membrane proteins; CCM, complete cell culture medium; SDS-PAGE, sodium dodecyl sulfate polyacrylamide gel electrophoresis; nanoHPLC, nano high performance liquid chromatography; MALDI, matrix-assisted laser desorption ionization; TOF, time of flight.

serum proteins as they may be widely used in medical applications. A reduced protein affinity was clearly observed for the non-sulfated variant dPGOH compared with dPGS, which indicates that serum proteins preferably interact with negatively charged NP surfaces, as also shown by others.[28] Differences in protein binding with respect to NP size were also observed. However, the influence of size on the protein composition of the NP protein corona seems to be minor compared with the influence of the surface charge. The effect of size on the composition of the protein corona may be explained by the different curvature of NPs, which could affect the binding of differently shaped proteins to different extents. Often, globular proteins absorbed on small particles seem to retain their native conformation with increasing cur-

Table 3 Selected identified membrane proteins after pull-down approach

Protein	Accession	MW (kDa)	MASCOT score	Unique peptides
Integrin β-II	ITB2_HUMAN	84.7	30	1
Transferrin receptor protein 1	TFR1_HUMAN	84.8	224.4	5

Notes: The dPGS-Au50 NPs were pre-incubated with CCM containing 10% FBS and then incubated with isolated membrane protein fraction. Proteins were eluted, separated through SDS-PAGE, and analyzed by using nanoHPLC coupled with MS/MS.
Abbreviations: NP, nanoparticle; CCM, complete cell culture medium; FBS, fetal bovine serum; SDS-PAGE, sodium dodecyl sulfate polyacrylamide gel electrophoresis; nanoHPLC, nano high performance liquid chromatography; MW, molecular weight; MS, mass spectrometry.

vature as shown for BSA on monodisperse silica spheres.[42] In contrast, fibrillar proteins may lose their native conformation with decreasing particle size as shown for fibrinogen.[42]

Here we could identify different serum proteins as components of the protein corona for each NP, among them constituents of the adaptive immune response, cell-adhesion (-migration, -motility, and -proliferation), activators, and regulators of the complement system. Some of these proteins may play a role in the cellular interaction of the NPs and thus could be interesting with respect to NP targeting.

In order to further analyze the interactions between NP protein corona and cell membranes, pull-down experiments were performed to identify possible interaction partners for dPGS. Through this approach, the transferrin receptor protein, HLA class 1 histocompatibility antigens, and a member of the integrin receptor family, which could be potentially involved in cellular recognition and uptake of the dPGS NPs, could be identified.

Others have already performed intensive research on the role of transferrin in NP uptake. Transferrin has been frequently identified in the protein coronas of several NPs, for example, silver, iron oxide, and silica.[43–45] Here we could identify serotransferrin in the corona of dPGS but not in the corona of dPGOH NPs. Serotransferrin can interact with the transferrin receptor and mediate an endocytotic uptake through clathrin-mediated endocytosis.[46] It was shown that
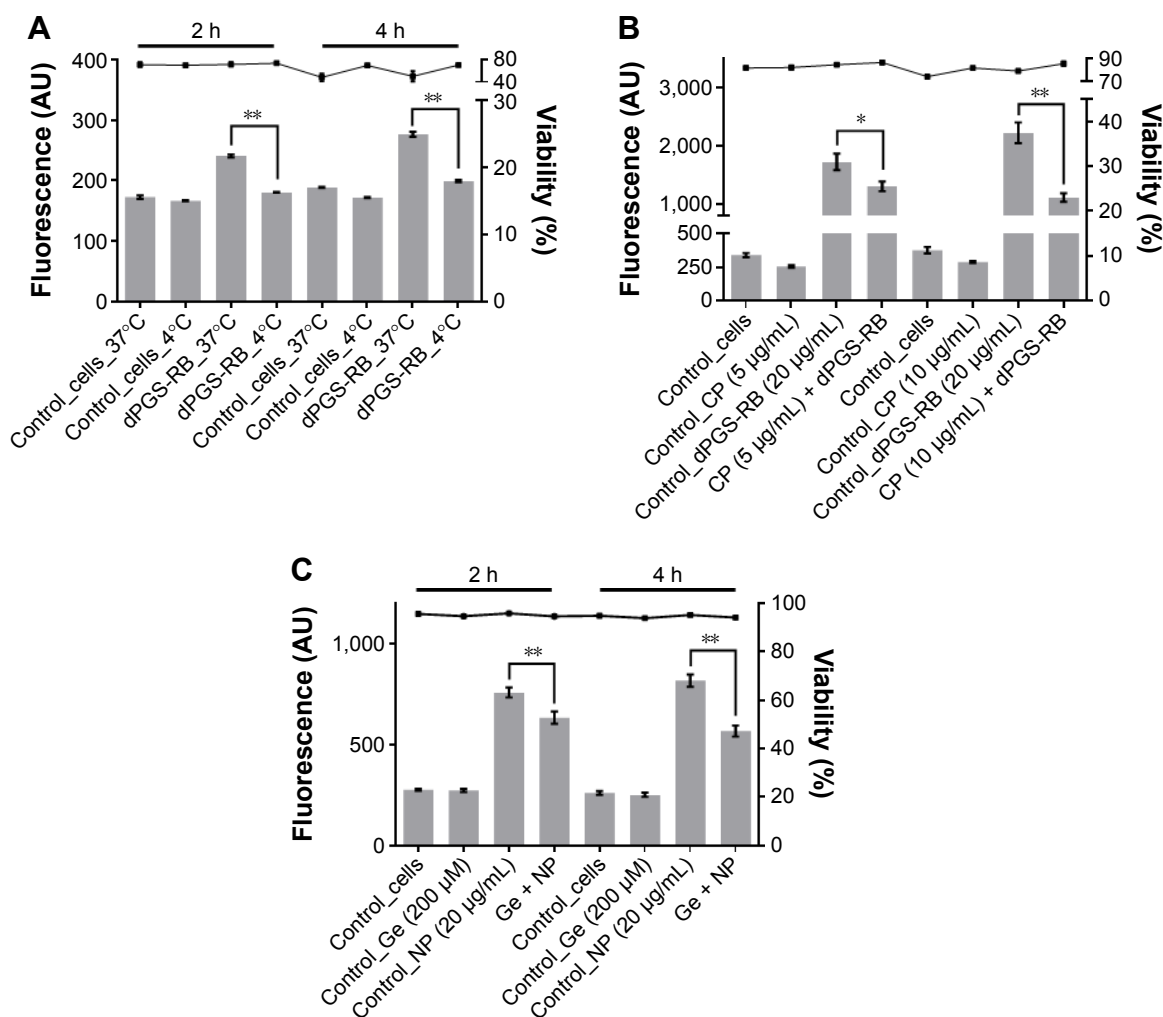
Figure 6 Investigation of possible uptake pathways of dPGS NPs.
Notes: (**A**) THP-1 cells were incubated for 2 or 4 h with pre-incubated dPGS-RB NPs at different temperatures (4°C or 37°C). THP-1 cells were pre-incubated for 2 h either with serum-free RPMI-1640 medium or medium containing 5 or 10 µg/mL CP (**B**) or with 200 µM genistein (Ge) (**C**). NPs, that is, dPGS-RB, which were pre-incubated for 2 h with RPMI-1640 medium containing 10% serum, were then added for another 2 h. Mean fluorescence values are depicted as analyzed by flow cytometry including SEM (n=9–12 biological repeats) as bars (with significance: **P<0.01 and *P<0.05), and the percentage of viable cells is depicted as a line including SEM (n=9–12 biological repeats).
Abbreviations: NP, nanoparticle; PBS, phosphate-buffered saline; CP, chlorpromazine; Ge, genistein.

the presence of transferrin enhanced the endocytosis of lipid-coated NPs in A549 cells in vitro.[26] In this study, the transferrin receptor could be identified as a possible cellular interaction partner of CCM pre-incubated dPGS NPs using a pull-down approach. Furthermore, by using CP, a known inhibitor of clathrin-mediated endocytosis, cellular uptake of dPGS was decreased by 50% in this study. Therefore, clathrin-mediated endocytosis plays a major role in cellular uptake of dPGS. However, other pathways, in particular caveolin-mediated endocytosis seem to contribute as well.

In addition, a membrane protein of the integrin family was identified, which can also be involved in mediating cellular uptake of dPGS NPs. Integrins have the ability to recognize multiple ligands and may bind to interaction partners with

an RGD sequence (Arg-Gly-Asp), an acidic motif termed "LDV," or a collagenous GFOGER motif.[47–53] VN, which was identified as a component of the serum corona for dPGS but not for dPGOH NPs, can interact with αvβ3 integrin and could thus possibly be important for the uptake of dPGS NPs as well.[54–56] For FBS-treated TiO$_2$ NPs, it was already shown that cellular uptake into human lung carcinoma cells (A549) was reduced when cells were pre-treated with anti-VN antibodies.[57]

Taken together, several lines of evidence that the protein coronas of dPG NPs can alter the NP cell interactions and influence cellular uptake are presented. These data indicate that clathrin-mediated endocytosis is the major cellular uptake pathway for dPGS, whereas other pathways such as

caveolin-mediated endocytosis contribute as well. Therefore, most likely different proteins and different pathways are involved in parallel in cellular uptake of dPGS NPs. Indeed, for the first time, a few possible cellular uptake receptors for dPGS were identified. As shown by others, different proteins in the protein corona can be involved in the cellular uptake of NPs. A study performed by Ritz et al showed that binding of ApoA4 and ApoC3 to four polymeric NPs was increasing the uptake while the binding of ApoH was decreasing it.[58] Therefore, as NPs are typically covered by a protein corona consisting of plenty of different proteins, there seems to be a complex interplay of different corona components. Different proteins may influence cellular uptake through different pathways.

Conclusion

In this study, different dPG-coated gold NPs were synthesized, and it could be shown that the surface charge had a large influence on the protein corona compared to size, which only had a minor effect on corona composition in this study. Sulfated dPG NPs (dPGS) showed a higher tendency to interact with serum proteins compared to the non-sulfated dPG NPs (dPGOH). The different protein affinities were well reflected by different rates of cellular uptake with dPGS but not dPGOH being strongly taken up by human monocytes. A pull-down approach allowed us to identify possible cellular interaction partners for dPGS in human monocytes such as the transferrin receptor or an integrin, which correlated well with the presence of serotransferrin or VN, respectively, in the corona of dPGS. Thus, this approach allows for the first time to get insights into the role of specific proteins of the dPGS corona in cellular uptake and thereby to better understand possible uptake mechanisms. Furthermore, these data indicate that clathrin-mediated endocytosis is the major though not the only cellular uptake pathway for cellular uptake. It may be concluded that most likely different pathways involving different receptors exist for mediating cellular uptake of dPGS NPs.

Acknowledgments

Disclosure

The authors have no affiliation or financial involvement with any organization or entity with a financial interest. This paper was presented at the 2nd NanoSafety Forum for Young Scientists in Visby, Gotland, Sweden in September 2016 as an oral presentation with interim findings. The authors report no other conflicts of interest in this work.

References

1. Torchilin VP. Targeted pharmaceutical nanocarriers for cancer therapy and imaging. *AAPS J*. 2007;9(2):E128–E147.
2. Arachchige MC, Reshetnyak YK, Andreev OA. Advanced targeted nanomedicine. *J Biotechnol*. 2015;202:88–97.
3. Petre CE, Dittmer DP. Liposomal daunorubicin as treatment for Kaposi's sarcoma. *Int J Nanomedicine*. 2007;2(3):277–288.
4. Caminade A-M, Turrin C-O. Dendrimers for drug delivery. *J Mater Chem B*. 2014;2(26):4055–4066.
5. Madaan K, Kumar S, Poonia N, Lather V, Pandita D. Dendrimers in drug delivery and targeting: drug-dendrimer interactions and toxicity issues. *J Pharm Bioallied Sci*. 2014;6(3):139–150.
6. Owens DEr, Peppas NA. Opsonization, biodistribution, and pharmacokinetics of polymeric nanoparticles. *Int J Pharm*. 2006;307(1):93–102.
7. Oh N, Park JH. Endocytosis and exocytosis of nanoparticles in mammalian cells. *Int J Nanomedicine*. 2014;9(Suppl 1):51–63.
8. Jones SW, Roberts RA, Robbins GR, et al. Nanoparticle clearance is governed by Th1/Th2 immunity and strain background. *J Clin Invest*. 2013;123(7):3061–3073.
9. Li SD, Huang L. Stealth nanoparticles: high density but sheddable PEG is a key for tumor targeting. *J Control Release*. 2010;145(3):178–181.
10. Allard-Vannier E, Cohen-Jonathan S, Gautier J, et al. Pegylated magnetic nanocarriers for doxorubicin delivery: a quantitative determination of stealthiness in vitro and in vivo. *Eur J Pharm Biopharm*. 2012;81(3):498–505.
11. Kreuter J, Ramge P, Petrov V, et al. Direct evidence that polysorbate-80-coated poly(butylcyanoacrylate) nanoparticles deliver drugs to the CNS via specific mechanisms requiring prior binding of drug to the nanoparticles. *Pharm Res*. 2003;20(3):409–416.
12. Kurakhmaeva KB, Djindjikhashvili IA, Petrov VE, et al. Brain targeting of nerve growth factor using poly(butyl cyanoacrylate) nanoparticles. *J Drug Target*. 2009;17(8):564–574.
13. Lin Y, Pan Y, Shi Y, Huang X, Jia N, Jiang JY. Delivery of large molecules via poly(butyl cyanoacrylate) nanoparticles into the injured rat brain. *Nanotechnology*. 2012;23(16):165101.
14. Kreuter J. Nanoparticulate systems for brain delivery of drugs. *Adv Drug Deliv Rev*. 2001;47(1):65–81.
15. Mulik RS, Monkkonen J, Juvonen RO, Mahadik KR, Paradkar AR. ApoE3 mediated polymeric nanoparticles containing curcumin: apoptosis induced in vitro anticancer activity against neuroblastoma cells. *Int J Pharm*. 2012;437(1–2):29–41.
16. Jo DH, Kim JH, Lee TG, Kim JH. Size, surface charge, and shape determine therapeutic effects of nanoparticles on brain and retinal diseases. *Nanomedicine*. 2015;11(7):1603–1611.
17. Walczyk D, Bombelli FB, Monopoli MP, Lynch I, Dawson KA. What the cell "sees" in bionanoscience. *J Am Chem Soc*. 2010;132(16):5761–5768.
18. Lynch I, Dawson KA. Protein-nanoparticle interactions. *Nano Today*. 2008;3(1–2):40–47.
19. Mahmoudi M, Lynch I, Ejtehadi MR, Monopoli MP, Bombelli FB, Laurent S. Protein-nanoparticle interactions: opportunities and challenges. *Chem Rev*. 2011;111(9):5610–5637.
20. Monopoli MP, Walczyk D, Campbell A, et al. Physical-chemical aspects of protein corona: relevance to in vitro and in vivo biological impacts of nanoparticles. *J Am Chem Soc*. 2011;133(8):2525–2534.
21. Zanganeh S, Spitler R, Erfanzadeh M, Alkilany AM, Mahmoudi M. Protein corona: Opportunities and challenges. *Int J Biochem Cell Biol*. 2016;75:143–147.
22. Cheng X, Tian X, Wu A, et al. Protein corona influences cellular uptake of gold nanoparticles by phagocytic and nonphagocytic cells in a size-dependent manner. *ACS Appl Mater Interfaces*. 2015;7(37):20568–20575.

23. Ritz S, Schottler S, Kotman N, et al. Protein corona of nanoparticles: distinct proteins regulate the cellular uptake. *Biomacromolecules*. 2015;16(4):1311–1321.

24. Salvati A, Pitek AS, Monopoli MP, et al. Transferrin-functionalized nanoparticles lose their targeting capabilities when a biomolecule corona adsorbs on the surface. *Nature Nanotechnol*. 2013;8(2):137–143.

25. Mirshafiee V, Mahmoudi M, Lou K, Cheng J, Kraft ML. Protein corona significantly reduces active targeting yield. *Chem Commun*. 2013;49(25):2557–2559.

26. Guo Y, Wang L, Lv P, Zhang P. Transferrin-conjugated doxorubicin-loaded lipid-coated nanoparticles for the targeting and therapy of lung cancer. *Oncol Lett*. 2015;9(3):1065–1072.

27. Kainthan RK, Janzen J, Levin E, Devine DV, Brooks DE. Biocompatibility testing of branched and linear polyglycidol. *Biomacromolecules*. 2006;7(3):703–709.

28. Dernedde J, Rausch A, Weinhart M, et al. Dendritic polyglycerol sulfates as multivalent inhibitors of inflammation. *Proc Natl Acad Sci U S A*. 2010;107(46):19679–19684.

29. Khandare J, Calderon M, Dagia NM, Haag R. Multifunctional dendritic polymers in nanomedicine: opportunities and challenges. *Chem Soc Rev*. 2012;41(7):2824–2848.

30. Weinhart M, Groger D, Enders S, et al. The role of dimension in multivalent binding events: structure-activity relationship of dendritic polyglycerol sulfate binding to L-selectin in correlation with size and surface charge density. *Macromol Biosci*. 2011;11(8):1088–1098.

31. Weinhart M, Groger D, Enders S, Dernedde J, Haag R. Synthesis of dendritic polyglycerol anions and their efficiency toward L-selectin inhibition. *Biomacromolecules*. 2011;12(7):2502–2511.

32. Vonnemann J, Liese S, Kuehne C, et al. Size dependence of steric shielding and multivalency effects for globular binding inhibitors. *J Am Chem Soc*. 2015;137(7):2572–2579.

33. Lou X, Wang C, He L. Core-shell Au nanoparticle formation with DNA-polymer hybrid coatings using aqueous ATRP. *Biomacromolecules*. 2007;8(5):1385–1390.

34. Ziegler C, Eychmüller A. Seeded growth synthesis of uniform gold nanoparticles with diameters of 15–300 nm. *J Phys Chem C*. 2011;115(11):4502–4506.

35. Vonnemann J, Sieben C, Wolff C, et al. Virus inhibition induced by polyvalent nanoparticles of different sizes. *Nanoscale*. 2014;6(4):2353–2560.

36. Groger D, Kerschnitzki M, Weinhart M, et al. Selectivity in bone targeting with multivalent dendritic polyanion dye conjugates. *Adv Healthcare Mater*. 2014;3(3):375–385.

37. Rabilloud T, Strub J-M, Luche S, Girardet J, van Dorsselaer A, Lunardi J. Ruthenium II tris (bathophenanthroline disulfonate), a powerful fluorescent stain for detection of proteins in gel with minimal interference in subsequent mass spectrometry analysis. *Proteome*. 2000;1(1):1–14.

38. Vonnemann J, Beziere N, Bottcher C, et al. Polyglycerolsulfate functionalized gold nanorods as optoacoustic signal nanoamplifiers for in vivo bioimaging of rheumatoid arthritis. *Theranostics*. 2014;4(6):629–641.

39. Walkey CD, Chan WC. Understanding and controlling the interaction of nanomaterials with proteins in a physiological environment. *Chem Soc Rev*. 2012;41(7):2780–2799.

40. Le Roy C, Wrana JL. Clathrin- and non-clathrin-mediated endocytic regulation of cell signalling. *Nat Rev Mol Cell Biol*. 2005;6(2):112–126.

41. Wang LH, Rothberg KG, Anderson RG. Mis-assembly of clathrin lattices on endosomes reveals a regulatory switch for coated pit formation. *J Cell Biol*. 1993;123(5):1107–1117.

42. Roach P, Farrar D, Perry CC. Surface tailoring for controlled protein adsorption: effect of topography at the nanometer scale and chemistry. *J Am Chem Soc*. 2006;128(12):3939–3945.

43. Shannahan JH, Lai X, Ke PC, Podila R, Brown JM, Witzmann FA. Silver nanoparticle protein corona composition in cell culture media. *PLoS One*. 2013;8(9):e74001.

44. Sakulkhu U, Mahmoudi M, Maurizi L, Salaklang J, Hofmann H. Protein corona composition of superparamagnetic iron oxide nanoparticles with various physico-chemical properties and coatings. *Sci Rep*. 2014;4:5020.

45. Tenzer S, Docter D, Rosfa S, et al. Nanoparticle size is a critical physicochemical determinant of the human blood plasma corona: a comprehensive quantitative proteomic analysis. *ACS Nano*. 2011;5(9):7155–7167.

46. McMahon HT, Boucrot E. Molecular mechanism and physiological functions of clathrin-mediated endocytosis. *Nat Rev Mol Cell Biol*. 2011;12(8):517–533.

47. Plow EF, Haas TA, Zhang L, Loftus J, Smith JW. Ligand binding to integrins. *J Biol Chem*. 2000;275(29):21785–21788.

48. Ruoslahti E. RGD and other recognition sequences for integrins. *Annu Rev Cell Dev Biol*. 1996;12:697–715.

49. Campbell ID, Humphries MJ. Integrin structure, activation, and interactions. *Cold Spring Harb Perspect Biol*. 2011;3(3):a004994.

50. Emsley J, Knight CG, Farndale RW, Barnes MJ, Liddington RC. Structural basis of collagen recognition by integrin alpha2beta1. *Cell*. 2000;101(1):47–56.

51. Arosio D, Casagrande C. Advancement in integrin facilitated drug delivery. *Adv Drug Deliv Rev*. 2016;97:111–143.

52. Raj A, Saraf P, Javali NM, Li X, Jasti B. Binding and uptake of novel RGD micelles to the alphavbeta3 integrin receptor for targeted drug delivery. *J Drug Target*. 2014;22(6):518–527.

53. Lahti M, Heino J, Kapyla J. Leukocyte integrins alphaLbeta2, alphaM-beta2 and alphaXbeta2 as collagen receptors – receptor activation and recognition of GFOGER motif. *Int J Biochem Cell Biol*. 2013;45(7):1204–1211.

54. Horton MA. The alpha v beta 3 integrin "vitronectin receptor". *Int J Biochem Cell Biol*. 1997;29(5):721–725.

55. Pytela R, Pierschbacher MD, Ruoslahti E. A 125/115-kDa cell surface receptor specific for vitronectin interacts with the arginine-glycine-aspartic acid adhesion sequence derived from fibronectin. *Proc Natl Acad Sci U S A*. 1985;82(17):5766–5770.

56. Li R, Luo M, Ren M, et al. Vitronectin regulation of vascular endothelial growth factor-mediated angiogenesis. *J Vasc Res*. 2014;51(2):110–117.

57. Tedja R, Lim M, Amal R, Marquis C. Effects of serum adsorption on cellular uptake profile and consequent impact of titanium dioxide nanoparticles on human lung cell lines. *ACS Nano*. 2012;6(5):4083–4093.

58. Ritz S, Schöttler S, Kotman N, et al. Protein corona of nanoparticles: distinct proteins regulate cellular uptake. *Biomacromolecules*. 2015;16:1311–1321.

3.2 Amphiphilic nanogels: influence of surface hydrophobicity on protein corona, biocompatibility and cellular uptake

Tony Bewersdorff, Alexandra Gruber, Murat Eravci, Malti Dumbani, Daniel Klinger, Andrea Haase

The supplementary material to the publication embedded on the following pages is contained in Annex II.

The authors contribution:

Sample preparation for DLS

Data analysis

Cell culture

Sample preparation for cell viability assay, protein corona analysis and cellular uptake studies

Analysis of proteomic results (2D-SDS-PAGE and LC-ESI-MS/MS)

Investigation of the cellular uptake by flow cytometry

Discussion and evaluation of the results (with other authors)

Preparation of the manuscript (with other authors)

ORIGINAL RESEARCH

Amphiphilic nanogels: influence of surface hydrophobicity on protein corona, biocompatibility and cellular uptake

Tony Bewersdorff[1]
Alexandra Gruber[2]
Murat Eravci[1]
Malti Dumbani[1]
Daniel Klinger[2]
Andrea Haase[1]

[1]German Federal Institute for Risk Assessment (BfR), Department of Chemical and Product Safety, Berlin, Germany; [2]Freie Universität Berlin, Institute of Pharmacy (Pharmaceutical Chemistry), Berlin, Germany

Correspondence: Andrea Haase,
German Federal Institute for Risk Assessment, Department of Chemical and Product Safety, Max-Dohrn-Strasse 8–10, Berlin 10589, Germany
Tel +49 30 184 122 7600
Email Andrea.Haase@bfr.bund.de

Daniel Klinger
Freie Universität Berlin, Institute of Pharmacy (Pharmaceutical Chemistry), Königin-Luise Street 2-4, Berlin 14195, Germany
Tel +49 308 386 0001
Email Daniel.Klinger@fu-berlin.de

Background and purpose: Nanogels (NGs) are promising drug delivery tools but are typically limited to hydrophilic drugs. Many potential new drugs are hydrophobic. Our study systematically investigates amphiphilic NGs with varying hydrophobicity, but similar colloidal features to ensure comparability. The amphiphilic NGs used in this experiment consist of a hydrophilic polymer network with randomly distributed hydrophobic groups. For the synthesis we used a new synthetic platform approach. Their amphiphilic character allows the encapsulation of hydrophobic drugs. Importantly, the hydrophilic/hydrophobic balance determines drug loading and biological interactions. In particular, protein adsorption to NG surfaces is dependent on hydrophobicity and critically determines circulation time. Our study investigates how network hydrophobicity influences protein binding, biocompatibility and cellular uptake.

Methods: Biocompatibility of the NGs was examined by WST-1 assay in monocytic-like THP-1 cells. Serum protein corona formation was investigated using dynamic light scattering and two-dimensional gel electrophoresis. Proteins were identified by liquid chromatography-tandem mass spectrometry. In addition, cellular uptake was analyzed via flow cytometry.

Results: All NGs were highly biocompatible. The protein binding patterns for the two most hydrophobic NGs were very similar to each other but clearly different from the hydrophilic ones. Overall, protein binding was increased with increasing hydrophobicity, resulting in increased cellular uptake.

Conclusion: Our study supports the establishment of structure–property relationships and contributes to the accurate balance between maximum loading capacity with low protein binding, optimal biological half-life and good biocompatibility. This is an important step to derive design principles of amphiphilic NGs to be applied as drug delivery vehicles.

Keywords: adjustable amphiphilic nanogels, tuneable hydrophilic/hydrophobic balance, biocompatibility, cellular uptake, protein corona, THP-1 cells

Introduction

Nanogels (NGs) as cross-linked polymeric nanoparticles (NPs) are emerging as flexible, versatile drug carriers,[1] being interesting for many applications ranging from cancer therapy to nanoantibiotics.[2–8] However, conventional NGs exhibit one major drawback: their overall hydrophilicity dramatically limits their application for hydrophobic drugs.

Amphiphilic NGs, based on a hydrophilic polymer matrix containing hydrophobic groups, recently emerged as new carriers for hydrophobic drugs.[9–11] Accurately tuning delivery properties can be achieved by changing the network's hydrophilic/hydrophobic balance. In general, increasing hydrophobicity enables higher loading capacities and more sustained release profiles,[12] but may lead to several undesired effects such as decreased systemic circulation time and reduced biocompatibility.[13,14] In blood, plasma proteins selectively adsorb to NG surfaces, forming a specific protein corona. The identity and amount of bound proteins are mainly determined by surface characteristics with hydrophobicity and surface charge being the most important ones.[13–19] The corona represents the actual bio-nano-interface, mediates cellular interactions and depicts the biological identity of a NP.[20,21] Hydrophobic surfaces favor binding of opsonins, specific plasma proteins, that label NPs for uptake and removal by the reticuloendothelial system (RES).[22,23,24] Consequently, blood circulation time is dramatically reduced, limiting the therapeutic potential of the NPs.[25] In contrast, hydrophilic surface moieties protect NPs from opsonization and prevent cellular uptake by the RES, described as "stealth effect".[26–29]

Amphiphilic NGs combine aspects from hydrophobic and hydrophilic surfaces in one single colloidal system. Thus, their protein interactions and biocompatibility are far less understood. It becomes obvious that structural optimization for drug delivery applications requires a careful balancing, as increasing hydrophobicity leads to increased loading capacities of hydrophobic cargoes but at the other side also results in a reduced half-life and biocompatibility. To correlate specific hydrophilic/hydrophobic network compositions to loading/release profiles and to NG behavior in biological systems, systematic investigations are needed.

However, up to now such systematic studies are highly challenging since conventional synthetic approaches to generate amphiphilic NGs also change the colloidal features, such as size, size distribution and morphology. The protein corona is also dependent on NP size, curvature and shape.[30–32] Consequently, it would be impossible to discriminate whether a different NG behavior results from altered size or modified amphiphilicity.

Thus, a new synthetic approach is required. We have recently developed a synthetic platform approach based on the functionalization of reactive precursor particles with hydrophilic and hydrophobic moieties,[12,33] allowing to tuning of amphiphilicity while providing a majority of similar colloidal features. Therefore, we now have access

to a library of comparable NGs with varying network composition but similar colloidal properties. All NGs are based on an amphiphilic network of poly(methacrylamide) copolymers containing 80 mol-% of hydrophilic 2-hydroxypropylamin (HPA) groups but 20 mol-% of different hydrophobic amides, ie, benzyl, hexyl, cholesteryl and dodecyl moieties referred to as BENZA-20, HEXA-20, CHOLA-20 and DODA-20.

This allows us, for the first time, to systematically investigate the influence of network composition on the interaction with biological systems. Human monocytic like THP-1 cells are used as a model system for human monocytes, which are a main component of the RES. We investigated biocompatibility and cellular uptake in THP-1 cells. Protein binding was analyzed by two-dimensional gel electrophoresis (2DE) and liquid chromatography-tandem mass spectrometry (LC-MS/MS) combined with the Top 3 approach for quantification.[34,35] To the best of our knowledge, this is the first systematic investigation on highly comparable amphiphilic NGs with different hydrophobicities, their specific protein coronas and the resulting effects in terms of cellular uptake and biocompatibility. In combination with our previously determined loading capacities and release profiles,[12] these results are important to establish structure–property and structure–activity relationships.

Materials and methods
Synthesis of amphiphilic NGs

All reagents were purchased from commercial sources and used without further purification, unless otherwise stated. Anhydrous solvents were obtained from a MB-SPS-800 (MBraun, Germany) solvent purification system and ultrapure water (MQ) from a LaboStar Pro UV 2 (Evoqua, Germany) water system. Pentafluorophenyl methacrylate (PFPMA),[36,37] poly(pentafluorophenyl methacrylate) (PPFPMA),[38] CHOLA[39,40] and [2-(aminoethyl)-carbamothioyl]-5-aminofluorescein (FITCA)[41] and post-modification of PPFPMA[12,42] were prepared according to literature procedures. Moisture or air-sensitive reactions were carried out in dry glassware under nitrogen atmosphere. Dialysis was performed in benzoylated cellulose dialysis tubes (width: 32 mm, molecular weight cutoff 2000 g/mol, Sigma-Aldrich, Germany).

Reactive precursor particles

Amphiphilic NGs were synthesized as recently described.[12] First, reactive PPFPMA precursor particles were synthesized via miniemulsion polymerization. Briefly, an oil phase

consisting of 10 g PFPMA, 0.4 g ethylene glycol dimethacrylate (EGDMA, 5 mol-% w.r.t PFPMA), hexadecane (0.44 g) and 195 mg 2,2′-azobis(2-methylpropionitrile) (AIBN) was dispersed in an aqueous phase of sodium dodecyl sulfate (SDS) dissolved in deionized (DI) water (1.25 mg/mL, in 200 mL DI water, 2.5 wt-% w.r.t PFPMA) by pre-sonication in a sonication bath (Elmasonic P30 H, Elma, Germany) for 10 mins. Full dispersion was achieved by ultrasonication with a Digital Sonifier SFX 550 (Branson, Germany). The emulsion was purged with nitrogen for 10 mins before the reaction was allowed to proceed for 24 hrs at 70°C. Particle dispersions were purified via repeated centrifugation-washing-redispersion steps and freeze-dried for storage.

Amphiphilic NGs

Post-modification of reactive precursor particles was carried out on dispersed PPFPMA particles (400 mg, 1.59 mmol w.r.t monomer units of PPFPMA particles, 1.0 eq) in dimethylformamide (DMF) by adding different molar ratios of amine functionalized moieties (3.0 eq w.r.t. monomer units) and triethylamine (TEA) (660 µL, 4.77 mmol, 3.0 eq w.r.t. monomer units), as summarized in Table S1.

The reaction was allowed to proceed at 50°C for 24 hrs. Afterward, the particles were purified by extensive dialysis first against DMF (1 week) and subsequently against DI water (1 week) and MQ (1 week). The particles were then freeze-dried for storage upon use. In this study, the following five NGs were used: poly(N-(2-hydroxypropyl)methacrylamide) (PHPMA) as hydrophilic control, bearing no hydrophobic groups and variants that each contained 80 mol-% hydrophilic HPA and 20 mol-% of a different hydrophobic group, ie, benzylamine (BENZA-20), hexylamine (HEXA-20), an amine-functionalized cholesteryl group (CHOLA-20) and dodecylamine (DODA-20). Estimated differences in NG hydrophobicities were calculated using http://www.molinspiration.com resulting in the theoretical logarithmic partition coefficients (logP).

FITC-labeled amphiphilic NGs

The synthesis of the fluorescence labeled NGs was carried out analog to the post-modification of the unlabeled NGs but in a two-step approach. Briefly, freeze-dried PPFPMA particles (2.00 g, 7.93 mmol w.r.t monomer units of PPFPMA particles, 1.0 eq) were dispersed in 400 mL DMF by short treatment in a sonication bath (Elmasonic P30 H, Elma). The particles were swollen overnight in DMF before amine functionalized fluorescein (FITCA) (71 mg, 0.16 mmol, 0.02 eq w.r.t monomer units) and

TEA (3.3 mL, 23.8 mmol, 3 eq w.r.t. monomer units) were added and heated to 50°C. After 24 hrs, 30 mL of the dispersion (150 mg PPFPMA-FITC particles) were reacted for another 24 hrs with different ratios of amine functionalized moieties (3.0 eq w.r.t. monomer units), as summarized in Table S2.

Afterward, the NGs were purified by extensive dialysis against DMF and subsequently against DI water and MQ. The NGs were then freeze-dried and obtained as pale-yellow powder. They can be stored and redispersed in DI water or PBS by vortex and short sonication treatment. Characterization of the NGs via dynamic light scattering (DLS) measurement after redispersion in DI water is shown in Table 1.

NG dispersion

NGs were dispersed in MQ or PBS by vortexing, followed by 30 min sonication at room temperature (RT).

Characterization of the NGs

The success of the post-modification reaction was monitored by attenuated total reflection- Fourier-transform infrared spectroscopy (ATR-FTIR spectroscopy) on freeze-dried particles as described previously.[12] The size of the NGs after post-modification was determined by DLS using a nicomp nano Z3000 (Particle Sizing Systems, USA) at a fixed scattering angle of 173°. The measurements were carried out at RT. In order to measure zeta potential, NGs were measured at 200 µg/mL in MQ or PBS at 25°C using Zetasizer Nano ZS (Malvern Instruments GmbH, Germany). A pre-equilibration time of 2 mins was used, attenuator and voltage were selected automatically and three runs of 30 measurements were used.

The size of the NGs in the dry state was investigated via transmission electron microscopy (TEM). Samples were prepared by applying a 10 µL droplet of the NG dispersion (1 mg/mL in MQ) on a carbon-coated copper grid (400 meshes, Quantifoil Micro Tools GmbH, Großlöbichau, Germany) for 45 s. The supernatant was removed with filter paper. This process was repeated 10 times and the grids were allowed to dry in air overnight. The TEM samples were measured afterward using the TEM mode of a Hitachi Scanning Electron Microscope (SU8030, Hitachi High-Technologies Corporation, Tokyo, Japan) with a working voltage of 30.0 kV at different magnifications. In order to evaluate the size and the size distribution of the NGs in the dried state, the diameter of

Table 1 Characterization of the physico-chemical properties of the NGs

Nanogels		Particle diameter D_h [nm] (from dls)		Size difference Δd_h [nm]	Zeta potential Z [mv]	
Type	Sample	MQ	CCM		MQ	PBS
Hydrophilic	PHPMA	210±45	225±5	15	−15.7	−12.4
Moderate hydrophobic	BENZA-20	185±35	235±25	50	−9.4	−5.8
	HEXA-20	170±65	255±10	85	−8.8	−5.1
Hydrophobic	CHOLA-20	170±40	220±5	50	−13.4	−7.0
	DODA-20	180±70	280±5	100	−18.7	−19.7

Notes: NGs were dispersed in MQ, PBS or CCM by vortexing, followed by 30-min sonication at RT. DLS was performed after 2 hrs. Particle sizes are denoted as the hydrodynamic diameter and the respective standard deviation.
Abbreviations: NGs, nanogels; DLS, dynamic light scattering; MQ, ultrapure water; CCM, complete cell culture medium (RPMI 1640 containing 10% FBS); RT, room temperature.

500 NGs each sample was determined with the software ImageJ (version 1.52e).

Measurement of the water contact angle

Polymer films were produced via spin-coating of polymer solutions on glass slides (Ø 25 mm, Neolab, Germany) with a spin processor WS-659MZ-23NPPB (Laurell Technologies Corporation, USA). Polymers solutions (1.5 wt-% in CHCl$_3$ with a few drops of MeOH, if needed) were dropped on the objects and coated at 11,000 rounds per minute (rpm) for 40 s. Polymer films were dried under vacuum (RT, 90 mins). Static contact angle measurements were performed using sessile drop method on a contact angle system OCA 20 (DataPhysics Instruments, Germany) and processed with SCA20 (Version 3.12.11, DataPhysics Instruments). Two microliters MQ were dropped on the substrate and allowed to equilibrate (20 s, RT). The contact angles of 18 measurements from three coating samples were determined and averaged.

Cell culture

The human monocytic like cell line THP-1 was obtained from DSMZ (German Collection of Microorganisms and Cell Cultures, Germany) and cultivated in RPMI 1640 complete cell culture medium (CCM) containing 10% FBS, 2 mM L-Glutamine, 100 mM 4-(2-hydroxyethyl) piperazine-1-ethanesulfonic acid (HEPES), 100 units/mL penicillin, 0.1 mg/mL streptomycin in an incubator (37°C, 5% CO$_2$). Cell culture medium, FBS and additives were obtained from PAN Biotech, Germany. Cells were counted using a Casy TTC (Roche Diagnostics GmbH, Germany).

Cell viability

Cells were seeded in 96-well plates (TPP, Germany) at 15,000 cells/100 µL CCM, incubated for 24 hrs (37°C, 5% CO$_2$), treated with NGs (final concentrations 20, 75 and 100 µg/mL) and incubated for additional 24 cells were washed twice with PBS. Next, WST-1 solution (4-[3-(4-iodophenyl)-2-(4-nitrophenyl)-2H-5-tetrazolio]-1,3-benzene disulfonate, Roche, Switzerland) was added according to manufacturer instruction and incubated for another 2 hrs (37°C, 5% CO$_2$). Absorbance was measured using a GENios plate reader at 450 nm (TECAN, Switzerland).

Protein corona analysis

The NGs were dispersed at 300 µg/mL in 5 mL CCM (with 10% FBS gold) in sterile glass vials containing magnetic stir bar by stirring (700 rpm, 30 mins, RT). NGs were loaded on top of 4.5 mL 1.5 M sucrose (except PHPMA, which was loaded on 1.25 M sucrose) and pelleted via ultracentrifugation (17,900 g, 2.5 hrs at RT). CCM without NGs served as control and was treated similarly. Pellets were washed twice with PBS (17,900 g, 30 mins at RT). Samples were divided into two equal parts, one for two-dimensional polyacrylamide gel electrophoresis (2D-PAGE) analysis and one for LC-MS/MS analysis.

2D-PAGE analysis of the protein corona

Unless otherwise stated, chemicals were purchased from Carl Roth GmbH (Germany). Proteins were eluted in 500 µL 2D lysis buffer (7 M urea, 2 M thiourea, 4% chaps, 2% pharmalyte pH 4–7, 1% dithiothreitol (DTT) and protease inhibitors). Total protein content was measured using the 2D Quant kit (GE Healthcare, Germany). For the isoelectric focusing-samples (500 µL) were loaded on nonlinear IPG strips (24 cm ImmobilineTM DrySrip pH 4–7 (NL), GE Healthcare) and equilibrated for 1 hr in equilibration buffer EB1 (360 mg/mL urea, 24 mg/mL SDS and 50.4 mM/mL Tris HCl, pH 8.6). Active rehydration and focusing were

performed (15 hrs at 30 V, 1.5 hrs at 200 V, 1 hr at 500 V, 13.5 hrs gradient 500–1000 V, 3 hrs gradient 1000–8000 V and 6 hrs at 8000 V) with the GE Ettan IPGphor 3 (GE Healthcare). Afterward proteins were reduced (1% DTT in EB1, 15 mins) and then alkylated (4% iodoacetamide in EB1, 15 mins). Stripes were transferred onto 12.5% SDS-polyacrylamide gels. Electrophoresis was carried out with the GE Ettan DALTtwelve System Separation Unit (GE Healthcare). Gels were fixed (30% ethanol, 10% acetic acid in water) and stained with ruthenium II tris (bathophenanthroline disulfate) chelate (0.4 µM RU-II and 20% ET in MQ).[43] Gels were scanned with a VersaDoc 4000MP imaging system (Bio-Rad, Germany) using excitation λ=473 nm/ detection λ=610 nm and analyzed with Delta2D version 4.6 (Decodon, Germany). Each sample was analyzed in three independent replicates.

LC-MS/MS
In solution digestion
Unless otherwise stated, chemicals were purchased from Carl Roth GmbH. NG pellets were reconstituted in 50 µL of denaturation buffer (6 M urea/2 M thiourea in 10 mM HEPES, pH 8.0), reduced for 30 mins at RT with 1 µL of 0.5 M DTT in 50 mM of ammonium bicarbonate (ABC) and alkylated for 30 mins at RT in the dark by adding 1 µL of 0.5 M iodoacetamide in ABC. Subsequently, 2 µL of Trypsin/Lys-C Mix (Promega, USA) at 0.5 µg/µL in ABC was added and incubated for 4 hrs at RT. The urea concentration was decreased to <2 M by addition of 150 µL of ABC for trypsin digestion overnight at RT. The digestion was stopped by acidification with 200 µL of 5% acetonitrile (ACN), 3% trifluoroacetic acid (TFA). Tryptic peptides were desalted with stage tips.[44]

Liquid chromatography-electrospray ionization-tandem mass spectroscopy (LC-ESI-MS/MS)
Unless otherwise stated, all devices were purchased from Thermo Scientific (USA) and all chemicals were purchased from Carl Roth GmbH. Desalted peptides were reconstituted in 20 µL of 0.1% (v/v) TFA, 5% (v/v) ACN and 4 µL were analyzed by a reversed-phase capillary nano-liquid chromatography system (Ultimate 3000), connected to an Orbitrap Velos mass spectrometer via a nanospray. The LC system was flexion source equipped with a stainless-steel emitter. Samples were injected and concentrated on a trap column (PepMap100 C18, 3 µm, 100 Å, 75 µm i.d. ×2 cm),

equilibrated with 0.05% TFA, 2% ACN in water. After switching the trap column inline, LC separations were performed on a capillary column (Acclaim PepMap100 C18, 2 µm, 100 Å, 75 µm i.d. ×25 cm) at an eluent flow rate of 300 nL/min using a linear gradient of 3–50% B in 50 mins. Mobile phase A contained 0.1% formic acid (FA) in water, and mobile phase B contained 0.1% FA in ACN. Mass spectra were acquired in a data-dependent mode utilizing a single MS survey scan with a resolution of 60,000 in the Orbitrap, and MS/MS scans of the 20 most intense precursor ions in the linear trap quadrupole. The MS survey range was m/z 350–1500. The dynamic exclusion time (for precursor ions) was set to 60 s and automatic gain control was set to 1×10^6 and 5.000 for Orbitrap-MS and LTQ-MS/MS scans, respectively.

Protein identification and label-free quantification of protein abundance
MS and MS/MS data from each LC/MS run were analyzed using the MaxQuant software (Version 1.6.0.16). Identification of proteins was performed using the MaxQuant-implemented Andromeda peptide search engine against a reference proteome database of Bos taurus (Bovine/Uniprot proteome ID: UP000009136, Version October 1, 2017). Initial maximum precursor and fragment mass deviations were set to 7 ppm and 0.5 Da, respectively. Variable modification (methionine oxidation and N-terminal acetylation) and fixed modification (cysteine carbamidomethylation) were set for the search and trypsin with a maximum of two missed cleavages were chosen for searching. The minimum peptide length was set to 7 amino acids and the false discovery rate for peptide and protein identification was set to 0.01. Relative protein abundance was determined using the Top 3 approach. Top 3 intensities of the identified proteins were calculated by summing up the intensities of the three most intense unique peptides for each protein.[34,35] Table S3 summarizes the quantification of NG protein coronas.

Cellular uptake of FITC-labeled NGs in THP-1 cells
Data for physico-chemical characterization of the FITC-labeled NGs are included in Table S4. NGs were sonicated in a Sonorex RK510 water bath (30 mins, RT). Subsequently, 40 µg/mL of the pre-incubated NGs (2 hrs, RT, CCM containing 10% FBS) were incubated with THP-1 cells for 2 hrs (37°C, 5% CO_2). After washing with PBS three times (500 g, 5 mins), uptake was analyzed using a FACS Aria III

(BD Biosciences, Germany), equipped with a blue laser (488 nm), a fluorescence detector (582/42 nm) and a 70 μm nozzle. An example for the differentiation panels we used during the flow cytometry is given in Figure S1.

Results

Physico-chemical characterization of the NGs

In order to investigate the influence of NG hydrophobicity on protein interaction, biocompatibility and cellular uptake, a library of amphiphilic NGs (Figure 1) with varying hydrophobicities but similar colloidal properties was synthesized. For this, we used our recently developed synthetic platform approach which is based on the functionalization of reactive precursor particles with hydrophilic and hydrophobic moieties (Figure 1A).[12] Well-defined reactive precursor particles with narrow size distribution were obtained from miniemulsion polymerization (respective DLS curve can be found in Figure S2). The colloidal features of these precursor particles, ie, crosslinking density, size and size distribution, are then translated into the different amphiphilic NGs equally. Table 1 summarizes particles sizes and the respective standard deviation, as a measure for particle size dispersity (DLS curves are included in Figure S2). To further demonstrate the similarity in colloidal features between precursor particles and the amphiphilic NGs, TEM images of PPFPMA and NGs were compared (TEM images and statistical evaluations of PPFPMA precursors and CHOLA-20 NGs as representative samples for the amphiphilic NGs are included in Figure S3). Following this approach (Figure 1A), we now have access to a library of comparable NGs with varying network composition, including a hydrophilic NG (PHPMA) and four different amphiphilic NGs (Figure 1B) with each containing 80 mol-% hydrophilic HPA in combination with 20 mol-% of a specific hydrophobic group, ie, benzylamine (BENZA-20), hexylamine (HEXA-20), an amine-functionalized cholesteryl (CHOLA-20) or dodecylamine (DODA-20). Having demonstrated equal molar incorporation of the specific hydrophobic groups (20 mol-% each), we assessed hydrophobicity of the different NGs. First, the logarithmic partition coefficients (logP) of the resulting hydrophilic/hydrophobic methacrylamide repeating units on the network copolymer were calculated allowing for a first classification of the five NGs into three groups: 1) hydrophilic, 2) moderate hydrophobic and 3) hydrophobic (Figure 1B). The hydrophilic group only contains PHPMA (logP =1.52) while BENZA-20 (logP =3.18) and HEXA-20 (logP =4.23) were assigned to the moderately

hydrophobic NGs. DODA-20 (logP =7.26) and CHOLA-20 (logP =8.86) represent the hydrophobic NGs.

To reinforce these theoretical values, the hydrophobicity of each NG was examined by static contact angle measurements using the sessile drop method. However, as contact angle measurements on dried NP films could be misleading due to capillary forces at interparticulate cavities,[45] the measurements were carried out on linear polymer analogs, confirming the above-described classification (Figure 2). The hydrophilic PHPMA (Figure 2A) has a contact angle of θ 23±2°. BENZA-20 (Figure 2B) and HEXA-20 (Figure 2C) of the moderate hydrophobic group showed θ 70±3° and θ 76±1°, respectively. The largest contact angles were found for the members of the hydrophobic group, ie, CHOLA-20 (Figure 2D) and DODA-20 (Figure 2E) with θ 80±1° and θ 92±1°.

In addition, loading and release experiments with Nile red as hydrophobic model cargo have been carried out previously to determine the influence of the polymer composition on the internal network hydrophobicity.[12] The incorporation of 20 mol-% of hydrophobic groups increased the loading capacity in the order: BENZA-20<HEXA-20<DODA-20<CHOLA-20. The loading capacity of CHOLA-20 was increased threefold compared to PHPMA while the corresponding release rate was significantly reduced.[12] These results not only fortify the classification based on hydrophobicity but also demonstrate the high potential of the amphiphilic NGs as nanocarriers for hydrophobic compounds. However, for evaluating the therapeutic potential the interactions of the NGs with biological systems should be determined next.

Increasing hydrodynamic diameters of the NGs upon incubation in physiological medium as assessed via comparative DLS measurements already indicate formation of protein coronas. Table 1 summarizes the size increases as differences of the hydrodynamic diameters in CCM and MQ (Δd_h), which is also graphically depicted in Figure 3. Size increases are largely consistent with reported changes due to protein corona formation.[46] In addition, the zeta potential in MQ and PBS was determined (Table 1). Neutral to slightly negative values in MQ and PBS suggest that colloidal stability of the NGs can mainly be attributed to neutral PHPMA segments on the particle surface.

Biocompatibility of NGs

PHPMA, which is the main component (80 mol-%) of the amphiphilic NGs, is known to be biocompatible.[42,47]
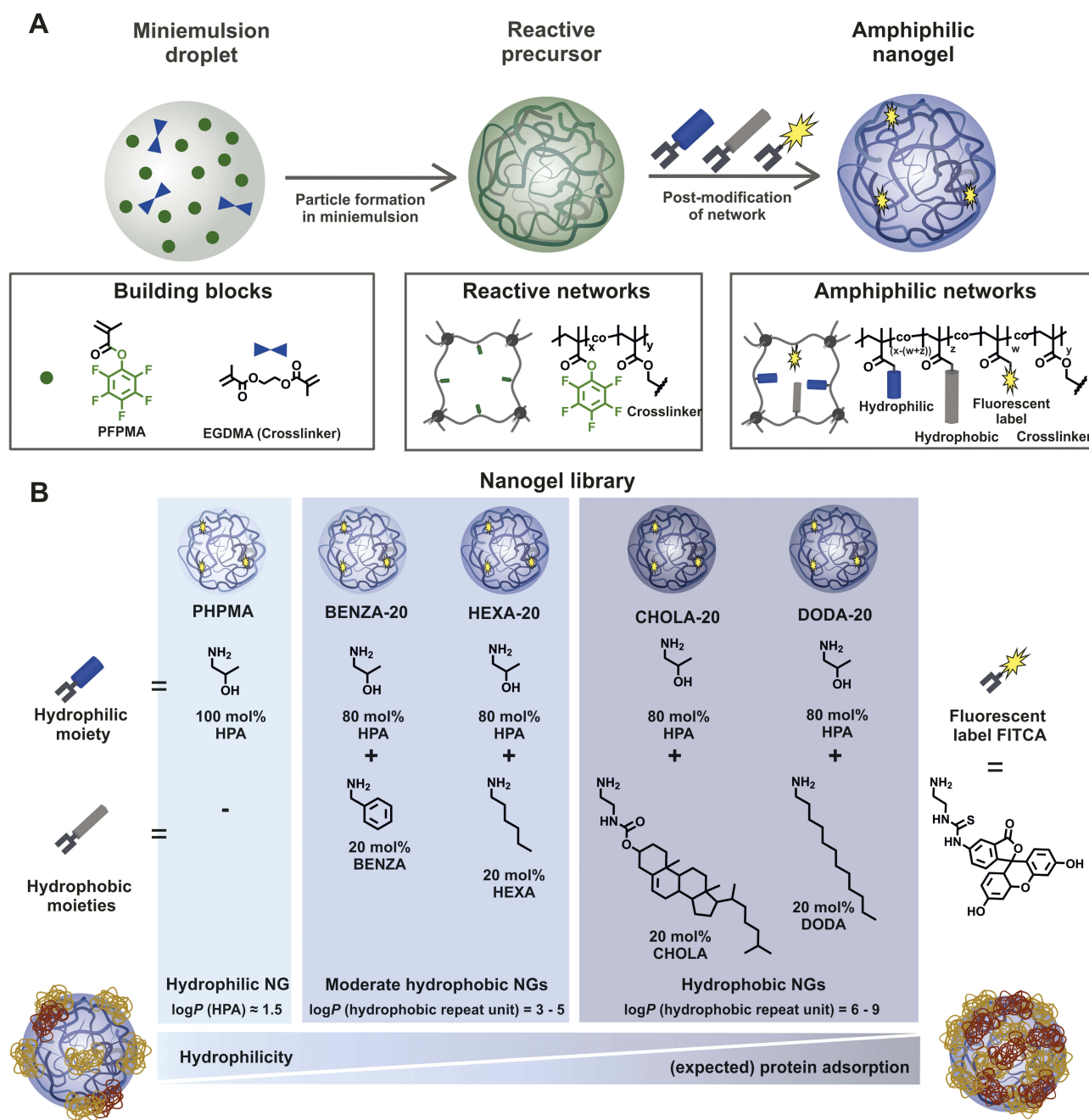
Figure 1 A reactive precursor particle approach gives access to a NG library with varying hydrophobicity and similar colloidal features.

Notes: Schematic synthesis of the NGs is depicted (**A**) based on precursor particles being subsequently amine functionalized (**B**). We used HPA that translates to PHPMA and four modified variants that each contained 80 mol-% HPA and 20 mol-% of a different hydrophobic group, ie hexylamine (HEXA-20), benzylamine (BENZA-20), linear dodecylamine (DODA-20) as well as an amine functionalized cholesteryl group (CHOLA-20).

Abbreviations: NG, nanogel; NGs, nanogels; HPA, 2-hydroxypropylamine; PHPMA, poly(N-(2-hydroxypropyl)methacrylamide); FITCA, amine functionalized fluorescein; EGDMA, ethylene glycol dimethacrylate.

However, the amphiphilic networks also contain additional 20 mol-% of hydrophobic groups, which may influence the interaction of the NGs with lipid membranes and cause some toxicity. Previously, we have already demonstrated that amphiphilic NGs with varying amphiphilicity showed no cytotoxic effect on normal human keratinocytes, suggesting good biocompatibility.[12] Reasoned by the fact that monocytes are a main component of the RES, we assessed the biocompatibility in the monocytic like human cell line THP-1 (Figure 4). All NGs were found to be biocompatible, which is in line with our previous study.
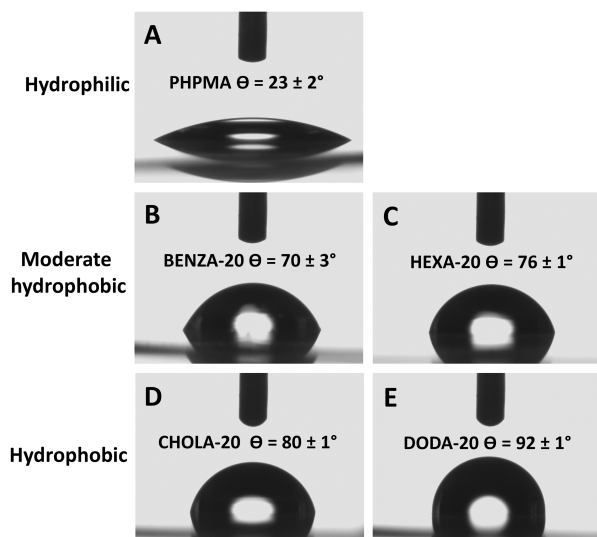
Figure 2 Contact angle measurement allows for the categorization of the NGs.
Notes: We could differentiate three groups: with PHPMA (**A**) as hydrophilic, BENZA-20 (**B**) and HEXA-20 (**C**) as moderate hydrophobic and CHOLA-20 (**D**) and DODA-20 (**E**) as hydrophobic.
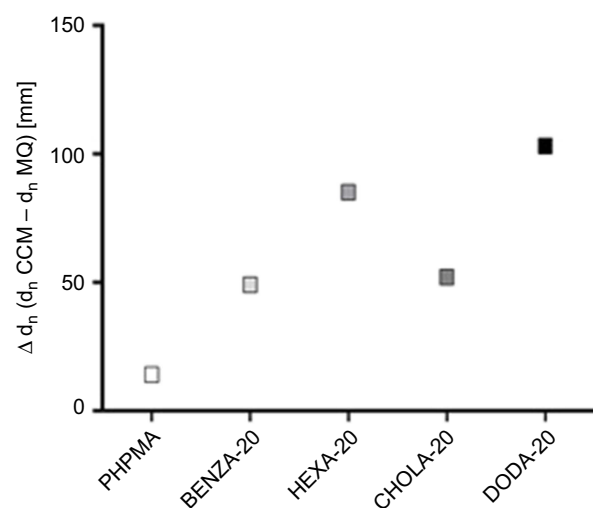**Abbreviations:** NGs, nanogels; PHPMA, poly(N-(2-hydroxypropyl)methacrylamide).

Figure 3 Illustration of size differences (Δd_h) between incubation of NGs in MQ and CCM.
Notes: NGs were dispersed in MQ and CCM by vortexing, followed by 30 min sonication at RT. DLS was performed after 2 hrs.
Abbreviations: NGs, nanogels; MQ, ultrapure water; CCM, complete cell culture medium (RPMI 1640 containing 10% FBS); RT, room temperature; DLS, dynamic light scattering; PHPMA, poly(N-(2-hydroxypropyl)methacrylamide).

Investigation of protein corona of NGs by 2DE

To further investigate the protein corona that is suggested by the observed size increase by DLS measurements in CCM, the protein binding of all NGs was examined using 2DE. The resulting 2D gel images obtained after 30 min incubation in CCM revealed significant qualitative and
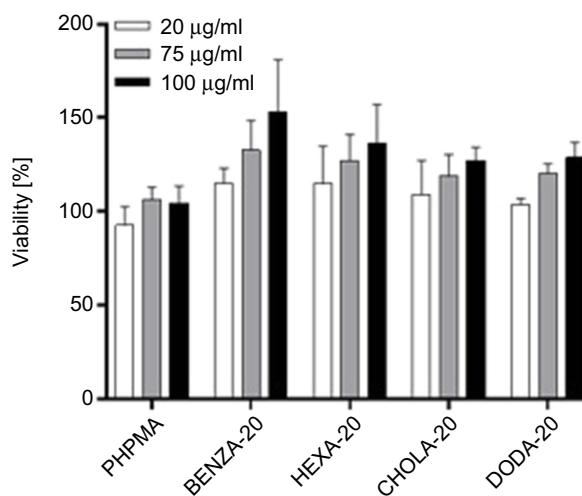

Figure 4 Viability of monocytic like THP-1 cells shows good biocompatibility of the NGs with different network hydrophobicities.
Notes: Depicted are mean values of three biological repeats and standard error of mean (SEM).
Abbreviation: NGs, nanogels.

quantitative differences between the coronas of all NGs. Each NG displayed a unique and individual spot pattern (Figure 5, Figures S4A–E), where also the amount and intensity of spots varied significantly. While the hydrophilic NG PHPMA showed the lowest number of protein spots, considerable increased spot numbers were observed with increasing hydrophobicity. Hence, the protein binding was far less prominent for PHPMA (Figure 5A) compared to all other NGs. In particular, when compared to the moderate hydrophobic NG BENZA-20 (Figure 5B) and the hydrophobic DODA-20 (Figure 5C), the observed increase in spot number and intensity supports the assumption of an increased protein binding with increased hydrophobicity. The spot patterns of all NGs were analyzed and compared to PHPMA, serving as a benchmark. All protein spots with significantly increased intensity compared to PHPMA (ie, intensity increased >1.5, $p<0.05$, n=3) were taken into account. Largest differences were found for one of the most hydrophobic NGs, ie DODA-20, where in total 49 significantly increased protein spots compared to PHPMA were detected (Figure 5D). Concerning the number of spots being different from PHPMA the NGs can be ranked as such: DODA-20>CHOLA-20=BENZA-20>HEXA-20.

Protein binding patterns between the two hydrophobic NGs showed a high degree of similarity, ie, DODA-20 and CHOLA-20 had 16 protein spots in common. Whereas DODA-20 had only 11 and 6 spots in common with the moderate hydrophobic NGs BENZA-20 and HEXA-20,
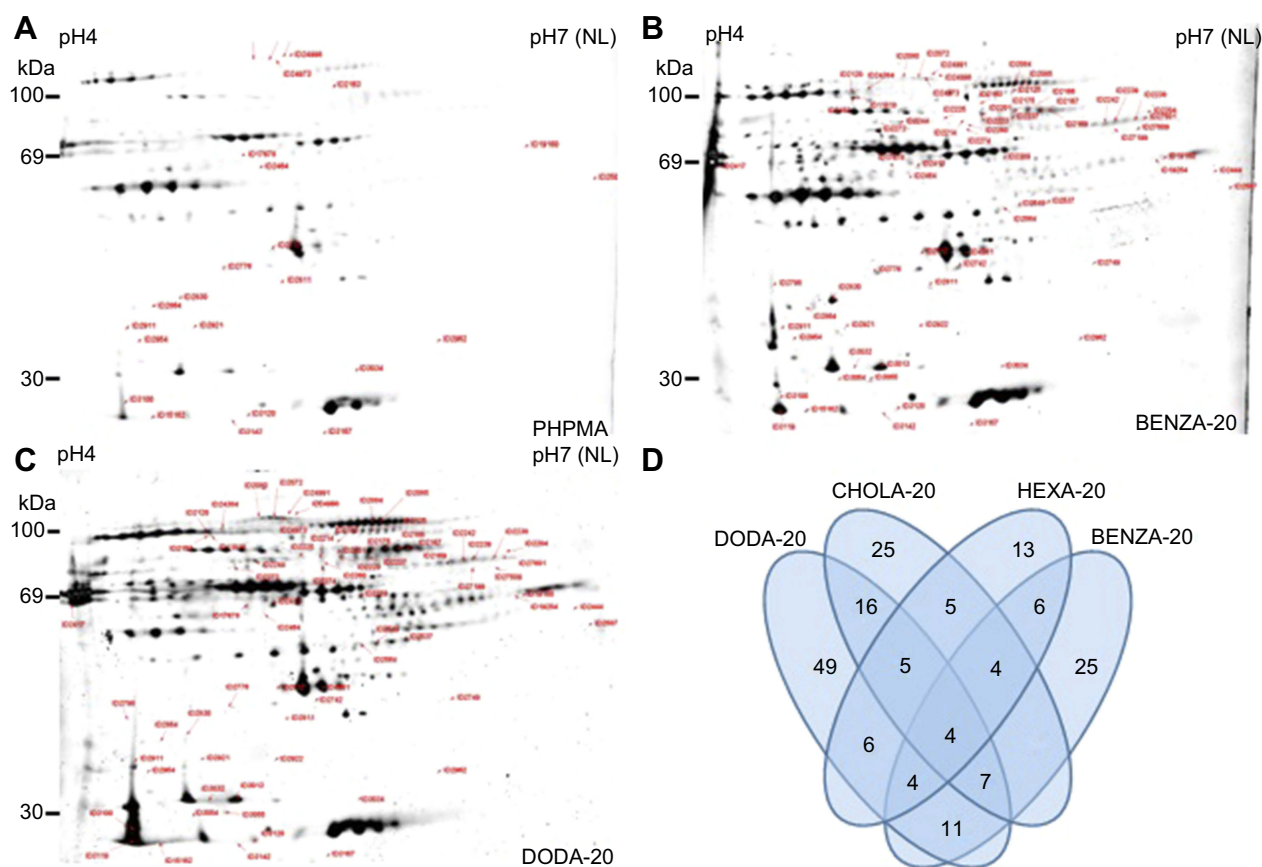
Figure 5 Differences in the protein coronas are illustrated using the spot patterns of the obtained 2DE analysis from representative NGs.
Notes: NGs (300 µg/mL) were incubated in CCM for 30 mins. Bound proteins were eluted and analyzed using 2DE analysis. Depicted are the resulting representative 2D gels for (**A**) PHPMA, (**B**) BENZA-20 and (**C**) DODA-20. All other 2D images are depicted in Figure S4. In comparison to blank control (no NGs), labels indicate significantly modified proteins within the respective NGs. Similarities and differences regarding the number of significant spots (ie, intensity increased >1.5, $p<0.05$, n=3) in each corona relative to PHPMA as a benchmark are visualized in a Venn diagram (**D**).
Abbreviations: 2DE, two-dimensional gel electrophoresis; NGs, nanogels; CCM, complete cell culture medium (RPMI 1640 containing 10% FBS); PHPMA, poly(N-(2-hydroxypropyl)methacrylamide).

respectively. Similarities and differences in the protein coronas are visualized in a Venn diagram based on the spot numbers (Figure 5D). It becomes obvious that the number of significant spots follows roughly the same trend as the NG hydrophobicity. When comparing the two NGs within the respective group (ie, moderate hydrophobic and hydrophobic), it is remarkable that the slightly less hydrophobic NG in the respective cluster each has a higher number of pronounced spots. This suggests that the formation and composition of the protein corona is not only dependent on the overall hydrophobicity but may also depend on the molecular structure of the hydrophobic groups.

Identification of the corona proteins via LC-MS/MS

Having demonstrated qualitative differences in the protein corona, quantitative investigations of protein binding were conducted using LC-MS/MS using the Top 3 approach (Table S3). Again, DODA-20 showed the highest protein binding, while all the other NGs showed similar protein binding (Figure 6). Interestingly, total bound protein does not necessarily match with the total number of different proteins identified in each corona. This can occur when a single protein binds to a NG with an increased amount, while several proteins bind to another NG in smaller amounts. For example, the highest number of different individual proteins was found in HEXA-20 (Table 2) where 111 different proteins could be identified, while slightly fewer proteins (105) could be identified on DODA-20, despite the far higher amount of total bound proteins.

In order to address this context more precisely, the next step was to compare the specific composition of the protein coronas of the NGs with each other. Figure 7 shows the summary of the 15 most abundant proteins across all
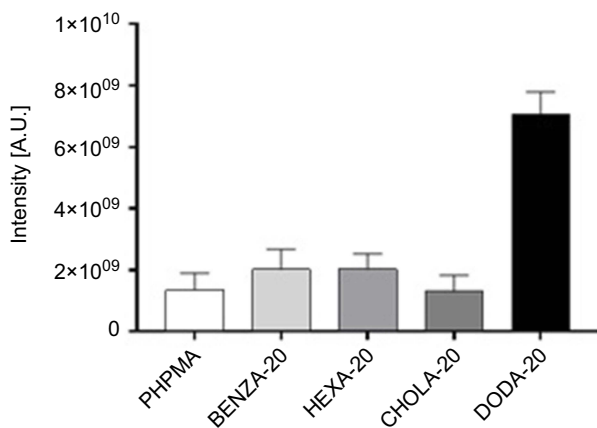
Figure 6 Comparison of the amount of bound proteins in the corona of the respective NGs using the Top 3 approach.

Notes: Proteins in the NG coronas were identified using LC-MS/MS and abundancies were determined using the Top 3 approach. The intensity for each protein is obtained by summing up the intensities of the three most intense unique peptides for that protein. Based on that, total protein intensities for each NG were determined.

Abbreviations: NGs, nanogels; LC-MS/MS, liquid chromatography-tandem mass spectrometry; A.U., arbitrary unit; PHPMA, poly(N-(2-hydroxypropyl) methacrylamide).

NGs, which make up at least 78% of the total coronas. As our NGs only differ in hydrophobicity while colloidal properties are largely similar, we can directly observe the influence of hydrophobicity on the protein corona composition. By applying a uniform color scheme, differences in the corona composition can be easily visualized. It is quite self-evident that the NGs have different influences on the corona compositions. We also wanted to investigate whether our groups (moderate hydrophobic and hydrophobic) are similar with regard to their protein corona. Therefore, the obtained protein intensities of the Top 3 approach were used. We compared the composition of the different protein coronas of each NG relative to PHPMA. As a result, a classification of the respective protein into

the group, increased or decreased compared to PHPMA, could be made. The results of the NGs with BENZA-20 and HEXA-20 as representatives of the moderate hydrophobic and CHOLA-20 and DODA-20 as members of the hydrophobic group were then compared. The visualization is depicted as cluster analysis (Figure 8) and clearly shows the increased (red) and decreased (green) proteins of the respective corona compared to PHPMA. The protein coronas of DODA-20 and CHOLA-20 are very similar to each other and distinctly distinguishable to the coronas of BENZA-20 and HEXA-20. This can be seen by the very similar color pattern. The majority of proteins (one box each) display the same behavior with respect to increased or decreased intensity compared to PHPMA within the hydrophobic group. Thus, the hydrophobicity of the individual NGs seems to act as an important factor for the composition of the protein corona.

Subsequently, we were able to detect a number of different proteins that were significantly reduced (factor <0.5) or increased (factor >1.5) regarding their intensities compared to PHPMA (Table 2). Protein intensities were normalized using PHPMA as a reference, log(2) transformed and the Z-score was calculated. Profiles of altered proteins were then compared between the two groups of amphiphilic NGs (moderate hydrophobic group versus hydrophobic group). We found proteins that behaved alike, eg, being rather low in intensity on the moderate hydrophobic NGs (BENZA-20 and HEXA-20) and increased on the hydrophobic ones (CHOLA-20 and DODA-20) or vice versa (Figure 9A and B, Table 3). For example, proteins such as pentraxin, complement factor I and complement factor B (Figure 9C–E) bound stronger to the more hydrophobic NGs (DODA-20 and CHOLA-20). Apolipoprotein E and serum albumin, on

Table 2 Overview on number of corona proteins identified via LC-MS/MS compared to the hydrophilic NG PHPMA

Nanogels		Number of identified proteins in the corona		
Type	Sample	Total (specific for this corona)	Comparison to PHPMA	
			Decreased (intensity factor <0.5)	Increased (intensity factor >1.5)
Moderate hydrophobic	BENZA-20 HEXA-20	88 (1) 111 (4)	18 19	32 62
Hydrophobic	CHOLA-20 DODA-20	104 (4) 105 (4)	9 11	62 58

Notes: Given is the total number of all identified proteins for the respective NG (total). The number of proteins found only on this NG is given in brackets. The number of proteins with a lower (<0.5) or higher (>1.5) intensity compared to PHPMA are listed in the following columns.

Abbreviations: LC-MS/MS, liquid chromatography-tandem mass spectrometry; NG, nanogel.
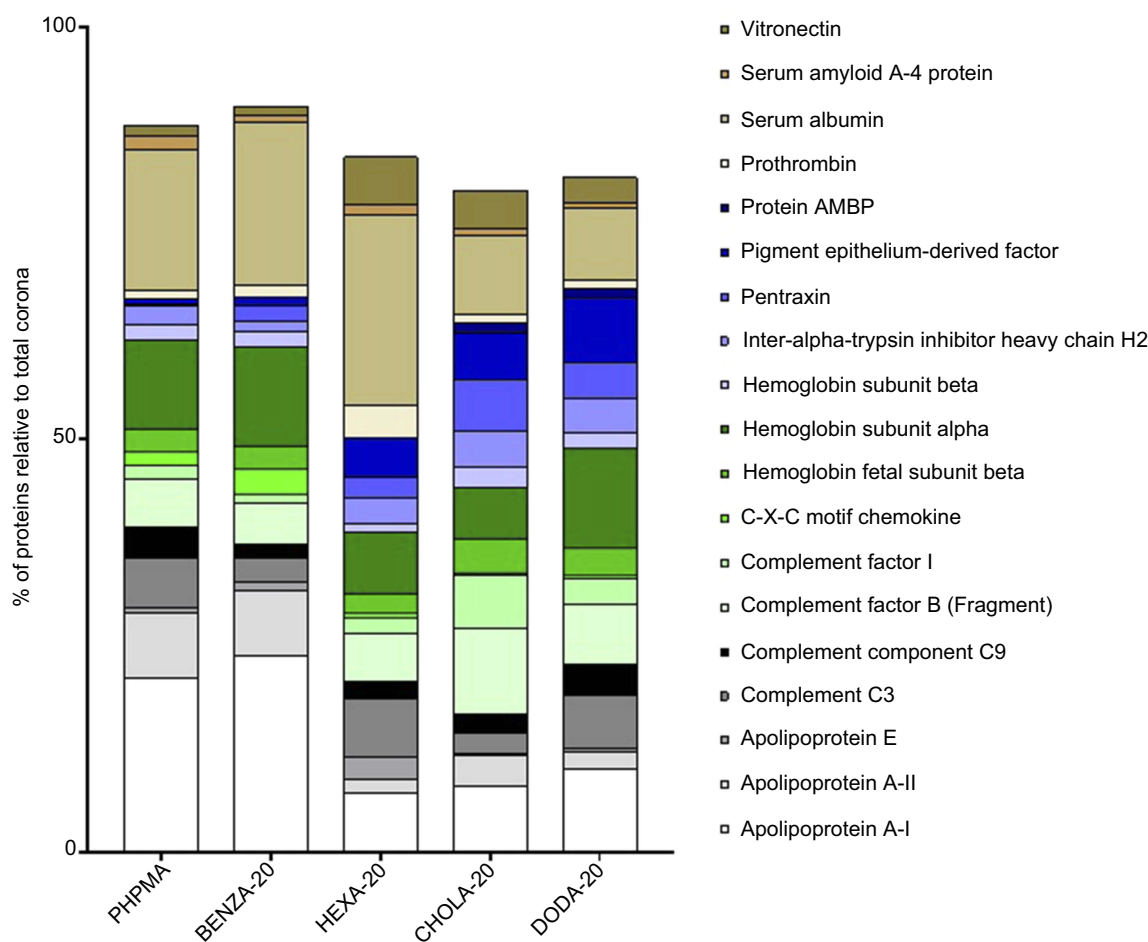
Figure 7 Impact of the various NGs upon the relative distribution of the most abundant proteins among all protein coronas.
Notes: Depicted are the 15 most abundant proteins of each single protein corona (summarized overall), which were identified via LC-MS/MS and relative percentages were calculated using the Top 3 approach. Results for each protein are given in percentage of the total bound proteins in that corona. Remaining proteins (residual % up to 100) are not depicted.
Abbreviations: NGs, nanogels; LC-MS/MS, liquid chromatography-tandem mass spectrometry; PHPMA, poly(N-(2-hydroxypropyl)methacrylamide).
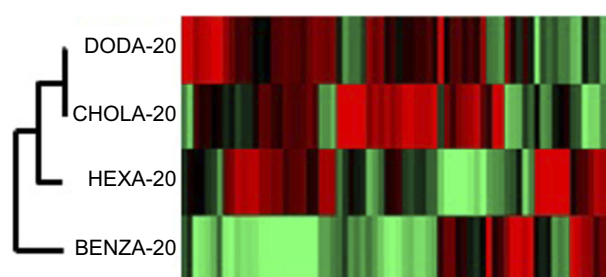

Figure 8 Cluster analysis for comparison of the NG corona proteins shows the grouping of the NGs regarding similarity within the protein corona.
Notes: Similarities and differences in the protein coronas of the NGs are visualized using a HCA. Each protein (every rectangle stands for a different identified protein) is compared to PHPMA, which serves as a benchmark particle (values are normalized) and values are transformed into a heat map. Red shows a higher intensity and green a lower intensity compared to PHPMA.
Abbreviations: NGs, nanogels; HCA, hierarchical cluster analysis; PHPMA, poly (N-(2-hydroxypropyl)methacrylamide).

the other hand, were found in much lower amounts (Figure 9F and G). Thus, we can conclude that the hydrophobicity

of the NGs significantly influenced the amount and the identity of proteins in the corona.

Cellular uptake of NGs

Finally, we investigated how changes in protein binding are reflected by an altered cellular uptake in THP-1 cells. For this, we used analogous amphiphilic NGs but containing covalently attached FITC as fluorescent label, which facilitated easy quantification using flow cytometry based on a methodology recently established.[48] The respective NGs are denoted as PHPMA-FITC, BENZA-20-FITC, HEXA-20-FITC, DODA-20-FITC and CHOLA-20-FITC. The physico-chemical characterization of the FITC-labeled NGs is summarized in Table 4. NGs were pre-incubated for 2 hrs in CCM such that a protein corona can form and were then incubated with THP-1 cells for 2 hrs. Figure 10 shows clear variations in the cellular uptake with PHPMA-FITC being
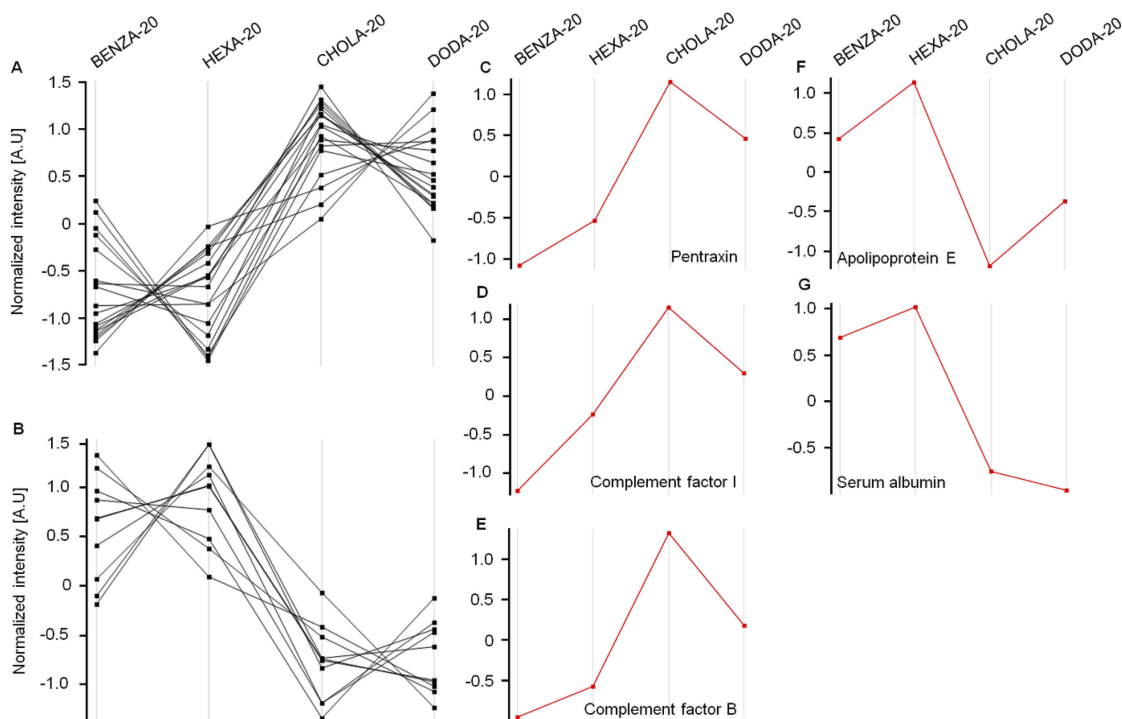
Figure 9 The comparison, with regard to their intensities, of normalized expression profiles of the identified corona proteins supports the grouping of the investigated NGs.
Notes: Protein intensities were normalized (PHPMA as reference), log(2) transformed and the Z-score was calculated using Perseus Version 1.6.1.3. The expression profiles were then examined for similarities. With increasing hydrophobicity, corona proteins of the two groups of NGs, namely moderate hydrophobic (BENZA-20+HEXA-20) and hydrophobic (DODA-20+CHOLA-20), display either an increase (**A**) or a decrease (**B**) in their expression profiles. Pentraxin (**C**), complement factor I (**D**) and complement factor B (**E**) are depicted as examples for proteins with an increased intensity among the hydrophobic NGs compared to the moderately hydrophobic NGs. Apolipoprotein E (**F**) and serum albumin (**G**) on the other hand show a decreased intensity among the hydrophobic NGs compared to the moderate NGs.
Abbreviations: NGs, nanogels; A.U., arbitrary unit; PHPMA, poly(N-(2-hydroxypropyl)methacrylamide).

taken up least, while the more hydrophobic NGs, ie, CHOLA-20-FITC, showed an enhanced uptake. All four NGs were significantly ($p<0.0005$) increased in uptake compared to the control NG PHPMA-FITC. Furthermore, it was observed that the uptake of the hydrophobic NG CHOLA-20-FITC in THP-1 cells compared to both moderate hydrophobic NGs (BENZA-20-FITC and HEXA-20-FITC) is also significantly ($p<0.0005$) increased. For the second representative of the hydrophobic group, DODA-20-FITC, this was only the case in comparison to BENZA-20-FITC ($p<0.0005$). These results correlate well with the increased amount of protein adsorption and demonstrate that increasing hydrophobicity led to an increase in cellular uptake in THP-1 cells, emphasizing the correlation between protein corona and cellular uptake.

Discussion

Here, we investigated protein binding, biocompatibility and cellular uptake of amphiphilic NGs. This new family of NGs is based on a cross-linked amphiphilic copolymer network allowing for solubilization of hydrophobic drugs in the interior. As previously shown, network hydrophobicity can be

modified to accurately tailor loading and release profiles,[12] demonstrating the high potential of these new carriers for medical applications. However, accurately determining their therapeutic potential requires a more detailed investigation of the interactions of the NGs with biological systems. In particular, the adsorbed protein corona is of importance as this links to rapid blood clearance and limits the therapeutic potential of the NGs.

We prepared a library of well-defined amphiphilic NGs with varying hydrophobicity (Figure 1) but similar colloidal features, ie, crosslinking density, size, size distribution, thus enabling true comparability between different NGs. Even though polydispersity can play a role in interaction of particles with biological systems, our concept allows the reduction of this effect to a systematic influence that is assumed to contribute to all samples equally. As can be seen in Table 1, only slight deviations in particle sizes and size distributions of NGs can be observed, which are within the margin of error for DLS. Only the hydrophilic PHPMA NG is larger than the hydrophobically modified ones. This is suggested to stem from a higher network hydration, resulting in a greater extent of swelling. The monocytic like human cell line THP-1 was

Table 3 Comparative assessment of protein coronas

Expression pattern	Protein	Accession number
A Increased protein adsorption with increasing hydrophobicity of the NGs	Complement factor B (Fragment)	Q3KUS7
	Pentraxin	C4T8B4
	Haemoglobin fetal subunit beta	P02081
	Complement factor I	F1N4M7
	Haemoglobin subunit beta	P02070
	Plasma serine protease inhibitor	Q9N2I2
	Haptoglobin (Zonulin)	Q2TBU0
	Thrombospondin-1	Q28178
	Alpha-2-macroglobulin	Q7SIH1
	Apolipoprotein B	E1BNR0
	Histidine-rich glycoprotein	F1MKS5
	Alpha-1-antiproteinase	P34955
	Alpha-1B-glycoprotein	Q2KJF1
	Actin, cytoplasmic 2	P63258
	Uncharacterized protein (F1MI18)	F1MI18
	Hemopexin	Q3SZV7
	Coagulation factor XII	P98140
	Fetuin-B	Q58D62
B Decreased protein adsorption with increasing hydrophobicity of the NGs	Serum albumin	A0A140T897
	Prothrombin	P00735
	Serum amyloid A-4 protein	Q32L76
	Apolipoprotein E	Q03247
	Alpha-fetoprotein	Q3SZ57
	ApoN protein	Q2KIH2
	Carboxypeptidase B2	Q2KIG3
	Apolipoprotein C-IV	Q3SYR5
	ECM1 protein	A5PJT7
	Alpha-2-antiplasmin (Alpha-2-AP)	P28800

Notes: The intensities of the adsorbed corona proteins identified by LC-MS/MS were normalized and the Z-score was determined with Perseus (Version 1.6.1.3). Proteins with increasing (A) or decreasing (B) profiles depending on the hydrophobicity of NGs have been grouped and are shown here.
Abbreviations: LC-MS/MS, liquid chromatography-tandem mass spectrometry; NGs, nanogels.

chosen as a cell model, as monocytes are a main component of the RES being responsible for fast uptake and clearance. At first, biocompatibility was assessed as amphiphilicity may represent a risk factor due to unfavorably interactions with lipid membranes.[49,50,51] All NGs were highly biocompatible (Figure 4), which is in line with our previous experiments on normal human keratinocytes.[12] The increased viability of the cells to more than 100% can be attributed to several factors. It may also indicate a general possible influence of NPs on colorimetric assays[52] or also on the mitochondrial reductase system. However, these experiments strengthen our assumption that the highly hydrophilic nature of PHPMA as the main network component translates to the amphiphilic NGs and ensures good biocompatibility.

Next, we focused on the determination of protein binding in physiological fluids as the resulting protein corona determines the biological identity of the NGs in vivo.[53,54]

Protein adsorption is largely determined by surface charge and hydrophobicity.[17,55] Our study confirmed that similarities in protein binding profiles were well correlated with the estimated hydrophobicity of the NGs. The increase of hydrodynamic diameters (Table 1 and Figure 3) indicates differences in corona formation with varying NG hydrophobicity. While the truly hydrophilic PHPMA NG shows only a marginal size increase, the more hydrophobic NGs show significantly increased sizes, suggesting increased protein adsorption. These findings correlate very well with the results from 2DE (Figure 5, Figures S4A–E), confirming a significantly increased number and intensity of spots for the moderate hydrophobic NG BENZA-20 and the hydrophobic NG DODA-20 compared to PHPMA. Similar results were obtained by LC-MS/MS investigations (Figure 6), showing an increase of protein adsorption for the hydrophobic NG DODA-20. While similar trends
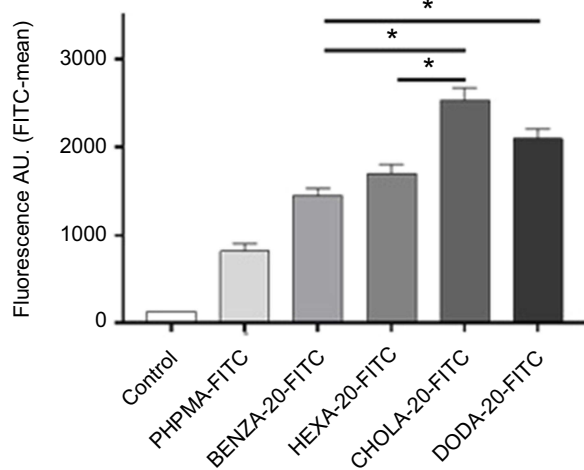
Figure 10 Flow cytometry data reveal a correlation between the uptake of NGs in human monocytic like THP-1 cells and the hydrophobicity of NGs.
Notes: NGs were pre-incubated for 2 hrs with CCM containing 10% FBS. After 2 hrs of incubation with THP-1 cells in an incubator (37°C, 5% CO_2) uptake was measured using flow cytometry. Mean fluorescence values including SEM (n=3 biological repeats) as bars with significance (*$P<0.0005$) are depicted. All four NGs were significantly ($p<0.0005$) increased in uptake versus the control PHPMA (not depicted).
Abbreviations: NGs, nanogels; CCM, complete cell culture medium (RPMI 1640 with 10% FBS); SEM, standard error of mean; A.U., arbitrary unit; PHPMA, poly(N-(2-hydroxypropyl)methacrylamide).

have been observed for other NP systems,[17,18] our study revealed that for NGs with comparable hydrophobicity but different functional hydrophobic moieties (ie, BENZA-20 vs HEXA-20 and DODA-20 vs CHOLA-20) the increase in protein adsorption varied significantly. This becomes especially obvious by comparing DODA-20 and CHOLA-20. Even though both hydrophobic repeating units in the network show similar logP-values (7.3 and 8.9), the size increase for DODA-20 was double (Δs=100 nm) compared to CHOLA-20 (Δs=50 nm) and intensity of total bound proteins was almost four times higher for DODA-20 compared to CHOLA-20 (Figure 6). Thus, protein binding does not appear to be governed by overall hydrophobicity alone, but is influenced by the molecular structure, as well.

We also examined the quantitative composition of the protein coronas, which typically is unique for different particles.[56] However, it is assumed that specific protein binding profiles also share commonalities that may result in similar biological consequences. It is of high interest to identify specific particle characteristics that define the occurrence of particular protein corona commonalities, which in turn will help to determine a well-defined biological response. Here we focused on the influence of NG network composition (and corresponding surface hydrophobicity) on the process of opsonization, which is

responsible for removal of the particles by uptake into cells of the RES. This is mediated by binding of specific proteins, called opsonins. While there are also opsonins triggering hemolysis and thrombogenicity, adsorption of opsonins belonging to the complement system leads to rapid clearance of NPs from the systemic blood cycle via complement receptor-mediated phagocytosis.[57]

Thus, we focused on correlating network hydrophobicity with adsorption of these types of opsonins. Up to now, this task was highly challenging since varying the network hydrophobicity also resulted in changes to the colloidal features which can also cause changes in protein adsorption profiles. Our synthetic platform approach, which generates well-defined NGs with similar colloidal features, represents a unique opportunity to systematically study the influence of network composition of protein binding.

Interestingly, we found a higher overlap among the hydrophobic NGs. Among the protein spots that were significantly increased in intensity (2DE, Figure 5D) compared to PHPMA (factor >1.5), the hydrophobic NGs CHOLA-20 and DODA-20 have a total of 16 spots in common. If we consider the group of the moderately hydrophobic NGs (BENZA-20 and HEXA-20), we only find six protein spots in common. Similarities between comparable structures (Figure 1B) are smaller. We find only six common protein spots in HEXA-20 and DODA-20 (linear moieties) and nine in BENZA-20 and CHOLA-20 (non-linear moieties). This suggests that the NG hydrophobicity has a greater influence on the corona composition than, for example, the structure. This relationship is also evident in the cluster analysis of the protein corona (Figure 8), which confirms an increased similarity between the hydrophobicities of the NGs than between similar structures, strengthening the impression from the 2D gels.

For a deeper understanding, we took a closer look at the 15 most abundant proteins for each corona (Figure 7). We identified proteins with different adsorption characteristics in the group of the moderate hydrophobic NGs (BENZA-20 and HEXA-20) compared to the hydrophobic group (CHOLA-20 and DODA-20). To improve visualization, we normalized the expression profiles of the intensities of the proteins to the reference particle PHPMA (Figure 9). The increase (Figure 9A) or decrease (Figure 9B) of protein adsorption with increasing hydrophobicity is now clearly visible. Interestingly, we found an enrichment of complement activation components such as pentraxin (Figure 9C), complement factor I (Figure 9D) and B (Figure 9E) for the most hydrophobic NGs, ie, CHOLA-20 and DODA-20. In comparison, the moderate hydrophobic NGs BENZA-20

and HEXA-20 show lower binding of these complement activation factors. Pentraxins are plasma proteins with a pentameric structure that serve as recognition molecules for foreign substances (eg, antigens) and label them for activation of the innate immune system. They also interact with the classical cascade of the complement system through binding of complement component 1q (C1q) as well as Fc receptors to activate immune responses.[58] With complement factors I and B two other interesting candidates were found in the corona of the hydrophobic NGs. Complement factor I plays a role in the regulation of the complement cascade, while complement factor B is involved in the activation of the alternative pathway of complement activation.[59,60] These opsonin corona components could drastically reduce blood retention time and thus the biological half-life, hampering medical application.

Since CHOLA-20 and DODA-20 NGs contain several components of this complement system in their protein coronas, we expect that these NGs will be cleared much faster compared to the moderate hydrophobic NGs BENZA-20, HEXA-20 and the hydrophilic PHPMA NG. Indeed, this expectation is supported by our cell uptake experiments. We could clearly show that increasing hydrophobicity and the resulting specific adsorption of opsonins leads to an increased cellular uptake in human monocytic like THP-1 cells (Figure 10). This is in line with other reports, showing that in general an increased hydrophobicity often leads to a much faster uptake of NPs.[13,17,24] In our study, we were able to demonstrate that the protein adsorption also crucially depends on the molecular structure of the respective functional hydrophobic groups. As demonstrated for CHOLA-20 and DODA-20 NGs of comparable hydrophobicity (logP around 7–8), the amount of protein adsorption varied significantly. However, composition of the protein coronas showed commonalities, translating to a similar cellular uptake. Our platform approach resulting in NGs with varying hydrophilicity but comparable colloidal features allowed the accurate identification of this difference in protein binding patterns on the molecular composition of amphiphilic NGs for the first time. These results show the importance of not only tuning drug delivery vehicles with respect to one aspect (eg, high loading capacities) but rather investigating them in their entirety to account for opposing effects. For the amphiphilic NGs used here, this means the hydrophilic/hydrophobic balance needs to be accurately adjusted to enable high drug loading and desirable release kinetics while providing an optimum biological half-life.

Conclusion

In this study, amphiphilic NGs with tuneable hydrophobicity but similar colloidal features were used to systematically examine the influence of network composition and hydrophobicity on the interactions with biological systems. We investigated not only biocompatibility and protein binding but also cellular uptake of the NGs in human monocytic like THP-1 cells. It could be shown that increasing network hydrophobicity increases interactions with proteins. For example, DODA-20, as one of the most hydrophobic representative NGs used in this study, showed a much higher protein intensity in LC-MS/MS compared to PHPMA, being the most hydrophilic NGs. Strikingly, it was also observed that for DODA-20 and CHOLA-20 NGs of similar hydrophobicity, significant differences in the amount of adsorbed proteins could be detected. This suggests a strong additional influence of the molecular structure of the hydrophobic groups on protein binding. This was confirmed as well using 2DE gels.

In addition to these qualitative investigations, quantitative studies showed that the composition of the protein corona also varied in dependence on the hydrophobicity. Specifically, a higher amount of opsonins was determined for the protein coronas of the hydrophobic NGs CHOLA-20 and DODA-20 compared to the moderate NGs BENZA-20 and HEXA-20 as well as to the hydrophilic NG PHPMA. These findings correlated well with the increased uptake of these NGs into THP-1 cells. Thus, hydrophobicity and molecular structure of the respective hydrophobic groups not only influenced protein binding (both qualitative and quantitative), but also the interactions of the NGs with cells of the RES. Therefore, these results, together with our recent investigation on the loading and release of a hydrophobic model compound, allow the design of optimal drug carriers systems for hydrophobic drugs. For this, the nanocarrier's network amphiphilicity needs to be balanced with respect to maximum loading capacity on one side and low protein binding on the other side, resulting in an increased biological half-life. As an example, the moderate hydrophobic BENZA-20 NGs represent a compromise between the enhanced loading capacity compared to PHPMA NGs and moderate cellular uptake in monocytic THP-1 cells. To further exploit the benefits of CHOLA-20 NGs, namely high loading capacity and slow release kinetics, the protein binding should be reduced to gain an increased biological half-life. In this regard, amphiphilic NGs with a covalent bound PEG-shell will be synthesized for further studies.

Acknowledgments

The authors thank their institutions for supporting this project. Furthermore, we would like to acknowledge the assistance of the Core Facility BioSupraMol supported by the Deutsche Forschungsgemeinschaft (DFG). This work was supported by Bundesinstitut für Risikobewertung (BfR; SFP 1322-502) and by the Collaborative Research Center (CRC) 1112 with funding for instrumentation. We acknowledge additional financial support for consumables from Verband der Chemischen Industrie eV (VCI) and Focus Area Nanoscale of the Freie Universität Berlin. A Gruber especially thanks the CRC 1112 and Focus area Nanoscale for scholarships to finance her PhD.

Disclosure

The authors have no affiliation or financial involvement with any organization or entity with a financial interest. Andrea Haase reports grants from German Federal Institute for Risk Assessment, during the conduct of the study. The authors report no other conflicts of interest in this work.

References

1. Klinger D, Landfester K. Stimuli-responsive microgels for the loading and release of functional compounds: fundamental concepts and applications. *Polymer.* 2012;53(23):5209–5231. doi:10.1016/j.polymer.2012.08.053
2. Huh AJ, Kwon YJ. "Nanoantibiotics": a new paradigm for treating infectious diseases using nanomaterials in the antibiotics resistant era. *J Control Release.* 2011;156(2):128–145. doi:10.1016/j.jconrel.2011.07.002
3. Kar M, Fechner L, Nagel G, Glitscher E, Noe Rimondino G, Calderón M. Chapter 12 responsive nanogels for anti-cancer therapy. In: Vashist A, Kaushik AK, Ahmad S, Nair M, editors. *Nanogels for Biomedical Applications.* London: The Royal Society of Chemistry; 2018:210–260. doi:10.1039/9781788010481
4. Molina M, Asadian-Birjand M, Balach J, Bergueiro J, Miceli E, Calderón M. Stimuli-responsive nanogel composites and their application in nanomedicine. *Chem Soc Rev.* 2015;44(17):6161–6186.
5. Molina M, Wedepohl S, Miceli E, Calderon M. Overcoming drug resistance with on-demand charged thermoresponsive dendritic nanogels. *Nanomedicine (Lond).* 2017;12(2):117–129. doi:10.2217/nnm-2016-0308
6. Shatsberg Z, Zhang X, Ofek P, et al. Functionalized nanogels carrying an anticancer microRNA for glioblastoma therapy. *J Control Release.* 2016;239:159–168. doi:10.1016/j.jconrel.2016.08.029
7. Guo B, Zhao J, Wu C, et al. One-pot synthesis of polypyrrole nanoparticles with tunable photothermal conversion and drug loading capacity. *Colloids Surf B Biointerfaces.* 2019;177:346–355. doi:10.1016/j.colsurfb.2019.02.016
8. Wu C, Zhao J, Hu F, et al. Design of injectable agar-based composite hydrogel for multi-mode tumor therapy. *Carbohydr Polym.* 2018;180:112–121. doi:10.1016/j.carbpol.2017.10.024
9. Schulte B, Rahimi K, Keul H, Demco DE, Walther A, Möller M. Blending of reactive prepolymers to control the morphology and polarity of polyglycidol based microgels. *Soft Matter.* 2015;11(5):943–953. doi:10.1039/c4sm02116a

10. Tiwari R, Heuser T, Weyandt E, Wang B, Walther A. Polyacid microgels with adaptive hydrophobic pockets and ampholytic character: synthesis, solution properties and insights into internal nanostructure by cryogenic-TEM. *Soft Matter.* 2015;11(42):8342–8353. doi:10.1039/c5sm01327e
11. Wischke C, Kruger A, Roch T, et al. Endothelial cell response to (co) polymer nanoparticles depending on the inflammatory environment and comonomer ratio. *Eur J Pharm Biopharm.* 2013;84(2):288–296. doi:10.1016/j.ejpb.2013.01.025
12. Gruber A, Işık D, Fontanezi BB, Böttcher C, Schäfer-Korting M, Klinger D. A versatile synthetic platform for amphiphilic nanogels with tunable hydrophobicity. *Polym Chem.* 2018;9(47):5572–5584. doi:10.1039/C8PY01123K
13. Simon J, Wolf T, Klein K, Landfester K, Wurm FR, Mailander V. Hydrophilicity regulates the stealth properties of polyphosphoester-coated nanocarriers. *Angew Chem Int Ed Engl.* 2018;57(19):5548–5553. doi:10.1002/anie.201800272
14. Aggarwal P, Hall JB, McLeland CB, Dobrovolskaia MA, McNeil SE. Nanoparticle interaction with plasma proteins as it relates to particle biodistribution, biocompatibility and therapeutic efficacy. *Adv Drug Deliv Rev.* 2009;61(6):428–437. doi:10.1016/j.addr.2009.03.009
15. Cedervall T, Lynch I, Foy M, et al. Detailed identification of plasma proteins adsorbed on copolymer nanoparticles. *Angew Chem Int Ed Engl.* 2007;46(30):5754–5756. doi:10.1002/anie.200700465
16. Cedervall T, Lynch I, Lindman S, et al. Understanding the nanoparticle-protein corona using methods to quantify exchange rates and affinities of proteins for nanoparticles. *Proc Natl Acad Sci U S A.* 2007;104(7):2050–2055. doi:10.1073/pnas.0608582104
17. Gessner A, Waicz R, Lieske A, Paulke BR, Mäder K, Müller RH. Nanoparticles with decreasing surface hydrophobicities: influence on plasma protein adsorption. *Int J Pharm.* 2000;196(2):245–249.
18. Lindman S, Lynch I, Thulin E, Nilsson H, Dawson KA, Linse S. Systematic investigation of the thermodynamics of HSA adsorption to N-iso-propylacrylamide/N-tert-butylacrylamide copolymer nanoparticles. Effects of particle size and hydrophobicity. *Nano Lett.* 2007;7(4):914–920. doi:10.1021/nl062743+
19. Luck M, Paulke BR, Schroder W, Blunk T, Muller RH. Analysis of plasma protein adsorption on polymeric nanoparticles with different surface characteristics. *J Biomed Mater Res.* 1998;39(3):478–485.
20. Pearson RM, Juettner VV, Hong S. Biomolecular corona on nanoparticles: a survey of recent literature and its implications in targeted drug delivery. *Front Chem.* 2014;2:108. doi:10.3389/fchem.2014.00108
21. Strojan K, Leonardi A, Bregar VB, Krizaj I, Svete J, Pavlin M. Dispersion of nanoparticles in different media importantly determines the composition of their protein corona. *PLoS One.* 2017;12(1): e0169552. doi:10.1371/journal.pone.0169552
22. Jones SW, Roberts RA, Robbins GR, et al. Nanoparticle clearance is governed by Th1/Th2 immunity and strain background. *J Clin Invest.* 2013;123(7):3061–3073. doi:10.1172/JCI66895
23. Oh N, Park JH. Endocytosis and exocytosis of nanoparticles in mammalian cells. *Int J Nanomedicine.* 2014;9(Suppl 1):51–63. doi:10.2147/IJN.S26592
24. Owens DE, Peppas NA. Opsonization, biodistribution, and pharmacokinetics of polymeric nanoparticles. *Int J Pharm.* 2006;307(1):93–102. doi:10.1016/j.ijpharm.2005.10.010
25. Schottler S, Landfester K, Mailander V. Controlling the stealth effect of nanocarriers through understanding the protein corona. *Angew Chem Int Ed Engl.* 2016;55(31):8806–8815. doi:10.1002/anie.201602233
26. Allen TM, Hansen CB, de Menezes DEL. Pharmacokinetics of long-circulating liposomes. *Adv Drug Deliv Rev.* 1995;16(2):267–284. doi:10.1016/0169-409X(95)00029-7
27. Amoozgar Z, Yeo Y. Recent advances in stealth coating of nanoparticle drug delivery systems. *Wiley Interdiscip Rev Nanomed Nanobiotechnol.* 2012;4(2):219–233. doi:10.1002/wnan.1157

28. Essa S, Rabanel JM, Hildgen P. Characterization of rhodamine loaded PEG-g-PLA nanoparticles (NPs): effect of poly(ethylene glycol) grafting density. *Int J Pharm*. 2011;411(1–2):178–187. doi:10.1016/j.ijpharm.2011.02.039

29. Reddy KR, Wright TL, Pockros PJ, et al. Efficacy and safety of pegy-lated (40-kd) interferon alpha-2a compared with interferon alpha-2a in noncirrhotic patients with chronic hepatitis C. *Hepatology (Baltimore, Md)*. 2001;33(2):433–438. doi:10.1053/jhep.2001.21747

30. García-Álvarez R, Hadjidemetriou M, Sánchez-Iglesias A, Liz-Marzán LM, Kostarelos K. In vivo formation of protein corona on gold nanoparticles. The effect of their size and shape. *Nanoscale*. 2018;10(3):1256–1264. doi:10.1039/c7nr08322j

31. Lundqvist M, Augustsson C, Lilja M, et al. The nanoparticle protein corona formed in human blood or human blood fractions. *PLoS One*. 2017;12(4):e0175871. doi:10.1371/journal.pone.0175871

32. Rahman M, Laurent S, Tawil N, Yahia LH, Mahmoudi M. Nanoparticle and protein corona. In: *Protein-Nanoparticle Interactions: The Bio-Nano Interface*. Berlin, Heidelberg: Springer Berlin Heidelberg; 2013:21–44.

33. Fleischmann C, Gopez J, Lundberg P, et al. A robust platform for functional microgels via thiol-ene achemistry with reactive polyether-based nanoparticles. *Polym Chem*. 2015;6(11):2029–2037. doi:10.1039/C4PY01766H

34. Silva JC, Denny R, Dorschel C, et al. Simultaneous qualitative and quantitative analysis of the Escherichia coli proteome: a sweet tale. *Mol Cell Proteomics*. 2006;5(4):589–607. doi:10.1074/mcp.M500321-MCP200

35. Silva JC, Gorenstein MV, Li GZ, Vissers JP, Geromanos SJ. Absolute quantification of proteins by LCMSE: a virtue of parallel MS acqui-sition. *Mol Cell Proteomics*. 2006;5(1):144–156. doi:10.1074/mcp.M500230-MCP200

36. Blazejewski J-C, Hofstraat JW, Lequesne C, Wakselman C, Wiersum UE. Formation of monomeric halogenoaryl acrylates in the presence of hindered pyridine bases. *J Fluor Chem*. 1998;91(2):175–177. doi:10.1016/S0022-1139(98)00222-X

37. Eberhardt M, Mruk R, Zentel R, Theato P. Synthesis of Pentafluorophenyl(meth)acrylate Polymers: New Precursor Polymers for the Synthesis of Multifunctional Materials. *European Polymer Journal*. 2005;41(7):1569–1575. doi:10.1016/j.eurpolymj.2005.01.025

38. Eberhardt M, Théato P. RAFT polymerization of pentafluorophenyl methacrylate: preparation of reactive linear diblock copolymers. *Macromol Rapid Commun*. 2005;26(18):1488–1493. doi:10.1002/(ISSN)1521-3927

39. Kearns MD, Donkor AM, Savva M. Structure-transfection activity studies of novel cationic cholesterol-based amphiphiles. *Mol Pharm*. 2008;5(1):128–139. doi:10.1021/mp700131c

40. Nie Y, Gunther M, Gu Z, Wagner E. Pyridylhydrazone-based PEGylation for pH-reversible lipopolyplex shielding. *Biomaterials*. 2011;32(3):858–869. doi:10.1016/j.biomaterials.2010.09.032

41. Gentsch R, Pippig F, Nilles K, et al. Modular approach toward bioactive fiber meshes carrying oligosaccharides. *Macromolecules*. 2010;43(22):9239–9247. doi:10.1021/ma101607a

42. Gibson MI, Fröhlich E, Klok H-A. Postpolymerization modification of poly(pentafluorophenyl methacrylate): synthesis of a diverse water-soluble polymer library. *J Polym Sci A Polym Chem*. 2009;47(17):4332–4345. doi:10.1002/pola.v47:17

43. Rabilloud T, Strub J-M, Luche S, Girardet JL, van Dorsselaer A, Lunardi J. Ruthenium II tris (bathophenanthroline disulfonate), a powerful fluorescent stain for detection of proteins in gel with minimal interference in subsequent mass spectrometry analysis. *Proteome*. 2000;1(1):1–14. doi:10.1007/s102160000002

44. Rappsilber J, Ishihama Y, Mann M. Stop and go extraction tips for matrix-assisted laser desorption/ionization, nanoelectrospray, and LC/MS sample pretreatment in proteomics. *Anal Chem*. 2003;75(3):663–670. doi:10.1021/ac026117i

45. Staufenbiel S, Merino M, Li W, et al. Surface characterization and protein interaction of a series of model poly[acrylonitrile-co-(N-vinyl pyrrolidone)] nanocarriers for drug targeting. *Int J Pharm*. 2015;485(1–2):87–96. doi:10.1016/j.ijpharm.2015.02.072

46. Walkey CD, Chan WC. Understanding and controlling the interaction of nanomaterials with proteins in a physiological environment. *Chem Soc Rev*. 2012;41(7):2780–2799. doi:10.1039/c1cs15233e

47. Lammers T, Ulbrich K. HPMA copolymers: 30 years of advances. *Adv Drug Deliv Rev*. 2010;62(2):119–121. doi:10.1016/j.addr.2009.12.004

48. Salvati A, Nelissen I, Haase A, et al. Quantitative measurement of nanoparticle uptake by flow cytometry illustrated by an interlabora-tory comparison of the uptake of labelled polystyrene nanoparticles. *NanoImpact*. 2018;9:42–50. doi:10.1016/j.impact.2017.10.004

49. Lee K, Yu Y. Lipid bilayer disruption induced by amphiphilic Janus nanoparticles: the non-monotonic effect of charged lipids. *Soft Matter*. 2019. doi:10.1039/C8SM02525H

50. Jones MC, Jones SA, Riffo-Vasquez Y, et al. Quantitative assessment of nanoparticle surface hydrophobicity and its influence on pulmon-ary biocompatibility. *J Control Release*. 2014;183:94–104. doi:10.1016/j.jconrel.2014.03.022

51. Li Y, Chen X, Gu N. Computational investigation of interaction between nanoparticles and membranes: hydrophobic/hydrophilic effect. *J Phys Chem B*. 2008;112(51):16647–16653. doi:10.1021/jp8051906

52. Ong KJ, MacCormack TJ, Clark RJ, et al. Widespread nanoparticle-assay interference: implications for nanotoxicity testing. *PLoS One*. 2014;9(3):e90650. doi:10.1371/journal.pone.0090650

53. Walczyk D, Bombelli FB, Monopoli MP, Lynch I, Dawson KA. What the cell "sees" in bionanoscience. *J Am Chem Soc*. 2010;132(16):5761–5768. doi:10.1021/ja910675v

54. Gunawan C, Lim M, Marquis CP, Amal R. Nanoparticle–protein corona complexes govern the biological fates and functions of nanoparticles. *J Mater Chem B*. 2014;2(15):2060–2083. doi:10.1039/c3tb21526a

55. Jo DH, Kim JH, Lee TG, Kim JH. Size, surface charge, and shape determine therapeutic effects of nanoparticles on brain and retinal dis-eases. *Nanomedicine*. 2015;11(7):1603–1611. doi:10.1016/j.nano.2015.04.015

56. Corbo C, Molinaro R, Parodi A, Toledano Furman NE, Salvatore F, Tasciotti E. The impact of nanoparticle protein corona on cytotoxi-city, immunotoxicity and target drug delivery. *Nanomedicine (Lond)*. 2016;11(1):81–100. doi:10.2217/nnm.15.188

57. Dobrovolskaia MA, Aggarwal P, Hall JB, McNeil SE. Preclinical studies to understand nanoparticle interaction with the immune sys-tem and its potential effects on nanoparticle biodistribution. *Mol Pharm*. 2008;5(4):487–495. doi:10.1021/mp800032f

58. Du Clos TW. Pentraxins: structure, function, and role in inflamma-tion. *ISRN Inflamm*. 2013;2013:379040. doi:10.1155/2013/379040

59. Roversi P, Johnson S, Caesar JJ, et al. Structural basis for comple-ment factor I control and its disease-associated sequence polymorph-isms. *Proc Natl Acad Sci U S A*. 2011;108(31):12839–12844. doi:10.1073/pnas.1102167108

60. Schwaeble WJ, Ali YM, Sim RB. Chapter 15 - the roles and contribu-tions of the complement system in the pathophysiology of autoimmune diseases A2 - rose, noel R. In: Mackay IR, editor. *The Autoimmune Diseases*. 5th ed. Boston: Academic Press; 2014:217–227.

3.3 The influence of shape and charge on protein corona composition in common gold nanostructures

Tony Bewersdorff, Emanuel A. Glitscher, Julian Bergueiro, Murat Eravci, Enrico Miceli, Andrea Haase, Marcelo Calderón

The supplementary material to the publication embedded on the following pages is contained in Annex III.

The authors contribution:

Sample preparation for protein corona investigation and LC-ESI-MS/MS measurements
Analysis of the proteomic results
Discussion and evaluation of the results (with other authors)
Preparation of the manuscript (with other authors)

The influence of shape and charge on protein corona composition in common gold nanostructures

Tony Bewersdorff[a,1], Emanuel A. Glitscher[b,1], Julian Bergueiro[c], Murat Eravci[a], Enrico Miceli[b], Andrea Haase[a,*], Marcelo Calderón[b,d,e,**]

[a] German Federal Institute for Risk Assessment (BfR), Department of Chemical and Product Safety, Berlin, Germany
[b] Freie Universität Berlin, Institute of Chemistry and Biochemistry, Takustrasse 3, 14195 Berlin, Germany
[c] Centro Singular de Investigación en Química Biolóxica e Materiais Moleculares (CIQUS), Departamento de Química Orgánica, Universidade de Santiago de Compostela, Santiago de Compostela, Spain
[d] POLYMAT and Applied Chemistry Department, Faculty of Chemistry, University of the Basque Country UPV/EHU, Paseo Manuel de Lardizabal 3, 20018 Donostia-San Sebastián, Spain
[e] IKERBASQUE, Basque Foundation for Science, 48013 Bilbao, Spain

A B S T R A C T

With increasing importance of gold nanoparticles (AuNPs) in the medical field, the understanding of their interactions in biological environments is essential. It is known that the exposure to biological fluids of particles in the nanometric range leads to accumulation of proteins on the particle surface proximity, generating the so-called protein corona. This fact can completely change the properties of AuNPs, thus drastically influencing the characteristics and intended purpose of the particles. Therefore, deep insight on the formation and composition of this protein corona is of extreme importance. Between the different factors that can alter the corona formation, our study focuses on the influence of the shape and particle surface charge. In detail, four different shapes of nanometrical scale (spheres, rods, stars and cages) of comparable size were used, all of them stabilized with three different heterofunctionalized poly(ethylene glycol) thiol (R-PEG-SH) linkers (R = OCH$_3$, COOH or NH$_2$) to check the effect of charge as well. After incubation with human serum, abundant proteins were identified via liquid chromatography-electrospray ionization-tandem mass spectroscopy (LC ESI MS/MS) and compared in terms of their relative abundance. On the basis of statistical evaluations, the shape of our AuNPs showed a greater influence than the surface charge. Especially, cage-shaped AuNPs showed a lower amount of total corona proteins. This shape showed differences in the abundances of individual proteins like albumin, vitronectin and members of the complement system. These results indicate that nanocages could present an improved biocompatibility compared with the other shapes due to the high curvature areas and dense ligation on the flat surfaces that could hinder opsonisation and fast removal by the immune system.

1. Introduction

Over the past decades, nanotechnology has led to manifold innovations. Especially in the field of medical applications, an increasing number of nanomaterials with different sizes, shapes and physico-chemical properties were described. Among them, especially gold nanoparticles (AuNPs) received an increased attention due to their efficient straightforward synthesis and high long-term stability that allows their use as biocompatible platforms [1–7]. Moreover, AuNPs present unique optical properties which qualifies them as Raman probes and light-to-heat transducers [8]. To improve biological applications of AuNPs (i.e. bio-imaging, analytical sensing, gene diagnostics, photothermal therapy and targeted delivery of biomolecular and chemical cargos), a wide spectrum of synthetic strategies have been designed to control

their size, shape and surface functionality [9–15].

Considering the described in vivo medical treatments that used colloidal dispersions of AuNPs, their administration occurs mainly by intravenous injection or oral ingestion [16]. Nevertheless, via both entry modes, AuNPs are exposed to a complex biological environment from either the blood or the digestive tract, right on the event of administration. Diverse biomolecules like metabolites, lipids, sugars, ions and especially proteins present in such environments, have the potential to interact with the AuNPs [17–20]. However, among all the possible interactions, the so called protein corona is the most dominant and important factor, influencing the behaviour of AuNPs in vivo. The corona composition is determined by the kinetic on and off rates (or rather the equilibrium binding constants) of the several thousand proteins present in biological fluids and tissues for the respective AuNPs,
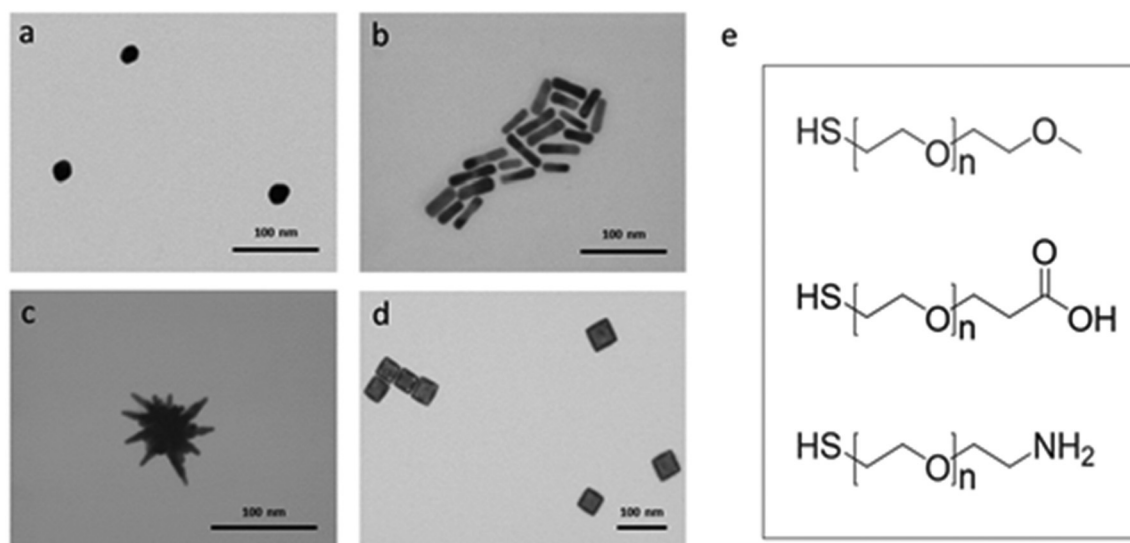

Fig. 1. TEM images of the differently shaped AuNPs used in this study, demonstrated by (a) spheres, (b) rods, (c) stars and (d) cages, each equipped with (e) one of three different functionalized PEG chains (–OCH₃, –COOH or –NH₂).

taking into account the complexity of the protein corona scenario [21–23]. Moreover, the bio-identity of the particle (the composition of the protein corona formed) has a dramatic impact on the fate of the AuNPs. For instance, it was shown that by altering the bio-identity of the AuNPs, parameters like biological interactions, cellular recognition, uptake and intracellular recognition of AuNPs are critically affected [24–28]. For example, AuNPs coated with transferrin or haemoglobin lose their targeting capabilities when a protein corona is formed [25,28–31].

The accumulation of proteins and thus the formation of a corona is highly dependent on the physico-chemical properties of the AuNPs. Size, shape and surface charges are the most prominent factors with a serious influence on the composition of the protein corona [25,32–34]. The dependence of protein adsorption on AuNP surfaces as a function of their size and surface curvature has already been investigated several times. With increasing curvature of the surface, for example, globular proteins appear to retain their native conformation, as shown for bovine serum albumin on monodisperse silica spheres. In comparison, fibrillar proteins such as fibrinogen may lose their native conformation with decreasing particle size [35–37]. Apart from size and curvature, we also found on a previous report that the surface charge on dendritic polyglycerol-coated AuNPs plays a crucial role with regard to the proteins present in the corona [38]. This is in good agreement with other studies, which demonstrate that the surface chemistry has a major influence on the corona composition [39]. Nevertheless, most of these studies mainly focus on the differences in sizes, surface modifications or colloidal stability on a limited collection of AuNPs. This situation motivated us to discuss the influence of shape and surface charge on a broader variety of particle shapes decorated with neutral, positively or negatively charged ligands.

Within this study, we present for the first time a comprehensive investigation of protein corona formation on AuNPs with comparable sizes, where the shape and the surface charge are systemically varied. We considered gold nano-spheres (AuNSPs) as an isotropic geometry which are predominant in biomedical research. Three anisotropic architectures widely used as near infra-red to heat transducers were considered as well: gold nano-rods (AuNRs), gold nano-stars (AuNSTs) and gold nano-cages (AuNCs). These structures have high appearance in literature and are of interest for different biomedical applications [40–44]. Particularly, AuNCs are of interest due to their hollowed interior, flat surface and superior optical properties. Given their relative novelty, they have not yet been studied so intensively as the other

anisotropies. To investigate potential variation between the different surface charges we chose three types of thiolated poly(ethylene glycol) (PEG) as ligands due to the good colloidal stability and easy functionalization with three different end-groups (-OCH₃, -COOH, -NH₂).

2. Results and discussion

2.1. Synthesis and characterization of the AuNPs

Protein corona formation on differently shaped and charged AuNPs was investigated with four different AuNP shapes (AuNSPs, AuNRs, AuNSTs and AuNCs). These structures have high appearance in literature and are of interest for different biomedical applications [40–44]. To have the targeted differently shaped AuNPs with comparable sizes, considering the synthetic limitations, we aimed for particles in a range of around 50 nm. Particles in this size range show prolonged circulation in vivo and increased accumulation in infected tissues and are therefore ideal candidates for optical imaging, photothermal therapy and drug delivery applications [45]. In detail, we applied different reduction protocols found in literature. Such synthetic methodologies of this particular AuNPs can provide particles with low dispersity for the targeted size range. AuNSPs were synthesized with sodium citrate as reductant by a modified Turkevich-Frens protocol [46]. CTAB capped AuNRs were formed in a one-pot protocol by Jana et al. with silver nitrate, ascorbic acid and sodium borohydride [47]. Star-shaped growth of AuNSTs was achieved by adding gold salt, silver nitrate and ascorbic acid to 2–3 nm spherical seed particles [48]. AuNCs were synthesized in a galvanic exchange reaction with silver nanocubes as templates [49]. Ionic stabilizing agents which were required during the synthesis of AuNPs where later exchanged with the desired functional moieties by exposing the AuNPs to an excess of mono-thiolated PEG (X-PEG-SH). Three different types of hetero-functionalized PEG were used, yielding particles with methoxy (-OCH₃), carboxylic acid (-COOH) and amine (-NH₂) end functionalization.

Transmission electron microscopy (TEM) pictures are revealing the particular size and shape of the synthesized AuNPs along with their typical absorption spectra. Targeted sizes of around 50 nm were successfully achieved and the particles show low polydispersity in TEM (Fig. 1). Absorption spectra show expected maxima around 540 nm for AuNSPs and between 720 and 860 nm for AuNRs, AuNSTs and AuNCs (Fig. S1). High-resolution TEM images are provided to show the internal hollow structure of the AuNCs in contrast to the other particle

Table 1
Characterization of AuNPs.

Nanoparticles shape moiety		Size in TEM [nm][a]	Size in MQ [nm]	Size in HS [nm]	Zeta [mV]	λ_{max} [nm]
AuNSPs	–OCH₃	49.2	56.4	108.9	−4.0	544
	–COOH		58.1	96.1	−17.4	539
	–NH₂		89.2	102.3	+7.1	543
AuNRs	–OCH₃	54.3	71.1	83.8	−5.4	771
	–COOH		69.6	75.9	−12.1	783
	–NH₂		572.1	> 1000	+4.4	770
AuNSTs	–OCH₃	52.5	67.3	148.0	−3.0	850
	–COOH		62.7	178.9	−25.7	820
	–NH₂		66.2	185.2	+9.9	867
AuNCs	–OCH₃	58.0	75.3	94.0	−5.6	736
	–COOH		73.8	91.7	−19.0	720
	–NH₂		87.8	217.1	−2.6	736

[a] TEM sizes are given as the average for all three variants as the initial synthesis of the AuNP core structure is identical. Sizes are given as the diameter for AuNSPs and AuNSTs, the longitudinal length for AuNRs, and the diagonal length for AuNCs. Histograms are shown in Fig. S3.

shapes (Fig. S2). Basic physico-chemical properties of the AuNPs are summarized in Table 1. Characterization with respect to their size distribution in dispersion was done with dynamic light scattering (DLS) in ultrapure water (MQ) and human serum (HS). Hydrodynamic diameters in MQ varied between 56 and 88 nm and show narrow size distributions (Fig. S4). Compared with the sizes evaluated by TEM, a minor increase in diameter was detected for most particles. Only the amine-functionalized particles showed a slight tendency for aggregation, illustrated by higher DLS values, but were still completely dispersed in solution when incubated with HS. Therefore, TEM sizes are accurate regarding the diameter and aggregation behaviour of the particles in solution and all AuNPs shall be comparable regarding their uniform size. In HS however, the hydrodynamic diameters of the AuNPs were slightly increased when compared to the measurements in MQ. These shifts may indicate an association of proteins and are reported as an evidence of the protein corona formation [50–53].

Additionally, the zeta potential was determined in MQ for all AuNPs to verify the exchange of surface functionalization (Table 1). All OCH₃-equipped AuNPs show neutral values. AuNPs functionalized with COOH show a high negative charge, NH₂-functionalized a slightly positive charge except for AuNCs. As AuNC-NH₂ show the fastest aggregation of all the particles. We assume that the charge is partially

shielded by interactions of amines with the gold surface which could also explain why the zeta potential remains neutral or slightly negative. The minor differences in zeta potential could not only mean a shielding of the end groups, but also differences in overall PEG-functionalization density. Indeed, it has already been shown, that high curvature, as present for e.g. spheres and the longitudinal ends of rod-shaped particles, shows a lower density of binding ligand than flat surfaces and ultimately leads to different protein binding patterns [54]. Nevertheless, within this study, we want to focus solely on the structural differences for protein composition dependant on the shape of the inorganic AuNP-core itself and possible variations of same structures by alternation of the end group functionalization.

2.2. Identification of the protein corona via LC-MS/MS

In total, by combination of the shapes and charges, twelve different types of AuNPs regarding their shape and surface functionalization were synthesized. All AuNPs were incubated with HS to study the individual formation of protein corona and the dependency on shape and charge. For comparison, we used same concentrations of particles as comparison by total surface volume is hardly achievable for highly anisotropic particles like AuNSTs and hinders the comparison with structures like AuNSPs and AuNRs in this context. Protein binding to the AuNPs was identified via liquid chromatography-tandem mass spectrometry (LC-MS/MS) and quantified using the TOP 3 approach [55]. Therefore, the intensities of the identified proteins were calculated by summing up the intensities of the three most intense unique peptides for each protein [56]. Although PEG is known to shield particles from protein adsorption, we could identify a total of more than 90 proteins for almost all shapes and surface charges. Only for the AuNCs, less proteins were abundant in the protein corona. Here, 81 (AuNC-OCH₃), 45 (AuNC-COOH) and 55 (AuNC-NH₂) proteins could be identified (Fig. 2A). The same tendency was observed in the overall intensities of the proteins identified by the TOP 3 approach. Highest amount of proteins per weight of AuNPs was bound to the AuNSTs which we attribute to their larger surface-to-volume ratio. For AuNSPs and AuNRs, we found similar intensities while clearly less total protein was present in the cage variants (Fig. 2B). This could indicate a hindrance in interaction between the serum proteins and AuNCs due to their structural appearance.

However, the amount of identified proteins does not correlate with the number of total bound proteins. For example, within the spherical variants, the AuNSPs-OCH₃ show the highest intensity although they
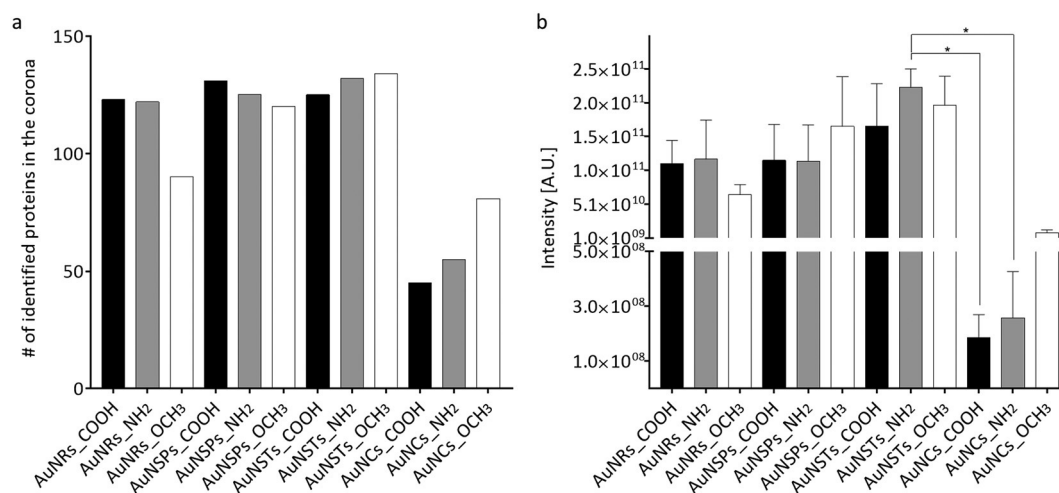
Fig. 2. (a) Total number of identified corona proteins and (b) the total intensities of proteins bound to the AuNPs are shown. Corona proteins were identified using LC-MS/MS and abundances were determined via TOP 3 approach. The intensity for each protein is obtained by summing up the three most intense unique peptides for each protein. The total intensities were determined based on this approach. The various functional surface groups are colour coded (–OCH₃ white; –COOH black; –NH₂ grey). One-way nonparametric ANOVA analysis with Tukey test for multiple comparison was used to assess differences between groups (* $p < 0.05$).

had the lowest number of identified proteins. For AuNSTs, the representatives of the AuNSTs-NH$_2$ group show a higher proportion of bound proteins compared to the AuNSTs-OCH$_3$ group, despite the fact that the number of identified corona proteins was less. Still, the amount of proteins identified is in good agreement with other studies for PEGylated AuNPs [57]. Only the AuNCs stand out as they show a huge difference in identified proteins between the negatively/positively charged and the neutral particles. It has already been investigated, that the grafting density of PEG increases with high curvature and that PVP-capped AuNCs show higher grafting densities than CTAB-coated AuNRs [58,59]. In this context, we assume that the higher PEG grafting density of AuNCs effects the adsorption of proteins as tightly packed PEG layers are more efficient in preventing protein association [60,61], and that the difference between –COOH, –NH$_2$ and –OCH$_3$ end-groups result from the increased number of charges at the surface. Although as the total numbers do not differ significantly within the other shape-groups, we conclude that the variation in end-group modification does not seem to have a strong influence on the total and relative numbers of bound proteins and that the density of the PEG layer – influenced by the shape – is the key factor here. Within this study, we were further interested on a closer insight in the individual protein compositions of the different shapes and surface charges.

2.3. Comparison of individual protein abundances

For analysis of the protein corona, the 15 most abundant proteins for each particle were determined. Across all we found a total of 22 proteins covering at least 67% of the total protein corona (Fig. 3). Hierarchical cluster analysis was used to show the similarities among the AuNPs (Fig. 4). For the method of hierarchical cluster analysis, we looked at the composition of the protein corona of each individual NP.
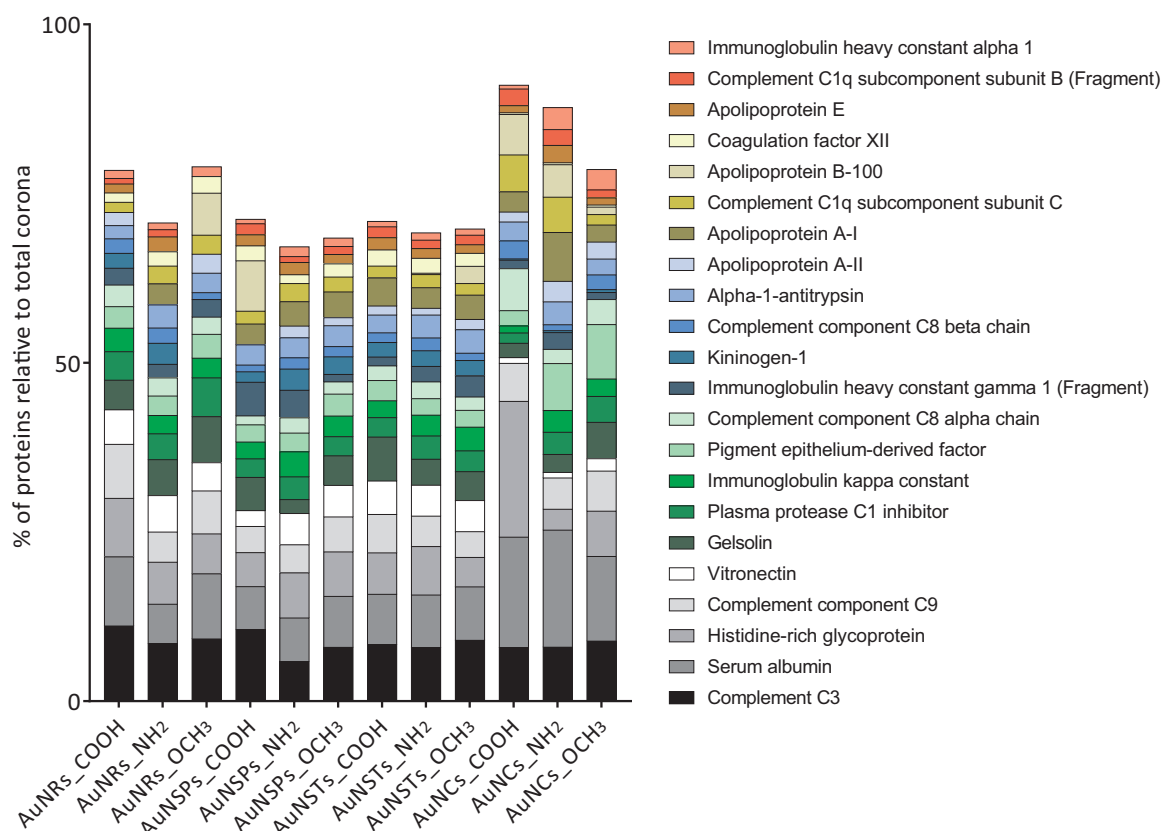

Fig. 4. Hierarchical cluster analysis (HCA) of the AuNPs for the comparison of the protein coronas. Similarities and differences are shown using HCA in Perseus (version 1.6.2.3).

Roughly speaking, it can be said that the distance between two links represents the similarity or better: dissimilarity of two NPs with respect to their protein corona. In our case, this would mean that AuNSTs-NH$_2$ and AuNSPs-OCH$_3$ are very similar in terms of their protein corona composition. While AuNCs-COOH should show a large difference in the protein corona due to the very late linkage with the cluster of the two mentioned nanoparticles. According to the hierarchical arrangement, in our case the 5 NPs with a similar protein corona (with decreasing similarity) are: AuNSTs-NH$_2$, AuNSPs-OCH$_3$, AuNRs-NH$_2$, AuNSTs-NH$_2$ and AuNSTs-COOH. Among these 5 NPs, there are already all 3 variants of the AuNSTs. This could lead to the conclusion that rather the form than the functionalization of the NPs could play a role in the formation of the protein corona. Interestingly, only few direct correlations could be observed. AuNCs seem to be further separated from the other

Fig. 3. Comparison of the most abundant proteins in the corona of AuNPs. The 15 most abundant proteins of each protein corona (summarized) are shown. These were calculated using the TOP 3 approach. Results are given in percentage of the total bound proteins in the specific corona (proteins are colour coded). Remaining proteins (missing percentage up to 100) are not shown.
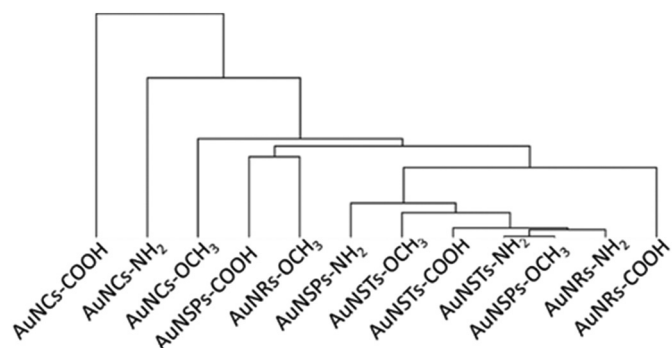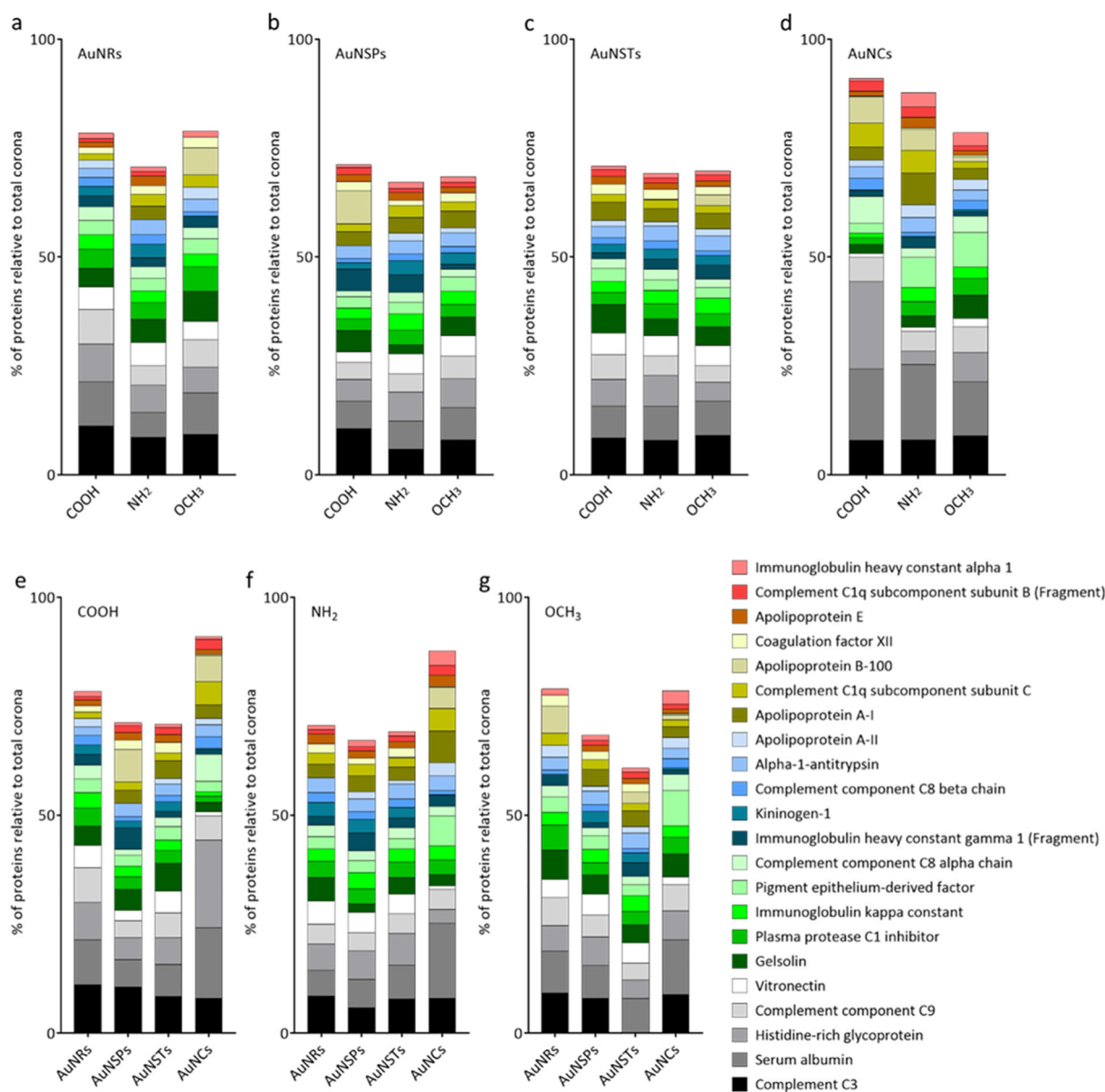
Fig. 5. Comparison of the most abundant proteins in the corona of each AuNP, grouped for different shapes and surface charges. Depicted are the 15 most abundant proteins of each protein corona (summarized). Classification is based on structure with (a) rod-, (b) sphere-, (c) star- and (d) cage-shaped AuNPs or according to the surface functionalization with (a) –COOH, (b) –NH₂ and (c) –OCH₃. Within one panel the different surface modifications (a–d) or the different shapes of the AuNPs (e-g) are shown. Intensities were calculated using the TOP 3 approach. Results are given in percentage of the total bound proteins in the specific corona (proteins are colour coded).

variants. Nevertheless, no dependence of the protein corona on surface charge could be determined. This indicates that same AuNP shapes are more likely to share similarities in protein corona composition than same end-group functionalizations.

A closer look into the individual groups reveals a more detailed distribution of the entire protein corona as well as to the 15 most abundant proteins. The examination of these corona proteins with regard to the structure or the surface charge (Fig. 5) of the individual AuNPs also confirmed the previously found relationship. AuNSTs generally show the most similar pattern with regard to intensity. The surface charge seems to have less influence on the star-shaped AuNPs (Fig. 5c) compared to the others. AuNRs and AuNCs show a much more pronounced altered pattern (Fig. 5a & d). But in general, the variation between the different surface modifications is not as pronounced as the influence of the shape on protein corona formation within a comparable surface charge. Even though, the band patterns of the graphs are very

different across all AuNPs, -NH₂ functionalized variants seem to have a more similar distribution than the -COOH and -OCH₃ particles. However, a closer look reveals that there is also a noticeable difference especially regarding the AuNCs which we contribute to the huge difference in identified proteins for the charged (45 and 55 identified proteins for -COOH and -NH₂, respectively) and neutral (81 for -OCH₃) AuNCs as previously discussed.

For a more detailed insight into the composition of the protein corona, some representative proteins were selected (Fig. 6). In these graphs, similarities and differences in the composition of the protein corona are more clearly visualized with respect to the individual proteins. For example, it becomes visible that an activator of the complement system (complement C3) is distributed over all AuNPs independent of charge or structure (Fig. 6a). In the case of serum albumin, we again find high abundances throughout all shapes and charges. Serum albumin usually shows a preferable adsorption onto
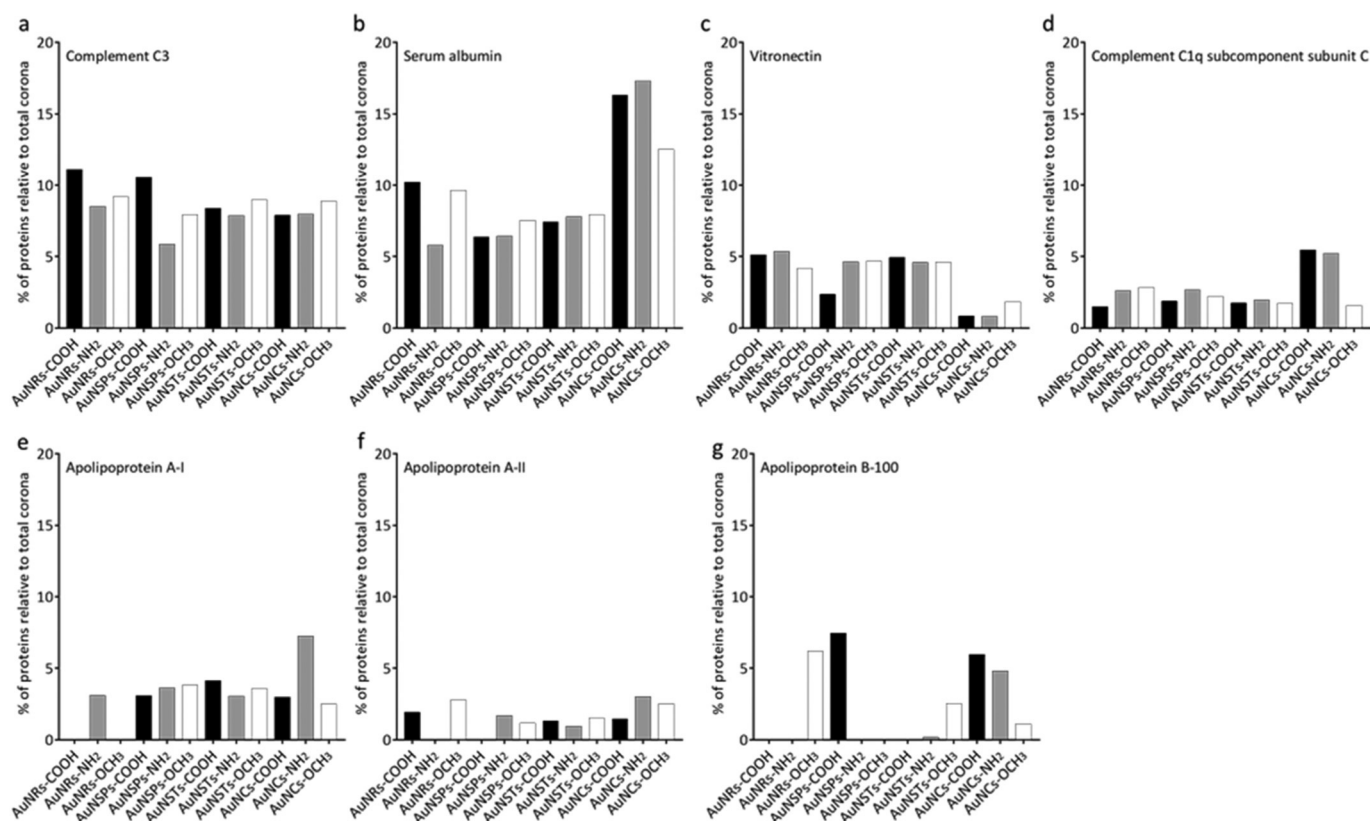
Fig. 6. Representation of selected corona proteins with different binding patterns among the AuNPs. Depicted are selected proteins of the 15 most abundant proteins. The values of the respective proteins correspond to the percentage of the total bound proteins in the corona of the AuNPs. Proteins displayed are (a) complement C3, (b) serum albumin, (c) vitronectin, (d) complement C1q subcomponent subunit C, (e) apolipoprotein A-I, (f) apolipoprotein A-II and (g) apolipoprotein B-100.

positively charged particles due to its low isoelectric point (< 5.5) [33], but for AuNPs, albumin is recognized as one of the most abundant proteins for particles with spherical, rod-like and star-like shapes [62,63].

As a new result, we find a higher abundance of serum albumin relative to the total amount of bound proteins in case of AuNCs (Fig. 6b). In general, albumin shows rapid adsorption onto nanoparticles upon administration but is usually replaced at a later stage by proteins, which show higher binding affinities. Previous studies have already shown that particles which bind less total proteins in their corona are particularly enriched in albumin [64]. We hypothesize that the high curvature at the edges and higher grafting density of the PEG layer for the AuNCs hinders other plasma components like vitronectin (Fig. 6c), a protein which regulates cell adhesion, apolipoproteins and members of the complement system from adsorption at later stages. That would explain the remaining of high relative amounts of serum albumin as well as other rapidly adsorbing proteins like some immunoglobulins (Ig). This assumption is supported by the overall low total intensity and number of abundant proteins for all variants of the AuNCs. Due to their structure, AuNCs have the smallest surface area and strong surface curvatures at the edges comparable to smaller spherical particles, which are also known to show lower total abundances [37]. In addition, it might also be possible that proteins can interact internally through their open structure and are therefore not determined by the methodology used in this study.

AuNCs also stand out from the rest regarding complement unit C1q (Fig. 6d). The C1 complex binds to antibodies adsorbing to the surface of pathogens or nanoparticles and initiates the classical complement pathway which results in opsonisation and phagocytosis [65]. C1q shows higher abundance for AuNCs compared to other members of the complement system. We conclude that the progression of the classical complement pathway might be hindered as C1q splits into further

fragments to promote opsonisation. A closer look into the structure of the protein reveals, that C1q differ from other plasma proteins with respect to its distinct collagen-like regions [66]. The polyproline helices in these collagen-like motifs could attach to the cages similarly to poly (vinyl pyrrolidone), a polymer often used in AuNC stabilization because of its preferable attachment to {100} facets [67]. As the surface of AuNCs, contrarily to other AuNP shapes, mostly consists of {100} facets, this could explain the stronger affinity of the C1q compared to other shapes. Another protein found enriched in the corona of the cages was the histidine-rich glycoprotein, which exhibits high binding affinity to C1q through its cystatin-like regions at the N-terminus and therefore also shows increased presence in the corona of the cages [68]. From these apparent differences, we conclude that the presence of {100} facets along with previously mentioned PEG grafting density and particle structure have a strong influence in the abundance of certain plasma proteins. In view of the fact that C1q is a component of the complement activation system (classical pathway) and the less abundant vitronectin also plays a role in the complement system, this might indicate a variation in the cellular uptake pathway of AuNCs. Since vitronectin can interact with αvβ3 integrin, it could also be of high importance in the cell uptake mechanisms [69,70].

Interestingly, the three most abundant apolipoproteins show a most diverse pattern regarding AuNRs (Fig. 6e–g). Apolipoprotein A-I was only present among the 15 most abundant proteins of AuNRs-NH2, whereas apolipoprotein A-II was missing only in this nanostructure. Apolipoprotein B-100 in contrast was not detected for AuNRs-COOH and AuNRs-NH2, but also not for other variants of AuNSPs and AuNSTs. In general, apolipoproteins were found to be more likely adsorbing onto liposomes and organic nanoparticles than inorganic surfaces [71]. This supports our findings that we could not detect several apolipoproteins among the 15 most abundant proteins for our particles.

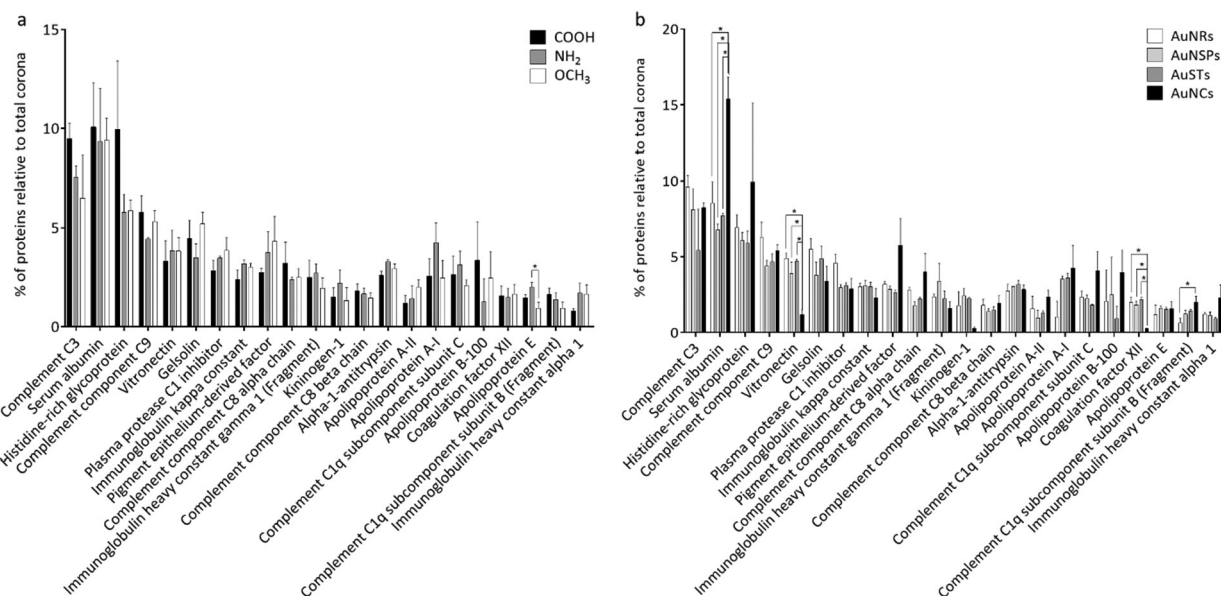In order to analyse whether the structure or the surface charge alone

Fig. 7. (a) Mean values for the same surface charge across all AuNP structures. The percentages of the proteins relative to the total protein corona were summarized for the same surface charge across all AuNP structures. Depicted are mean values of the summarized groups (COOH in black, NH_2 in grey and OCH_3 in white) with the SEM. (b) Mean values for the same AuNP structure across all surface charges. The percentages of the proteins relative to the total protein corona were summarized for the same structure across all AuNP surface charges. Depicted are mean values of the summarized groups (AuNRs in white, AuNSPs in light grey, AuNSTs in dark grey and AuNCs in black) with the SEM. One-way nonparametric ANOVA analysis with Tukey test for multiple comparison was used to assess differences between groups ($*p < 0.05$).

might have an influence on the formation of the protein corona, we have further summed up and compared the percentage of proteins relative to total corona either over all the identical charges or shapes (Fig. 7). The comparison of these two figures confirms that the structure may have a greater influence on the formation of the protein corona than surface charge. The more frequent and larger variations in the abundance of proteins can be clearly seen in the comparison of nanoparticle structures. Obviously, there are greater divergences in both graphs, nevertheless, it can be noted that the charge dependency graphs are generally more uniformly distributed. This is even more surprising when taking into account the isoelectric points (pI) of the different plasma proteins. Proteins with low pI should preferably adsorb onto positively charged particles and vice versa. We can point out a higher affinity for negatively charged particles in case of histidine-rich glycoprotein (pI ∼ 7.1), apolipoprotein B-100 (pI ∼ 6.6) and complement C3 (pI ∼ 6.3). For positively charged particles, only apolipoprotein A-I (pI ∼ 5.5) shows a significant enrichment (among rod- and cage-shaped AuNPs).

To visualize the relationship between different charges and shapes even better, we have calculated the mean values of the corresponding properties for all nanoparticles and determined the standard deviations. Subsequently, the percentage deviation of the standard deviation from the mean value was determined and displayed (Fig. S5). Using this representation, we notice again that the structure has a greater influence on the protein corona composition. If the structure is the variable variant, we still find 9 proteins with a 40% variation. If the surface charge is varied, there is only 1 protein with a 40% variation.

3. Conclusion

Within this project, we have focused on two essential physico-chemical properties (particle shape and surface charge) of AuNPs whose influence on the formation of a protein corona has been previously described [9,28]. The AuNPs used within this study featured four different structures and in addition each included three different surface functionalizations introduced by ligation with PEG. We investigated protein binding on the AuNPs and applied statistical methods to correlate the attachment with the physico-chemical properties.

Negatively charged surfaces of nanoparticles are supposed to lead to a stronger accumulation of proteins [31], which we could observe to a small extent in our experimental setup. AuNSP-COOH and AuNR-COOH showed this behaviour. Interestingly, we were able to identify a higher number of proteins for the neutral functionalized nanoparticles when compared to the other two representatives (AuNSTs and AuNCs). The 15 most abundant proteins did not show significant tendencies for any of the different moieties. Thus, we conclude that the interactions of proteins with PEGylated AuNPs might show low dependence on surface charge.

Regarding the size of the particles, we could not detect a difference of protein abundances in our set-up, as we aimed to use AuNPs with comparable dimensions. However, in the case of the slightly agglomerated AuNR-NH_2, the incubation with HS only led to further aggregation, but no noticeable difference in protein composition whether compared to the other AuNR-variances, nor NH_2-functionalized particles.

However, when considering the different structures, AuNSTs have a higher amount of total proteins present compared to AuNSPs and AuNRs due to their overall larger surface area. AuNCs however showed an interesting behaviour regarding its interaction with some proteins despite the fact that their surface-to-volume area is comparable with the other unbranched architectures. In relation to all shapes, AuNCs showed a lower total number and variety of proteins, but increased relative abundances for albumin and the complement C1q fragment. This leads to the conclusion that adsorption of other plasma proteins could be strongly hindered which we correlate to the high curvature at the edges, dense PEG-layers at the sides and predominance of {100} facets. The different composition in protein corona indicates the possibility of altered biological behaviour in contrast to spherical, rod-like and star-like AuNPs. Whether this has a direct effect on parameters like circulation time, cellular recognition and cellular uptake still needs to be investigated. Our findings indicate, that AuNCs could be a superior system for biomedical applications compared to other types of AuNPs as high relative amounts of albumin in the corona suggests improved biocompatibility and the high curvature and dense ligation could

protect the particles from opsonisation and fast removal by the immune system.

4. Experimental

4.1. Materials and methods

All chemicals were purchased from Sigma-Aldrich, Acros or Merck and used as received. Heterofunctionalized PEGs with molecular weights of 5 kDa were purchased from Rapp Polymere. Milli-Q water used for the experiments was obtained from a Millipore water purification system (18.2 MΩ·cm).

For UV/Vis spectroscopy, Scinco S 3150 multi-channel spectrophotometer was used. All samples were measured in Millipore water using disposable UV micro cuvettes from Brand.

Dynamic and electrophoretic light scattering measurements were recorded using Malvern Zetasizer Nano ZS ZEN3600 with a He−Ne laser (λ = 633 nm) or DPSS laser (λ = 532 nm) under a scattering angle of 173° at room temperature as not indicated otherwise. All samples were filtered with 0.2 μm or 0.45 μm syringe filters prior to the measurement to exclude large aggregates and dust. Measurements were analyzed using Malvern Zetasizer Software version 7.11. Size distribution of the particles is provided as the average of three measurements with 12–15 runs each. Zeta potential was measured by diluting the AuNPs in phosphate buffer (10 mM) and is given as the average of five measurements.

Electron microscopy was performed on Hitachi SU 8030 scanning electron microscope operating at 30 kV. For preparation, a droplet (2 μL) of the diluted sample solution was attached onto a carbon coated copper grid and dried at air. Size analysis was performed with ImageJ software.

4.2. Synthesis of gold nanospheres

The gold nanospheres were synthesized by citrate reduction. Briefly, 39.4 mg tetrachloroauric acid trihydrate (0.1 mmol) was dissolved in water (400 mL) and heated to 100 °C. Sodium citrate (2.36 mL, 1 wt% in water, 0.08 mmol) was quickly added. The solution was stirred under reflux for 15 min until which the colour changed from slightly yellow to deep red. After completion of the reaction, the particles were used without further purification.

4.3. Synthesis of gold nanorods

Gold nanorods were synthesized by dissolving 98.4 mg tetrachloroauric acid trihydrate (0.25 mmol) in water (250 mL) and heated to 45 °C. 18.23 g hexadecyltrimethylammonium bromide (50 mmol) was added and dissolved completely in the warm solution. After cooling down to room temperature, $AgNO_3$ solution in water (5 mL, 10 mM) and 88 mg ascorbic acid (0.5 mmol) were added followed by the addition of $NaBH_4$ solution in water (25 μL, 10 mM). After stirring for 1 h, the dark red solution was purified twice by centrifugation (6500 rpm, 2 h) and redispersion in water.

4.4. Synthesis of gold nanocages

For the synthesis of the nanocages, silver nanocubes were used as a scaffold and converted into gold nanocages by galvanic replacement. First, ethylene glycol (EG, 5 mL) was heated to 150 °C and stirred for 30 min. Disodium sulfide (60 μL, 3 mM in EG), polyvinylpyrrolidone (55 kDa, 1.25 mL, 20 mg/mL in EG) and HCl (0.5 mL, 3 mM in EG) were added and stirred for 2 min. Then, a solution of silver trifluoroacetate (0.4 mL, 282 mM in EG) was quickly injected and the particles were allowed to grow for 1 h while the colour changed from colorless to yellow/slightly greenish. The reaction was quenched by placing the reaction vessel into an ice bath. The particles were purified by centrifugation (2000 rpm, 15 min) and redispersion in 2 mL water. Afterwards, the particles were centrifuged three times (8000 rpm, 2 min), redispersed in water and stored in the dark at 4 °C.

For conversion into gold nanocages, a solution of polyvinylpyrrolidone (55 kDa, 5 mL, 1 mg/mL in water) was heated to 105 °C. Previously synthesized silver nanocubes were added and the mixture was stirred for 5 min. Afterwards, tetrachloroauric acid trihydrate (0.1 mM in water) was added dropwise via a syringe pump (0.75 mL/min). The replacement reaction was monitored by absorption spectroscopy and the addition of gold salt was stopped when the plasmon band reached 700 nm. After the addition, the solution was stirred for further 10 min at 105 °C and then cooled down in an ice bath. The particles were purified two times by centrifugation (3000 rpm, 30 min) and redispersion in water.

4.5. Functionalization of gold nanospheres, nanorods and nanocages

A known amount of the previously synthesized gold nanoparticles (spheres, rods, or cages) was added to a solution of excess bi functionalized poly(ethylene) glycol HS-PEG$_{5kDa}$-X (X = OCH$_3$, COOH, NH$_2$·HCl) and stirred for 48 h. The particles were purified by centrifugation and redispersion in water. For the gold nanocages, purification by dialysis (Spectra/Por Dialysis Tubing, molecular weight cut off = 50,000 Da) was additionally applied for 72 h against 2 L of ultrapure water.

4.6. Synthesis of gold nanostars

Small spherical particles served as seeds for the synthesis of gold nanostars. The seeds were produced by adding 6 mL of ice-cold sodium borohydride solution in water (0.1 M) to a solution of 19.7 mg tetrachloroauric acid trihydrate and 14.7 mg sodium citrate in 200 mL water. The formation of 3–4 nm spherical particles was confirmed by TEM and the particles were used without purification for the synthesis of nanostars. For that, 10 mL of tetrachloroauric acid trihydrate in water (0.25 mM) was mixed with 10 μL HCl (1 M) and 100 μL of the previously synthesized seed particle solution. 100 μL of silver nitrate solution (1 mM) and 50 μL of ascorbic acid solution (100 mM) were simultaneously added followed by 20 mg of bi-functionalized poly (ethylene) glycol HS-PEG$_{5kDa}$-X (X = OCH$_3$, COOH, NH$_2$·HCl). The solution was immediately centrifuged (5000 rpm, 10 min) and after redispersion in water further purified by centrifugation (6000 rpm, 3 min).

4.7. Incubation with human serum

For analysis of the protein corona all AuNPs (with 3 biological repeats for each NP) were dispersed at a final concentration of 300 μg/mL in 1.5 mL 70% human serum (diluted with PBS). Incubation was for 2 h in sterile glass vials containing magnetic stir bar by stirring (700 rpm at room temperature (RT)) with a magnetic stirring device (HMC Cyclone, HMC Europe, Germany). For the separation of the AuNPs with adsorbed corona from unbound proteins, the AuNP dispersions (1.5 mL) were loaded on top of 7.5 mL 2 M sucrose. The AuNPs were pelleted via ultracentrifugation (17,900g, 2.5 h at RT). 70% human serum without AuNPs served as control and was treated similarly. Pellets were washed twice with PBS (17,900g, 30 min at RT). Samples (n = 3 for each NP) were further prepared for LC-MS/MS analysis.

4.8. In solution digestion

The AuNP pellets (n = 3 for each NP) were reconstituted in 50 μL of denaturation buffer (6 M urea/2 M thiourea in 10 mM HEPES, pH 8.0) and reduced for 30 min at RT with 1 μL of 0.5 M DTT in 50 mM of ammonium bicarbonate (ABC, Carl Roth GmbH, Germany). The alkylation was carried out by adding 1 μL of 0.5 M IAA in ABC and

incubation for 30 min at RT in the dark. Subsequently, 2 µL of Trypsin/ Lys-C Mix (Promega) at a concentration of 0.5 µg/µL in ABC was added and incubated for 4 h at RT. The urea concentration was decreased to < 2 M by addition of 150 µL of ABC for trypsin digestion overnight at RT. The digestion was stopped by acidification with 200 µL of 5% acetonitrile (ACN), 3% trifluoroacetic acid. Tryptic peptides were desalted with stage tips [71].

4.9. Liquid chromatography-electrospray ionization-tandem mass spectroscopy (LC ESI MS/MS)

Desalted peptides were reconstituted in 20 µL of 0.1% (*v/v*) TFA, 5% (v/v) ACN and 4 µL were analyzed by a reversed-phase capillary nano-liquid chromatography system (Ultimate 3000, Thermo Scientific, United States of America) connected to an Orbitrap Velos mass spectrometer (Thermo Scientific). The LC system was coupled to the mass spectrometer via a nanospray flexion source equipped with a stainless-steel emitter (Thermo Scientific). Samples were injected and concentrated on a trap column (PepMap100 C18, 3 µm, 100 Å, 75 µm i.d. × 2 cm, Thermo Scientific) equilibrated with 0.05% TFA, 2% ACN in water. After switching the trap column inline, LC separations were performed on a capillary column (Acclaim PepMap100 C18, 2 µm, 100 Å, 75 µm i.d. × 25 cm, Thermo Scientific) at an eluent flow rate of 300 nL/min using a linear gradient of 3 50% B in 50 min. Mobile phase A contained 0.1% formic acid (FA) in water and mobile phase B contained 0.1% FA in ACN. Mass spectra were acquired in a data-dependent mode utilizing a single MS survey scan with a resolution of 60,000 in the Orbitrap and MS/MS scans of the 20 most intense precursor ions in the linear trap quadrupole. The MS survey range was *m/z* 350 1500. The dynamic exclusion time (for precursor ions) was set to 60 *s* and automatic gain control was set to 1×10^6 and 5.000 for Orbitrap-MS and LTQ-MS/MS scans, respectively.

4.10. Protein identification and label-free quantification of protein abundance

MS and MS/MS data from each LC/MS run were analyzed using the MaxQuant software (Version 1.6.0.16). Identification of proteins was performed using the MaxQuant-implemented Andromeda peptide search engine against a reference proteome database of *Homo sapiens* (Human/Uniprot proteome ID: UP000005640, Version October 1, 2017). Initial maximum precursor and fragment mass deviations were set to 7 ppm and 0.5 Da, respectively. Variable modification (methionine oxidation and N-terminal acetylation) and fixed modification (cysteine carbamidomethylation) were set for the search and trypsin with a maximum of two missed cleavages were chosen for searching. The minimum peptide length was set to 7 amino acids and the false discovery rate (FDR) for peptide and protein identification was set to 0.01. Relative protein abundance was determined using the TOP 3 approach. TOP 3 intensities of the identified proteins were calculated by summing up the intensities of the three most intense unique peptides for each protein [55].

CRediT authorship contribution statement

Tony Bewersdorff: Investigation, Methodology, Formal analysis, Writing - original draft. **Emanuel A. Glitscher**: Investigation, Methodology, Writing - original draft. **Julian Bergueiro**: Conceptualization, Supervision, Writing - review & editing. **Murat Eravci**: Investigation, Formal analysis. **Enrico Miceli**: Investigation, Writing - review & editing. **Andrea Haase**: Conceptualization, Supervision, Project administration, Writing - review & editing. **Marcelo Calderón**: Conceptualization, Supervision, Project administration, Writing - review & editing.

Declaration of competing interest

The authors declare that they have no known competing financial interests or personal relationships that could have appeared to influence the work reported in this paper.

Appendix A. Supplementary data

Supplementary data to this article can be found online at https:// doi.org/10.1016/j.msec.2020.111270.

References

[1] C.J. Ackerson, P.D. Jadzinsky, R.D. Kornberg, J. Am. Chem. Soc. 127 (2005) 6550–6551.
[2] M. Grzelczak, J. Perez-Juste, P. Mulvaney, L.M. Liz-Marzan, Chem. Soc. Rev. 37 (2008) 1783–1791.
[3] I. Hussain, S. Graham, Z. Wang, B. Tan, D.C. Sherrington, S.P. Rannard, A.I. Cooper, M. Brust, J. Am. Chem. Soc. 127 (2005) 16398–16399.
[4] N.R. Jana, L. Gearheart, C.J. Murphy, Langmuir 17 (2001) 6782–6786.
[5] S. Roux, B. Garcia, J.L. Bridot, M. Salome, C. Marquette, L. Lemelle, P. Gillet, L. Blum, P. Perriat, O. Tillement, Langmuir 21 (2005) 2526–2536.
[6] R. Sardar, J.S. Shumaker-Parry, J. Am. Chem. Soc. 133 (2011) 8179–8190.
[7] J.D. Wilton-Ely, Dalton Trans. 1 (2008) 25–29.
[8] M.C. Daniel, D. Astruc, Chem. Rev. 104 (2004) 293–346.
[9] Q. Cao, X. Wang, Q. Cui, Y. Yang, L. Li, Colloid. Surf. A Physicochem. Eng. Asp. 514 (2017) 117–125.
[10] J. Choi, H. Chung, J.-H. Yun, M. Cho, ACS Appl. Mater. Interfaces 8 (2016) 24008–24024.
[11] N.M. Danesh, P. Lavaee, M. Ramezani, K. Abnous, S.M. Taghdisi, Int. J. Pharm. 489 (2015) 311–317.
[12] A.R. Fernandes, J. Jesus, P. Martins, S. Figueiredo, D. Rosa, L.M. Martins, M.L. Corvo, M.C. Carvalheiro, P.M. Costa, P.V. Baptista, J. Control. Release 245 (2017) 52–61.
[13] T.-S. Lai, T.-C. Chang, S.-C. Wang, Sens. Actuators B Chem. 239 (2017) 9–16.
[14] S.M. Taghdisi, N.M. Danesh, P. Lavaee, A.S. Emrani, K.Y. Hassanabad, M. Ramezani, K. Abnous, Mater. Sci. Eng. C Mater. Biol. Appl. 61 (2016) 753–761.
[15] Y. Ye, J. Gao, H. Zhuang, H. Zheng, H. Sun, Y. Ye, X. Xu, X. Cao, Microchim. Acta 184 (2017) 245–252.
[16] D. Cabuzu, A. Cirja, R. Puiu, A.M. Grumezescu, Curr. Top. Med. Chem. 15 (2015) 1605–1613.
[17] C. Carrillo-Carrión, M. Nazarenus, S.S. Paradinas, S. Carregal-Romero, M.J. Almendral, M. Fuentes, B. Pelaz, P. del Pino, I. Hussain, M.J.D. Clift, B. Rothen-Rutishauser, X.-J. Liang, W.J. Parak, Curr. Opin. Chem. Eng. (4) (2014) 88–96.
[18] N. Feliu, D. Docter, M. Heine, P. del Pino, S. Ashraf, J. Kolosnjaj-Tabi, P. Macchiarini, P. Nielsen, D. Alloyeau, F. Gazeau, R.H. Stauber, W.J. Parak, Chem. Soc. Rev. 45 (2016) 2440–2457.
[19] L. Lartigue, C. Wilhelm, J. Servais, C. Factor, A. Dencausse, J.-C. Bacri, N. Luciani, F. Gazeau, ACS Nano 6 (2012) 2665–2678.
[20] S. Wan, P.M. Kelly, E. Mahon, H. Stöckmann, P.M. Rudd, F. Caruso, K.A. Dawson, Y. Yan, M.P. Monopoli, ACS Nano 9 (2015) 2157–2166.
[21] I. Lynch, T. Cedervall, M. Lundqvist, C. Cabaleiro-Lago, S. Linse, K.A. Dawson, Adv. Colloid Interf. Sci. 134-135 (2007) 167–174.
[22] M.P. Monopoli, D. Walczyk, A. Campbell, G. Elia, I. Lynch, F.B. Bombelli, K.A. Dawson, J. Am. Chem. Soc. 133 (2011) 2525–2534.
[23] B. Muthusamy, G. Hanumanthu, S. Suresh, B. Rekha, D. Srinivas, L. Karthick, B.M. Vrushabendra, S. Sharma, G. Mishra, P. Chatterjee, K.S. Mangala, H.N. Shivashankar, K.N. Chandrika, N. Deshpande, M. Suresh, N. Kannabiran, V. Niranjan, A. Nalli, T.S. Prasad, K.S. Arun, R. Reddy, S. Chandran, T. Jadhav, D. Julie, M. Mahesh, S.L. John, K. Palvankar, D. Sudhir, P. Bala, N.S. Rashmi, G. Vishnupriya, K. Dhar, S. Reshma, R. Chaerkady, T.K. Gandhi, H.C. Harsha, S.S. Mohan, K.S. Deshpande, M. Sarker, A. Pandey, Proteomics 5 (2005) 3531–3536.
[24] E. Casals, V.F. Puntes, Nanomedicine (Lond.) 7 (2012) 1917–1930.
[25] T. Cedervall, I. Lynch, S. Lindman, T. Berggard, E. Thulin, H. Nilsson, K.A. Dawson, S. Linse, Proc. Natl. Acad. Sci. U. S. A. 104 (2007) 2050–2055.
[26] M.P. Monopoli, C. Aberg, A. Salvati, K.A. Dawson, Nat. Nanotechnol. 7 (2012) 779–786.
[27] A.E. Nel, L. Madler, D. Velegol, T. Xia, E.M. Hoek, P. Somasundaran, F. Klaessig, V. Castranova, M. Thompson, Nat. Mater. 8 (2009) 543–557.
[28] D. Walczyk, F.B. Bombelli, M.P. Monopoli, I. Lynch, K.A. Dawson, J. Am. Chem. Soc. 132 (2010) 5761–5768.

[29] R. Del Cano, L. Mateus, G. Sanchez-Obrero, J.M. Sevilla, R. Madueno, M. Blazquez, T. Pineda, J. Colloid Interface Sci. 505 (2017) 1165–1171.
[30] A. Salvati, A.S. Pitek, M.P. Monopoli, K. Prapainop, F.B. Bombelli, D.R. Hristov, P.M. Kelly, C. Aberg, E. Mahon, K.A. Dawson, Nat. Nanotechnol. 8 (2013) 137–143.
[31] I. Lynch, K.A. Dawson, S. Linse, Sci. STKE 2006 (2006) 14.
[32] T. Cedervall, I. Lynch, M. Foy, T. Berggard, S.C. Donnelly, G. Cagney, S. Linse, K.A. Dawson, Angew. Chem. Int. Ed. Engl. 46 (2007) 5754–5756.
[33] M. Lundqvist, J. Stigler, G. Elia, I. Lynch, T. Cedervall, K.A. Dawson, Proc. Natl. Acad. Sci. U. S. A. 105 (2008) 14265–14270.
[34] M. Rahman, S. Laurent, N. Tawil, L.H. Yahia, M. Mahmoudi, Protein-Nanoparticle Interactions: The Bio-Nano Interface, Springer Berlin Heidelberg, 2013, pp. 21–44.
[35] P. Roach, D. Farrar, C.C. Perry, J. Am. Chem. Soc. 128 (2006) 3939–3945.
[36] Z.J. Deng, M. Liang, I. Toth, M.J. Monteiro, R.F. Minchin, ACS Nano 6 (2012) 8962–8969.
[37] S.H. Lacerda, J.J. Park, C. Meuse, D. Pristinski, M.L. Becker, A. Karim, J.F. Douglas, ACS Nano 4 (2010) 365–379.
[38] T. Bewersdorff, J. Vonnemann, A. Kanik, R. Haag, A. Haase, Int. J. Nanomedicine 12 (2017) 2001–2019.
[39] B.D. Johnston, W.G. Kreyling, C. Pfeiffer, M. Schaffler, H. Sarioglu, S. Ristig, S. Hirn, N. Haberl, S. Thalhammer, S.M. Hauck, M. SemmLer-Behnke, M. Epple, J. Huhn, P. Del Pino, W.J. Parak, Adv. Funct. Mater. 27 (2017) 1701956.
[40] G.N. Abdelrasoul, R. Magrassi, S. Dante, M. d'Amora, M.S. d'Abbusco, T. Pellegrino, A. Diaspro, Nanotechnology 27 (2016) 255101.
[41] W. Janetanakit, L. Wang, K. Santacruz-Gomez, P.B. Landon, P.L. Sud, N. Patel, G. Jang, M. Jain, A. Yepremyan, S.A. Kazmi, D.K. Ban, F. Zhang, R. Lal, ACS Appl. Mater. Interfaces 9 (2017) 27533–27543.
[42] M. Karimi, P.S. Zangabad, F. Mehdizadeh, H. Malekzad, A. Ghasemi, S. Bahrami, H. Zare, M. Moghoofei, A. Hekmatmanesh, M.R. Hamblin, Nanoscale 9 (2017) 1356–1392.
[43] P.C. Naha, P. Chhour, D.P. Cormode, Toxicol. in Vitro 29 (2015) 1445–1453.
[44] K.P. Steckiewicz, E. Barcinska, A. Malankowska, A. Zauszkiewicz-Pawlak, G. Nowaczyk, A. Zaleska-Medynska, I. Inkielewicz-Stepniak, J. Mater. Sci. Mater. Med. 30 (2019) 22.
[45] X. Yang, M. Yang, B. Pang, M. Vara, Y. Xia, Chem. Rev. 115 (2015) 10410–10488.
[46] G. Frens, Nature Phys. Sci. 241 (1973) 20–22.
[47] N.R. Jana, Small 1 (2005) 875–882.
[48] H. Yuan, C.G. Khoury, H. Hwang, C.M. Wilson, G.A. Grant, T. Vo-Dinh, Nanotechnology 23 (2012) 075102.
[49] S.E. Skrabalak, L. Au, X. Li, Y. Xia, Nat. Protoc. 2 (2007) 2182–2190.
[50] C.D. Walkey, W.C. Chan, Chem. Soc. Rev. 41 (2012) 2780–2799.
[51] E. Miceli, B. Kuropka, C. Rosenauer, E.R. Osorio Blanco, L.E. Theune, M. Kar, C. Weise, S. Morsbach, C. Freund, M. Calderon, Nanomedicine (Lond.) 13 (2018) 2657–2668.
[52] E. Miceli, M. Kar, M. Calderon, J. Mater. Chem. B 5 (2017) 4393–4405.
[53] K. Obst, G. Yealland, B. Balzus, E. Miceli, M. Dimde, C. Weise, M. Eravci, R. Bodmeier, R. Haag, M. Calderón, N. Charbaji, S. Hedtrich, Biomacromolecules 18 (2017) 1762–1771.
[54] L. Guerrini, R.A. Alvarez-Puebla, N. Pazos-Perez, Materials 11 (2018) 1154–1182.
[55] J.C. Silva, M.V. Gorenstein, G.Z. Li, J.P. Vissers, S.J. Geromanos, Mol. Cell. Proteomics 5 (2006) 144–156.
[56] J.C. Silva, R. Denny, C. Dorschel, M.V. Gorenstein, G.Z. Li, K. Richardson, D. Wall, S.J. Geromanos, Mol. Cell. Proteomics 5 (2006) 589–607.
[57] B. Pelaz, P. del Pino, P. Maffre, R. Hartmann, M. Gallego, S. Rivera-Fernandez, J.M. de la Fuente, G.U. Nienhaus, W.J. Parak, ACS Nano 9 (2015) 6996–7008.
[58] X. Xia, M. Yang, Y. Wang, Y. Zheng, Q. Li, J. Chen, Y. Xia, ACS Nano 6 (2012) 512–522.
[59] J. Lu, Y. Xue, R. Shi, J. Kang, C.-Y. Zhao, N.-N. Zhang, C.-Y. Wang, Z.-Y. Lu, K. Liu, Chem. Sci. 10 (2019) 2067–2074.
[60] R. Gref, M. Lück, P. Quellec, M. Marchand, E. Dellacherie, S. Harnisch, T. Blunk, R.H. Müller, Colloids Surf. B Biointerfaces 18 (2000) 301–313.
[61] P. Kingshott, H. Thissen, H.J. Griesser, Biomaterials 23 (2002) 2043–2056.
[62] R. García-Alvarez, M. Hadjidemetriou, A. Sánchez-Iglesias, L.M. Liz-Marzan, K. Kostarelos, Nanoscale 10 (2018) 1256–1264.
[63] E. Casals, T. Pfaller, A. Duschl, G.J. Oostingh, V. Puntes, ACS Nano 4 (2010) 3623–3632.
[64] W. Wohlleben, M.D. Driessen, S. Raesch, U.F. Schaefer, C. Schulze, B. von Vacano, A. Vennemann, M. Wiemann, C.A. Ruge, H. Platsch, S. Mues, R. Ossig, J.M. Tomm, J. Schnekenburger, T.A.J. Kuhlbusch, A. Luch, C.-M. Lehr, A. Haase, Nanotoxicology 10 (2016) 970–980.
[65] K.B.M. Reid, Front. Immunol. 9 (2018) 764.
[66] N.M. Thielens, F. Tedesco, S.S. Bohlson, C. Gaboriaud, A.J. Tenner, Mol. Immunol. 89 (2017) 73–83.
[67] S.E. Skrabalak, J. Chen, Y. Sun, X. Lu, L. Au, C.M. Cobley, Y. Xia, Acc. Chem. Res. 41 (2008) 1587–1595.
[68] I.K. Poon, K.K. Patel, D.S. Davis, C.R. Parish, M.D. Hulett, Blood 117 (2011) 2093–2101.
[69] M.A. Horton, Int. J. Biochem. Cell Biol. 29 (1997) 721–725.
[70] R. Pytela, M.D. Pierschbacher, E. Ruoslahti, Proc. Natl. Acad. Sci. U. S. A. 82 (1985) 5766–5770.
[71] P.P. Karmali, D. Simberg, Expert Opin. Drug Deliv. 8 (2011) 343–357.

3.4 Quantitative measurement of nanoparticle uptake by flow cytometry illustrated by an interlaboratory comparison of the uptake of labelled polystyrene nanoparticles

Anna Salvatia, Inge Nelissen, Andrea Haase, Christoffer Åberg, Sergio Moya, An Jacobs, Fatima Alnasser, Tony Bewersdorff, Sarah Deville, Andreas Luch, Kenneth A. Dawson

The authors contribution:

Sample preparation

Measurement of cellular uptake by flow cytometry

Evaluation of the own data

4   Summary and Conclusion

What the biological cell actually "sees" when it interacts with NPs dispersed in a biological medium probably is more important than the pure material properties of the bare particle itself.[133] Therefore, it is highly important to understand the interactions between NPs and proteins.

Within my thesis I focused on two main objectives. The influence of physico-chemical properties of NPs on the formation of a protein corona and the role of the protein-corona on cellular uptake.

4.1   Physico-chemical properties and formation of a protein corona

4.1.1   The influence of size and surface charge

In chapter 3.1 we dealt with dendritic polyglycerols and focused on two physico-chemical factors (size and surface charge). With the NPs used in this study, we were capable of showing that surface charge had a greater influence than size on protein corona formation. Thus, we were able to find significantly more proteins on the NPs that were negative (169 compared to 26) in terms of surface charge. This is in line with the results of other studies that have demonstrated that proteins tend to prefer negatively charged surfaces.[166] The comparison of the two different sizes (dPGS-Au50 vs. dPGS-Au20) did not reveal such a major difference in terms of protein numbers (169 compared to 114). Difference that still occur can be explained due to the varying curvature of the NPs. Depending on whether the protein is globular or fibrillar, the alteration of the surface curvature can lead to a change in the native conformation and thus alter the possibility of attachment. For example, fibrinogen, a fibrillar protein, can lose its native conformation as the surface curvature decreases and occupies more space on the nanoparticle.[167] Consequently, the surface area for the attachment of other proteins would be reduced.

After we had addressed the influence of size, we examined the influence of hydrophobicity.

4.1.2 Hydrophobicity and its impact on the formation of a protein corona

The NGs we used in chapter 3.2 deserve special attention, because their adjustable amphiphilic character makes them a well-suited candidate for embedding and transporting various drugs. With the recently developed synthetic platform approach by Klinger it is possible to tune the amphiphilicity while keeping the similar colloidal features of the NGs. Given this feature, we put our attention in chapter 3.3 to examine how the amphiphilic character affects protein binding. By using dynamic light scattering (DLS) measurement we could show that with ascending hydrophobicity the hydrodynamic diameter increases, indicating higher protein adsorption. These findings correlated with the results from 2D-PAGE, confirming significantly increased number and intensity of spots for increasing hydrophobicity. Comparable outcomes were obtained with liquid chromatography-tandem mass spectrometry (LC-MS/MS). Our study revealed that for NGs with a comparable hydrophobicity but various functional hydrophobic moieties the increase in protein adsorption varied significantly. Therefore, protein binding seems to be determined not only by the overall hydrophobicity, but is also affected by the molecular structure. In addition, the new synthetic platform approach allowed us to focus at the influence of hydrophobicity on the protein corona. Comparing the two groups of the hydrophobic NGs (moderate hydrophobic and hydrophobic), regarding the protein spots with significantly increased intensities, we found a higher overlap between the two most hydrophobic NGs (16 compared to 6). Similarities between comparable structures (linear versus non-linear moieties) were smaller, leading to the conclusion that the hydrophobicity has a higher influence than the structure.

After investigating the role of size and hydrophobicity, we addressed the influence of shape on the formation of a protein corona.

4.1.3 The shape of NPs and its effect on the protein-corona

Within the chapter 3.3 we investigated AuNPs with comparable sizes, where the shape and the surface charge could be changed systematically. We have compared 4 different shapes (spheres, rods, stars and cages), each with 3 different surface functionalization's (OCH_3, COOH, NH_2) in terms of their end groups. These end group functionalization's lead to different surface charges on the NPs. Therefore, it can be stated that we have NPs with a negative (COOH), positive (NH_2) and rather neutral (OCH_3) surface charge.

After the incubation of twelve different types of AuNPs (regarding shape and surface functionalization) with human serum we studied the individual formation of a protein corona. Protein binding was identified using liquid chromatography-tandem mass spectrometry and quantified via TOP 3 approach. We were able to identify more than 90 proteins for the different shapes and surface charges. Interestingly the gold nanocages (AuNCs) showed deviations, as we found less abundant proteins. This tendency was also visible in the overall intensities of the proteins identified by the TOP 3 approach. That may indicate a hindrance in the interaction between the serum proteins and the AuNCs by their structural appearance. For analysis of the protein corona 15 of the most abundant proteins for each NP were chosen. In total we found a total of 22 different proteins covering at least 67% of the total protein corona. The hierarchical clustering of the corona proteins suggests that rather the shape than the functional end groups have an influence on the formation of the corona. For a closer look at the similarities and differences within the protein coronas, we have selected some representative proteins. These allowed us to better illustrate the possible influence of shape or surface charge. As a result, we found that on the surface of the AuNCs, in relation to the total protein amount, significantly more albumin was bound than on the other NPs. It has already been shown that NPs that bind fewer different proteins in their corona show an enrichment of albumin.[168] In case of the AuNCs, we assume that the highly curved surface at the ends of the NPs and the higher grafting density of the PEG layer prevent other proteins from attaching. This also explains why we found high amounts of fast adsorbing proteins like albumin or immunoglobulins in the protein corona of all AuNCs. Due to their structure, AuNCs have the smallest surface area with strong curvatures and can therefore rather be compared to small spherical nanoparticles (which are known to show lower total abundances).[169]

On the other hand, due to the open structure of the AuNCs, there is a possibility that proteins bind inside and could not be determined with the method we used.

To analyze whether the structure or the surface charge has a greater influence on the composition, we summarized the proportion of proteins in the corona for the respective criteria across all NPs. The data summarized in this way obviously showed that there was greater variability within the structure. To further investigate the relationship between surface charge, shapes and protein corona, we calculated the mean values of the corresponding properties for all nanoparticles and determined the standard deviations. Subsequently, the percentage deviation of the standard deviation from the mean value was determined. Again, it is noticeable that the structure has a greater influence on the composition of the protein corona. Combining all our results and investigations, we can conclude that the structure of the NPs has a greater influence than the surface charge on the composition of the protein corona.

Following the studies concerning the influence of physico-chemical properties on protein corona formation, we were interested in the influence of the protein corona on cellular uptake of NPs.

4.2   The influence of the protein corona on cellular uptake

Crucial for the application of NPs in nanomedicine is whether they enter cells and the internalized amount. Considering the different compositions of the protein-coronas, varying cellular uptake pattern of the NPs should be evident. This will be displayed and discussed in the following chapters.

4.2.1 Effect of the size and surface charge on cellular uptake

The difference in the number of proteins on the surface (see 4.1.1) was also very well reflected in the uptake rates of the NPs. Negatively compared to positively charged NPs were strongly taken up into the cells. Which only reinforces the influence of the protein corona on the cellular uptake.

Generally speaking, the cell membrane has more negatively than positively charged areas on the surface. Consequently, positively charged NPs should be able to penetrate the cell membrane more easily than negatively charged NPs. Still negatively charged NPs were shown to be internalized and even be able to penetrate the cell membrane.[170, 171] Considering the possible influence of the proteins bound to the NP surface our results are in line with these observations.

In the following, we have investigated whether a similar correlation can also be found with hydrophobicity.

4.2.2 Impact of hydrophobicity on cellular uptake

We examined the composition of the protein coronas and took a closer look at the 15 most abundant proteins for each NG. Interestingly, we detected an enlargement of complement activation components like pentraxin, complement factor 1 and B for the most hydrophobic NGs in comparison to the moderate hydrophobic NGs. These opsonins could drastically reduce blood retention time and consequently even the biological half-life. Indeed, we were able to show this connection. Increased hydrophobicity and the resulting opsonin adsorption leaded to an increased cellular uptake in human monocytic like cells representing the RES.

4.3 Identification of possible uptake pathways

After characterization of the protein corona, we were interested in its influence on uptake. By performing a pull-down approach (chapter 3.1), subsequent experiments allowed us to identify several possible cellular interaction partners in the corona of the NPs. This gave us a first impression of the possible functioning of cellular uptake mechanisms and, in context with the NPs that were used, to pinpoint receptor-mediated uptake as a potentially key mechanism. Given the fact that NPs are typically covered by various proteins after entering the biological environment, there should be a complex interplay of different corona components. Therefore, either different proteins individually or in association may be responsible for the cellular uptake.

5   Outlook

This work contributes to the ongoing research on how the chemical properties of NPs influence the formation and composition of the protein corona. Our results can help preventing, limiting or even shifting protein accumulation in the desired direction. As a consequence, it might be possible to ensure that the blood circulation time of the NPs being prolonged and thus the administered dose being modifiable.

In this respect, further protein corona studies should be carried out with regard to the uptake behaviour in cells of the RES. A further step would also be the transition from *in vitro* to *in vivo*. Here it should be investigated whether the results obtained from the models can bear up against a "real life" application.

However, not only the addressing of NPs is of interest, but also the formation of the protein corona in biological environments. For the application of NPs as drug transporters, it is of utmost importance to know how they will behave in different biological environments. To achieve this, other models for biological environments, not only serum, should also be investigated for the formation of a protein corona on the surface of NPs.

The work presented in this thesis provides several starting points for further studies. For example, thanks to our pull-down experiment, good indications of possible ligand-receptor interactions could be found. These are particularly interesting for addressed NP delivery. Continuing investigations should identify further protein-ligand interactions between protein corona and receptors on the cell surface. To accomplish that, NPs with single protein coronas could be formed and examined for their uptake behaviour. In this context, the actual changes in the proteins on the surface of the nanoparticles could eventually also be explored. Furthermore, to get an even more detailed insight into the formation of the protein corona, the association and dissociation constants of the individual proteins could be measured.

The identification of receptors on cells of the RES with our pull-down experiment also offers the possibility to investigate the uptake pathways of NPs. With the identification of the receptors, further inhibitor experiments should also be carried out. We have already laid the foundation for further approaches with the identification of ligands and receptors.

6 Literature

1. Jeevanandam, J., et al., *Review on nanoparticles and nanostructured materials: history, sources, toxicity and regulations.* Beilstein J Nanotechnol, 2018. **9**: p. 1050-1074.
2. Kurniasih, I.N., J. Keilitz, and R. Haag, *Dendritic nanocarriers based on hyperbranched polymers.* Chem Soc Rev, 2015. **44**(12): p. 4145-64.
3. Griffin, S., et al., *Natural Nanoparticles: A Particular Matter Inspired by Nature.* Antioxidants (Basel), 2017. **7**(1).
4. Raab, C., et al., *Production of nanoparticles and nanomaterials*. 2015.
5. Zielonka, A. and M. Klimek-Ochab, *Fungal synthesis of size-defined nanoparticles.* Advances in Natural Sciences: Nanoscience and Nanotechnology, 2017. **8**(4): p. 043001.
6. Hamley, I.W., *Nanotechnology with soft materials.* Angew Chem Int Ed Engl, 2003. **42**(15): p. 1692-712.
7. Habiba, K., et al., *Fabrication of Nanomaterials by Pulsed Laser Synthesis*. 2014. p. 263-291.
8. Pinnell, S.R., et al., *Microfine zinc oxide is a superior sunscreen ingredient to microfine titanium dioxide.* Dermatol Surg, 2000. **26**(4): p. 309-14.
9. Rivero, P.J., et al., *Nanomaterials for Functional Textiles and Fibers.* Nanoscale Research Letters, 2015. **10**(1): p. 501.
10. Pitkethly, M.J., *Nanomaterials – the driving force.* Materials Today, 2004. **7**(12, Supplement): p. 20-29.
11. Mensah, F., H. Seyoum, and P. Misra, *Nanomaterials in Nanomedicine*, in *Applied Spectroscopy and the Science of Nanomaterials*, P. Misra, Editor. 2015, Springer Singapore: Singapore. p. 253-277.
12. De Jong, W.H. and P.J. Borm, *Drug delivery and nanoparticles:applications and hazards.* Int J Nanomedicine, 2008. **3**(2): p. 133-49.
13. Roduner, E., *Size matters: why nanomaterials are different.* Chem Soc Rev, 2006. **35**(7): p. 583-92.
14. Wang, Y., et al., *Enhanced dispersion stability of gold nanoparticles by the physisorption of cyclic poly(ethylene glycol).* Nature Communications, 2020. **11**(1): p. 6089.
15. Sanità, G., B. Carrese, and A. Lamberti, *Nanoparticle Surface Functionalization: How to Improve Biocompatibility and Cellular Internalization.* Frontiers in molecular biosciences, 2020. **7**: p. 587012-587012.
16. Singh, P., et al., *Gold Nanoparticles in Diagnostics and Therapeutics for Human Cancer.* Int J Mol Sci, 2018. **19**(7).
17. Xia, Q., et al., *Red blood cell membrane-camouflaged nanoparticles: a novel drug delivery system for antitumor application.* Acta Pharmaceutica Sinica B, 2019.
18. Ye, H., et al., *Manipulating nanoparticle transport within blood flow through external forces: an exemplar of mechanics in nanomedicine.* Proc Math Phys Eng Sci, 2018. **474**(2211): p. 20170845.
19. Gref, R., et al., *Biodegradable long-circulating polymeric nanospheres.* Science, 1994. **263**(5153): p. 1600-3.

20.   Frank, M.M. and L.F. Fries, *The role of complement in inflammation and phagocytosis.* Immunol Today, 1991. **12**(9): p. 322-6.

21.   Owens, D.E., 3rd and N.A. Peppas, *Opsonization, biodistribution, and pharmacokinetics of polymeric nanoparticles.* Int J Pharm, 2006. **307**(1): p. 93-102.

22.   Capjak, I., et al., *How protein coronas determine the fate of engineered nanoparticles in biological environment.* Arh Hig Rada Toksikol, 2017. **68**(4): p. 245-253.

23.   Lynch, I., A. Salvati, and K.A. Dawson, *What does the cell see?* Nature Nanotechnology, 2009. **4**: p. 546.

24.   Cedervall, T., et al., *Detailed identification of plasma proteins adsorbed on copolymer nanoparticles.* Angew Chem Int Ed Engl, 2007. **46**(30): p. 5754-6.

25.   Lynch, I., et al., *The nanoparticle-protein complex as a biological entity; a complex fluids and surface science challenge for the 21st century.* Adv Colloid Interface Sci, 2007. **134-135**: p. 167-74.

26.   Bewersdorff, T., et al., *The influence of surface charge on serum protein interaction and cellular uptake: studies with dendritic polyglycerols and dendritic polyglycerol-coated gold nanoparticles.* Int J Nanomedicine, 2017. **12**: p. 2001-2019.

27.   Bewersdorff, T., et al., *Amphiphilic nanogels: influence of surface hydrophobicity on protein corona, biocompatibility and cellular uptake.* Int J Nanomedicine, 2019. **14**: p. 7861-7878.

28.   Bewersdorff, T., et al., *The influence of shape and charge on protein corona composition in common gold nanostructures.* Materials Science and Engineering: C, 2020. **117**: p. 111270.

29.   Bangham, A.D., M.M. Standish, and J.C. Watkins, *Diffusion of univalent ions across the lamellae of swollen phospholipids.* J Mol Biol, 1965. **13**(1): p. 238-52.

30.   Langer, R. and J. Folkman, *Polymers for the sustained release of proteins and other macromolecules.* Nature, 1976. **263**(5580): p. 797-800.

31.   Goebel, F.D., et al., *Efficacy and safety of Stealth liposomal doxorubicin in AIDS-related Kaposi's sarcoma. The International SL-DOX Study Group.* Br J Cancer, 1996. **73**(8): p. 989-94.

32.   Hare, J.I., et al., *Challenges and strategies in anti-cancer nanomedicine development: An industry perspective.* Adv Drug Deliv Rev, 2017. **108**: p. 25-38.

33.   Brannon-Peppas, L. and J.O. Blanchette, *Nanoparticle and targeted systems for cancer therapy.* Adv Drug Deliv Rev, 2004. **56**(11): p. 1649-59.

34.   Kawasaki, E.S. and A. Player, *Nanotechnology, nanomedicine, and the development of new, effective therapies for cancer.* Nanomedicine, 2005. **1**(2): p. 101-9.

35.   Anselmo, A.C. and S. Mitragotri, *Nanoparticles in the clinic: An update.* Bioeng Transl Med, 2019. **4**(3): p. e10143.

36.   Hamidi, M., A. Azadi, and P. Rafiei, *Hydrogel nanoparticles in drug delivery.* Adv Drug Deliv Rev, 2008. **60**(15): p. 1638-49.

37.   Moghimi, S.M., A.C. Hunter, and J.C. Murray, *Long-circulating and target-specific nanoparticles: theory to practice.* Pharmacol Rev, 2001. **53**(2): p. 283-318.

38.   Panao Costa, J., et al., *Optimization of Chitosan-alpha-casein Nanoparticles for Improved Gene Delivery: Characterization, Stability, and Transfection Efficiency.* AAPS PharmSciTech, 2019. **20**(3): p. 132.

39.   Zepeda-Cervantes, J., et al., *Incorporation of ORF2 from Porcine Circovirus Type 2(PCV2) into genetically encoded nanoparticles as a novel vaccine using a self-aggregating peptide.* Vaccine, 2019. **37**(14): p. 1928-1937.

40. Ravichandran, R., *Nanotechnology-Based Drug Delivery Systems.* NanoBiotechnology, 2009. **5**(1): p. 17-33.

41. Sharma, H., et al., *Metal nanoparticles: a theranostic nanotool against cancer.* Drug Discov Today, 2015. **20**(9): p. 1143-51.

42. Wang, S., et al., *Three-photon luminescence of gold nanorods and its applications for high contrast tissue and deep in vivo brain imaging.* Theranostics, 2015. **5**(3): p. 251-266.

43. Matsumura, Y. and H. Maeda, *A new concept for macromolecular therapeutics in cancer chemotherapy: mechanism of tumoritropic accumulation of proteins and the antitumor agent smancs.* Cancer Res, 1986. **46**(12 Pt 1): p. 6387-92.

44. Maeda, H., et al., *Tumor vascular permeability and the EPR effect in macromolecular therapeutics: a review.* J Control Release, 2000. **65**(1-2): p. 271-84.

45. Choi, H.S. and J.V. Frangioni, *Nanoparticles for biomedical imaging: fundamentals of clinical translation.* Mol Imaging, 2010. **9**(6): p. 291-310.

46. Bishop, C.J., S.Y. Tzeng, and J.J. Green, *Degradable polymer-coated gold nanoparticles for co-delivery of DNA and siRNA.* Acta Biomater, 2015. **11**: p. 393-403.

47. Gossai, N.P., et al., *Drug conjugated nanoparticles activated by cancer cell specific mRNA.* Oncotarget, 2016. **7**(25): p. 38243-38256.

48. Guan, Y.H., et al., *Preparation of novel cisplatin-conjugated hollow gold nanospheres for targeting cervical cancer.* J Cell Physiol, 2019.

49. Luan, X., et al., *Anisamide-targeted PEGylated gold nanoparticles designed to target prostate cancer mediate: Enhanced systemic exposure of siRNA, tumour growth suppression and a synergistic therapeutic response in combination with paclitaxel in mice.* Eur J Pharm Biopharm, 2019. **137**: p. 56-67.

50. Ramchandani, D., et al., *Nanoparticle Delivery of miR-708 Mimetic Impairs Breast Cancer Metastasis.* Mol Cancer Ther, 2019. **18**(3): p. 579-591.

51. Woiski, T.D., et al., *Anti-hMC2RL1 Functionalized Gold Nanoparticles for Adrenocortical Tumor Cells Targeting and Imaging.* J Biomed Nanotechnol, 2017. **13**(1): p. 68-76.

52. Zhang, D., et al., *Nano-Gold Loaded with Resveratrol Enhance the Anti-Hepatoma Effect of Resveratrol In Vitro and In Vivo.* J Biomed Nanotechnol, 2019. **15**(2): p. 288-300.

53. Choi, C.H., et al., *Mechanism of active targeting in solid tumors with transferrin-containing gold nanoparticles.* Proc Natl Acad Sci U S A, 2010. **107**(3): p. 1235-40.

54. Cui, Y.N., et al., *Enhanced intracellular delivery and controlled drug release of magnetic PLGA nanoparticles modified with transferrin.* Acta Pharmacol Sin, 2017. **38**(6): p. 943-953.

55. Low, P.S. and S.A. Kularatne, *Folate-targeted therapeutic and imaging agents for cancer.* Curr Opin Chem Biol, 2009. **13**(3): p. 256-62.

56. Calderon, M., et al., *Dendritic polyglycerols for biomedical applications.* Adv Mater, 2010. **22**(2): p. 190-218.

57. Hawker, C.J., et al., *Exact Linear Analogs of Dendritic Polyether Macromolecules: Design, Synthesis, and Unique Properties.* Journal of the American Chemical Society, 1997. **119**(41): p. 9903-9904.

58. Wooley, K.L., J.M.J. Fréchet, and C.J. Hawker, *Influence of shape on the reactivity and properties of dendritic, hyperbranched and linear aromatic polyesters.* Polymer, 1994. **35**(21): p. 4489-4495.

59.   Ooya, T., J. Lee, and K. Park, *Effects of ethylene glycol-based graft, star-shaped, and dendritic polymers on solubilization and controlled release of paclitaxel.* J Control Release, 2003. **93**(2): p. 121-7.

60.   Kowalczuk, A., et al., *Loading of polymer nanocarriers: Factors, mechanisms and applications.* Progress in Polymer Science, 2014. **39**(1): p. 43-86.

61.   Tomalia, D.A., L.A. Reyna, and S. Svenson, *Dendrimers as multi-purpose nanodevices for oncology drug delivery and diagnostic imaging.* Biochem Soc Trans, 2007. **35**(Pt 1): p. 61-7.

62.   Gardikis, K., et al., *Dendrimers and the Development of New Complex Nanomaterials for Biomedical Applications.* Current Medicinal Chemistry, 2012. **19**(29): p. 4913-4928.

63.   Taghavi P.A, N., P. Mutlu, and U. Gunduz, *Bioapplications of poly(amidoamine) (PAMAM) dendrimers in nanomedicine*. Vol. 16. 2014.

64.   Markatou, E., et al., *Molecular interactions between dimethoxycurcumin and Pamam dendrimer carriers.* International Journal of Pharmaceutics, 2007. **339**(1): p. 231-236.

65.   Yu, G.S., et al., *Synthesis of PAMAM Dendrimer Derivatives with Enhanced Buffering Capacity and Remarkable Gene Transfection Efficiency.* Bioconjugate Chemistry, 2011. **22**(6): p. 1046-1055.

66.   Mukherjee, S.P., M. Davoren, and H.J. Byrne, *In vitro mammalian cytotoxicological study of PAMAM dendrimers – Towards quantitative structure activity relationships.* Toxicology in Vitro, 2010. **24**(1): p. 169-177.

67.   Mukherjee, S.P., et al., *Mechanistic studies of in vitro cytotoxicity of poly(amidoamine) dendrimers in mammalian cells.* Toxicology and Applied Pharmacology, 2010. **248**(3): p. 259-268.

68.   Jiang, Y.-H., et al., *SPL7013 Gel as a Topical Microbicide for Prevention of Vaginal Transmission of SHIV89.6P in Macaques.* AIDS Research and Human Retroviruses, 2005. **21**(3): p. 207-213.

69.   Hajebi, S., et al., *Stimulus-responsive polymeric nanogels as smart drug delivery systems.* Acta Biomater, 2019. **92**: p. 1-18.

70.   Soni, G. and K.S. Yadav, *Nanogels as potential nanomedicine carrier for treatment of cancer: A mini review of the state of the art.* Saudi Pharm J, 2016. **24**(2): p. 133-9.

71.   Soni, K.S., S.S. Desale, and T.K. Bronich, *Nanogels: An overview of properties, biomedical applications and obstacles to clinical translation.* J Control Release, 2016. **240**: p. 109-126.

72.   Rajar, K., et al., *One pot synthesis and characterization of Fe3O4 Nanorod-PNIPA Nanogel Composite for protein adsorption.* Mater Sci Eng C Mater Biol Appl, 2016. **68**: p. 59-64.

73.   Tsintou, M., et al., *5 - Nanogels for biomedical applications: Drug delivery, imaging, tissue engineering, and biosensors*, in *Nanobiomaterials Science, Development and Evaluation*, M. Razavi and A. Thakor, Editors. 2017, Woodhead Publishing. p. 87-124.

74.   Guo, B., et al., *One-pot synthesis of polypyrrole nanoparticles with tunable photothermal conversion and drug loading capacity.* Colloids Surf B Biointerfaces, 2019. **177**: p. 346-355.

75.   Huh, A.J. and Y.J. Kwon, *"Nanoantibiotics": a new paradigm for treating infectious diseases using nanomaterials in the antibiotics resistant era.* J Control Release, 2011. **156**(2): p. 128-45.

76.   Kar, M., et al., *Chapter 12 Responsive Nanogels for Anti-cancer Therapy*, in *Nanogels for Biomedical Applications*. 2018, The Royal Society of Chemistry. p. 210-260.

77. Klinger, D. and K. Landfester, *Stimuli-responsive microgels for the loading and release of functional compounds: Fundamental concepts and applications.* Polymer, 2012. **53**(23): p. 5209-5231.

78. Molina, M., et al., *Stimuli-responsive nanogel composites and their application in nanomedicine.* Chemical Society Reviews, 2015. **44**(17): p. 6161-6186.

79. Molina, M., et al., *Overcoming drug resistance with on-demand charged thermoresponsive dendritic nanogels.* Nanomedicine (Lond), 2017. **12**(2): p. 117-129.

80. Shatsberg, Z., et al., *Functionalized nanogels carrying an anticancer microRNA for glioblastoma therapy.* J Control Release, 2016. **239**: p. 159-68.

81. Wu, C., et al., *Design of injectable agar-based composite hydrogel for multi-mode tumor therapy.* Carbohydr Polym, 2018. **180**: p. 112-121.

82. Shah, S., et al., *"Nanogels as drug carriers – Introduction, chemical aspects, release mechanisms and potential applications".* International Journal of Pharmaceutics, 2020. **581**: p. 119268.

83. Hajebi, S., et al., *Hybrid and hollow Poly(N,N-dimethylaminoethyl methacrylate) nanogels as stimuli-responsive carriers for controlled release of doxorubicin.* Polymer, 2019. **180**: p. 121716.

84. Shah, S., et al., *"Nanogels as drug carriers - Introduction, chemical aspects, release mechanisms and potential applications".* Int J Pharm, 2020. **581**: p. 119268.

85. Choi, J.H., et al., *Multi-layered nanogels with MMP-sheddable PEG masks: Preparation and promotion of tumor cell uptake by controlling surface characteristics.* Colloids and Surfaces B: Biointerfaces, 2017. **156**: p. 71-78.

86. Pérez-Mas, L., et al., *Effect of dispersion forces on the behavior of thermosensitive nanogels: A coarse-grained simulation study.* Journal of Molecular Liquids, 2019. **288**: p. 111101.

87. Costa, D.F., L.P. Mendes, and V.P. Torchilin, *The effect of low- and high-penetration light on localized cancer therapy.* Advanced Drug Delivery Reviews, 2019. **138**: p. 105-116.

88. Tsai, W.-K. and Y.-H. Chan, *Semiconducting polymer dots as near-infrared fluorescent probes for bioimaging and sensing.* Journal of the Chinese Chemical Society, 2019. **66**(1): p. 9-20.

89. Kumarasamy, D. and T. Giri, *Biopolysaccharide-based hydrogel materials for drug delivery*. 2019. p. 585-613.

90. Lv, X., et al., *Influence of chitosan oligosaccharide on the gelling and wound healing properties of injectable hydrogels based on carboxymethyl chitosan/alginate polyelectrolyte complexes.* Carbohydr Polym, 2019. **205**: p. 312-321.

91. Fleischmann, C., et al., *A robust platform for functional microgels via thiol-ene achemistry with reactive polyether-based nanoparticles.* Polym Chem, 2015. **6**(11): p. 2029-2037.

92. Gruber, A., et al., *A versatile synthetic platform for amphiphilic nanogels with tunable hydrophobicity.* Polymer Chemistry, 2018. **9**(47): p. 5572-5584.

93. Chen, W., et al., *Cyclo(RGD)-Decorated Reduction-Responsive Nanogels Mediate Targeted Chemotherapy of Integrin Overexpressing Human Glioblastoma In Vivo.* Small, 2017. **13**(6).

94. Baklaushev, V.P., et al., *Treatment of glioma by cisplatin-loaded nanogels conjugated with monoclonal antibodies against Cx43 and BSAT1.* Drug Deliv, 2015. **22**(3): p. 276-85.

95. Sato, T., et al., *Evaluation of PLLA–collagen hybrid sponge as a scaffold for cartilage tissue engineering.* Materials Science and Engineering: C, 2004. **24**(3): p. 365-372.

96. Zhang, Y., et al., *New Gold Nanostructures for Sensor Applications: A Review.* Materials (Basel), 2014. **7**(7): p. 5169-5201.

97. Zhang, Y., et al., *Multifunctional Gold Nanorods with Ultrahigh Stability and Tunability for In Vivo Fluorescence Imaging, SERS Detection, and Photodynamic Therapy.* Angewandte Chemie International Edition, 2013. **52**(4): p. 1148-1151.

98. Zhang, Z., et al., *Near Infrared Laser-Induced Targeted Cancer Therapy Using Thermoresponsive Polymer Encapsulated Gold Nanorods.* Journal of the American Chemical Society, 2014. **136**(20): p. 7317-7326.

99. Cao, Q., et al., *Synthesis and application of bifunctional gold/gelatin nanocomposites with enhanced fluorescence and Raman scattering.* Colloids and Surfaces A: Physicochemical and Engineering Aspects, 2017. **514**: p. 117-125.

100. Choi, J., et al., *Molecular Dynamics Study on the Photothermal Actuation of a Glassy Photoresponsive Polymer Reinforced with Gold Nanoparticles with Size Effect.* ACS Appl Mater Interfaces, 2016. **8**(36): p. 24008-24.

101. Danesh, N.M., et al., *Targeted and controlled release delivery of daunorubicin to T-cell acute lymphoblastic leukemia by aptamer-modified gold nanoparticles.* Int J Pharm, 2015. **489**(1-2): p. 311-7.

102. Daniel, M.C. and D. Astruc, *Gold nanoparticles: assembly, supramolecular chemistry, quantum-size-related properties, and applications toward biology, catalysis, and nanotechnology.* Chem Rev, 2004. **104**(1): p. 293-346.

103. Fernandes, A.R., et al., *Multifunctional gold-nanoparticles: A nanovectorization tool for the targeted delivery of novel chemotherapeutic agents.* J Control Release, 2017. **245**: p. 52-61.

104. Grzelczak, M., et al., *Shape control in gold nanoparticle synthesis.* Chem Soc Rev, 2008. **37**(9): p. 1783-91.

105. Lai, T.-S., T.-C. Chang, and S.-C. Wang, *Gold nanoparticle-based colorimetric methods to determine protein contents in artificial urine using membrane micro-concentrators and mobile phone camera.* Sensors and Actuators B: Chemical, 2017. **239**: p. 9-16.

106. Saha, K., et al., *Gold nanoparticles in chemical and biological sensing.* Chem Rev, 2012. **112**(5): p. 2739-79.

107. Taghdisi, S.M., et al., *Double targeting, controlled release and reversible delivery of daunorubicin to cancer cells by polyvalent aptamers-modified gold nanoparticles.* Mater Sci Eng C Mater Biol Appl, 2016. **61**: p. 753-61.

108. Ye, Y., et al., *Electrochemical gene sensor based on a glassy carbon electrode modified with hemin-functionalized reduced graphene oxide and gold nanoparticle-immobilized probe DNA.* Microchimica Acta, 2017. **184**(1): p. 245-252.

109. Jana, N.R., *Gram-scale synthesis of soluble, near-monodisperse gold nanorods and other anisotropic nanoparticles.* Small, 2005. **1**(8-9): p. 875-82.

110. Skrabalak, S.E., et al., *Facile synthesis of Ag nanocubes and Au nanocages.* Nat Protoc, 2007. **2**(9): p. 2182-90.

111. Yuan, H., et al., *Gold nanostars: surfactant-free synthesis, 3D modelling, and two-photon photoluminescence imaging.* Nanotechnology, 2012. **23**(7): p. 075102.

112. Du, F., et al., *Hyaluronic acid-functionalized bismuth oxide nanoparticles for computed tomography imaging-guided radiotherapy of tumor.* International journal of nanomedicine, 2017. **12**: p. 5973-5992.

113. Silva, C.O., et al., *Bioproduction of gold nanoparticles for photothermal therapy.* Ther Deliv, 2016. **7**(5): p. 287-304.

114. Villar-Alvarez, E., et al., *Gold Nanorod-Based Nanohybrids for Combinatorial Therapeutics.* ACS Omega, 2018. **3**(10): p. 12633-12647.

115. Sztandera, K., M. Gorzkiewicz, and B. Klajnert-Maculewicz, *Gold Nanoparticles in Cancer Treatment.* Mol Pharm, 2019. **16**(1): p. 1-23.

116. Kobayashi, K., et al., *Surface engineering of nanoparticles for therapeutic applications.* Polymer Journal, 2014. **46**(8): p. 460-468.

117. Chen, W.H., et al., *Therapeutic nanomedicine based on dual-intelligent functionalized gold nanoparticles for cancer imaging and therapy in vivo.* Biomaterials, 2013. **34**(34): p. 8798-807.

118. Li, X., et al., *PEGylated PAMAM dendrimer-doxorubicin conjugate-hybridized gold nanorod for combined photothermal-chemotherapy.* Biomaterials, 2014. **35**(24): p. 6576-6584.

119. Muddineti, O.S., B. Ghosh, and S. Biswas, *Current trends in using polymer coated gold nanoparticles for cancer therapy.* Int J Pharm, 2015. **484**(1-2): p. 252-67.

120. Gotov, O., G. Battogtokh, and Y.T. Ko, *Docetaxel-Loaded Hyaluronic Acid-Cathepsin B-Cleavable-Peptide-Gold Nanoparticles for the Treatment of Cancer.* Mol Pharm, 2018. **15**(10): p. 4668-4676.

121. Zayed, G.M., et al., *Effect of Chemical Binding of Doxorubicin Hydrochloride to Gold Nanoparticles, Versus Electrostatic Adsorption, on the In Vitro Drug Release and Cytotoxicity to Breast Cancer Cells.* Pharm Res, 2018. **35**(6): p. 112.

122. Libutti, S.K., et al., *Phase I and pharmacokinetic studies of CYT-6091, a novel PEGylated colloidal gold-rhTNF nanomedicine.* Clin Cancer Res, 2010. **16**(24): p. 6139-49.

123. Spadavecchia, J., et al., *Targeted polyethylene glycol gold nanoparticles for the treatment of pancreatic cancer: from synthesis to proof-of-concept in vitro studies.* Int J Nanomedicine, 2016. **11**: p. 791-822.

124. Agency, E.M. *From laboratory to patient: the journey of a centrally authorised medicine.* 103813/2018 Rev. 1 2019 [cited 2022 04.02.2022]; Available from: https://www.ema.europa.eu/en/documents/other/laboratory-patient-journey-centrally-authorised-medicine_en.pdf.

125. Eifler, A.C. and C.S. Thaxton, *Nanoparticle therapeutics: FDA approval, clinical trials, regulatory pathways, and case study.* Methods Mol Biol, 2011. **726**: p. 325-38.

126. Aina, O.H., et al., *From Combinatorial Chemistry to Cancer-Targeting Peptides.* Molecular Pharmaceutics, 2007. **4**(5): p. 631-651.

127. Brooks, W.H., et al., *In Silico Chemical Library Screening and Experimental Validation of a Novel 9-Aminoacridine Based Lead-Inhibitor of Human S-Adenosylmethionine Decarboxylase.* Journal of Chemical Information and Modeling, 2007. **47**(5): p. 1897-1905.

128. Ferrari, M., *Cancer nanotechnology: opportunities and challenges.* Nature Reviews Cancer, 2005. **5**(3): p. 161-171.

129. Dobrovolskaia, M.A. and S.E. McNeil, *Immunological properties of engineered nanomaterials.* Nature Nanotechnology, 2007. **2**(8): p. 469-478.

130. Leonard, E.M., *Quality assurance and the drug development process: an FDA perspective.* Qual Assur, 1994. **3**(2): p. 178-86.

131. Monopoli, M.P., et al., *Biomolecular coronas provide the biological identity of nanosized materials.* Nat Nanotechnol, 2012. **7**(12): p. 779-86.

132. Ge, C., et al., *Towards understanding of nanoparticle-protein corona.* Arch Toxicol, 2015. **89**(4): p. 519-39.

133. Walczyk, D., et al., *What the Cell "Sees" in Bionanoscience.* Journal of the American Chemical Society, 2010. **132**(16): p. 5761-5768.

134. Hellstrand, E., et al., *Complete high-density lipoproteins in nanoparticle corona.* FEBS J, 2009. **276**(12): p. 3372-81.

135. Wan, S., et al., *The "sweet" side of the protein corona: effects of glycosylation on nanoparticle-cell interactions.* ACS Nano, 2015. **9**(2): p. 2157-66.

136. Cheng, X., et al., *Protein Corona Influences Cellular Uptake of Gold Nanoparticles by Phagocytic and Nonphagocytic Cells in a Size-Dependent Manner.* ACS Appl Mater Interfaces, 2015. **7**(37): p. 20568-75.

137. Jo, D.H., et al., *Size, surface charge, and shape determine therapeutic effects of nanoparticles on brain and retinal diseases.* Nanomedicine, 2015. **11**(7): p. 1603-11.

138. Lynch, I. and K.A. Dawson, *Protein-nanoparticle interactions.* Nano Today, 2008. **3**(1): p. 40-47.

139. Mahmoudi, M., et al., *Protein-nanoparticle interactions: opportunities and challenges.* Chem Rev, 2011. **111**(9): p. 5610-37.

140. Monopoli, M.P., et al., *Physical-chemical aspects of protein corona: relevance to in vitro and in vivo biological impacts of nanoparticles.* J Am Chem Soc, 2011. **133**(8): p. 2525-34.

141. Ritz, S., et al., *Protein corona of nanoparticles: distinct proteins regulate the cellular uptake.* Biomacromolecules, 2015. **16**(4): p. 1311-21.

142. Zanganeh, S., et al., *Protein corona: Opportunities and challenges.* Int J Biochem Cell Biol, 2016. **75**: p. 143-7.

143. Dee, K.C., D.A. Puleo, and R.J.A.i.t.t.-b.i. Bizios, *Protein-surface interactions.* 2002: p. 37-52.

144. Latour, R.A., *Fundamental Principles of the Thermodynamics and Kinetics of Protein Adsorption to Material Surfaces.* Colloids and Surfaces B: Biointerfaces, 2020. **191**: p. 110992.

145. Vroman, L., et al., *Interaction of high molecular weight kininogen, factor XII, and fibrinogen in plasma at interfaces.* Blood, 1980. **55**(1): p. 156-9.

146. Walkey, C.D. and W.C. Chan, *Understanding and controlling the interaction of nanomaterials with proteins in a physiological environment.* Chem Soc Rev, 2012. **41**(7): p. 2780-99.

147. Fleischer, C.C. and C.K. Payne, *Nanoparticle-cell interactions: molecular structure of the protein corona and cellular outcomes.* Acc Chem Res, 2014. **47**(8): p. 2651-9.

148. Lundqvist, M., et al., *The evolution of the protein corona around nanoparticles: a test study.* ACS Nano, 2011. **5**(9): p. 7503-9.

149. Panariti, A., G. Miserocchi, and I. Rivolta, *The effect of nanoparticle uptake on cellular behavior: disrupting or enabling functions?* Nanotechnol Sci Appl, 2012. **5**: p. 87-100.

150. Donahue, N.D., H. Acar, and S. Wilhelm, *Concepts of nanoparticle cellular uptake, intracellular trafficking, and kinetics in nanomedicine.* Adv Drug Deliv Rev, 2019. **143**: p. 68-96.

151. Conner, S.D. and S.L. Schmid, *Regulated portals of entry into the cell.* Nature, 2003. **422**(6927): p. 37-44.

152. Brown, C.M. and N.O. Petersen, *Free clathrin triskelions are required for the stability of clathrin-associated adaptor protein (AP-2) coated pit nucleation sites.* Biochem Cell Biol, 1999. **77**(5): p. 439-48.

153. Hirst, J. and M.S. Robinson, *Clathrin and adaptors.* Biochimica et Biophysica Acta (BBA) - Molecular Cell Research, 1998. **1404**(1): p. 173-193.

154. Praefcke, G.J. and H.T. McMahon, *The dynamin superfamily: universal membrane tubulation and fission molecules?* Nat Rev Mol Cell Biol, 2004. **5**(2): p. 133-47.

155. Sousa de Almeida, M., et al., *Understanding nanoparticle endocytosis to improve targeting strategies in nanomedicine.* Chemical Society Reviews, 2021. **50**(9): p. 5397-5434.

156. Zhao, J. and M.H. Stenzel, *Entry of nanoparticles into cells: the importance of nanoparticle properties.* Polymer Chemistry, 2018. **9**(3): p. 259-272.

157. Benyettou, F., et al., *Synthesis of silver nanoparticles for the dual delivery of doxorubicin and alendronate to cancer cells.* J Mater Chem B, 2015. **3**(36): p. 7237-7245.

158. Haddad, D., et al., *Role of Caveolin-1 in Diabetes and Its Complications.* Oxidative medicine and cellular longevity, 2020. **2020**: p. 9761539-9761539.

159. Pelkmans, L. and A. Helenius, *Endocytosis via caveolae.* Traffic, 2002. **3**(5): p. 311-20.

160. Raja, S.A., et al., *Caveolin-1 and dynamin-2 overexpression is associated with the progression of bladder cancer.* Oncol Lett, 2019. **18**(1): p. 219-226.

161. Sens, P. and M.S. Turner, *Budded membrane microdomains as tension regulators.* Physical Review E, 2006. **73**(3): p. 031918.

162. Blanco, E., H. Shen, and M. Ferrari, *Principles of nanoparticle design for overcoming biological barriers to drug delivery.* Nature biotechnology, 2015. **33**(9): p. 941-951.

163. Carver, L.A. and J.E. Schnitzer, *Caveolae: mining little caves for new cancer targets.* Nat Rev Cancer, 2003. **3**(8): p. 571-81.

164. Rejman, J., M. Conese, and D. Hoekstra, *Gene transfer by means of lipo- and polyplexes: role of clathrin and caveolae-mediated endocytosis.* J Liposome Res, 2006. **16**(3): p. 237-47.

165. Gradishar, W.J., *Albumin-bound paclitaxel: a next-generation taxane.* Expert Opin Pharmacother, 2006. **7**(8): p. 1041-53.

166. Dernedde, J., et al., *Dendritic polyglycerol sulfates as multivalent inhibitors of inflammation.* Proc Natl Acad Sci U S A, 2010. **107**(46): p. 19679-84.

167. Roach, P., D. Farrar, and C.C. Perry, *Surface tailoring for controlled protein adsorption: effect of topography at the nanometer scale and chemistry.* J Am Chem Soc, 2006. **128**(12): p. 3939-45.

168. Wohlleben, W., et al., *Influence of agglomeration and specific lung lining lipid/protein interaction on short-term inhalation toxicity.* Nanotoxicology, 2016. **10**(7): p. 970-80.

169. Lacerda, S.H., et al., *Interaction of gold nanoparticles with common human blood proteins.* ACS Nano, 2010. **4**(1): p. 365-79.

170. Gupta, R. and B. Rai, *Effect of Size and Surface Charge of Gold Nanoparticles on their Skin Permeability: A Molecular Dynamics Study.* Sci Rep, 2017. **7**: p. 45292.

171. Ma, N., et al., *Influence of nanoparticle shape, size, and surface functionalization on cellular uptake.* J Nanosci Nanotechnol, 2013. **13**(10): p. 6485-98.

Annex I

Supplementary information

Title:

The influence of surface charge on serum protein interaction and cellular uptake: studies with dendritic polyglycerols and dendritic polyglycerol-coated gold nanoparticles

Authors:

Tony Bewersdorff, Jonathan Vonnemann, Asiye Kanik, Rainer Haag, Andrea Haase

Journal:

International Journal of Nanomedicine on 14 March 2017

DOI: 10.2147/IJN.S124295

Link: https://doi.org/10.2147/IJN.S124295
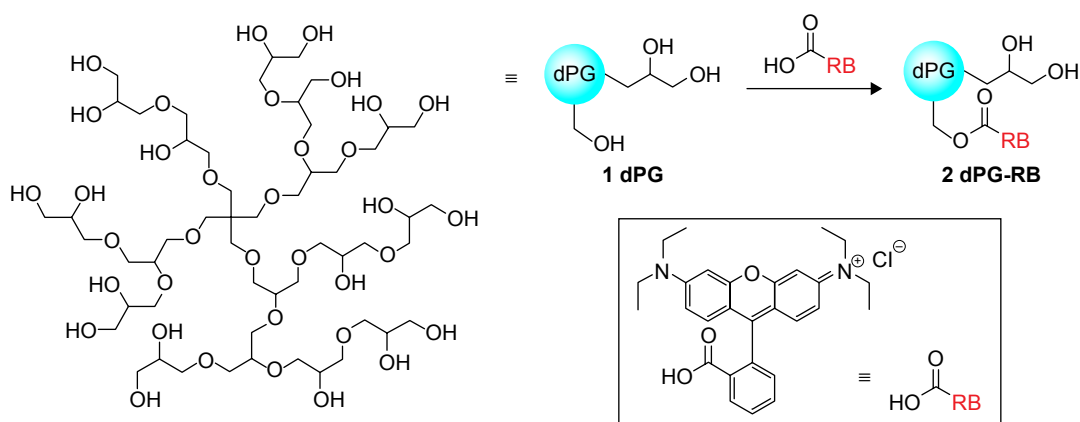
Supplementary materials

Figure S1 Schematic illustration of the synthesis of rhodamine-B-labeled dendritic polyglycerol (dPGOH-RB).

Notes: The synthesis through esterification is described in detail elsewhere.[1] Briefly, dry dendritic polyglycerol (dPGOH) was dissolved in anhydrous DMF and cooled to 0°C. Rhodamine B (159.67 mg, 0.33 mmol), DMAP (5.0 mg, 40.93 mol), NHS (134.27 mg, 1.17 mmol), and DCC (241.4 mg, 1.17 mmol) were added, and the mixture was allowed to achieve the room temperature. The mixture was stirred overnight, and the solvent was evaporated. Later, water was added. The obtained solution was extracted with DCM, and the phases were separated. Then, the solvent was evaporated, and chloroform was added. After ultrasonification (1 h), the solvent was decanted. Purification was accomplished by ultrafiltration in water and Sephadex™ G-25 SEC in water. Freeze-drying yielded the pure product. Average number of dye molecule incorporation (1.6) per polymer was determined by UV-Vis-spectroscopy.

Abbreviations: DMF, dimethylformamide; DMAP, 4-dimethylaminopyridine; NHS, N-hydroxysuccinimide; DCC, N,N′-dicyclohexylcarbodiimide; DCM, dichloromethane.
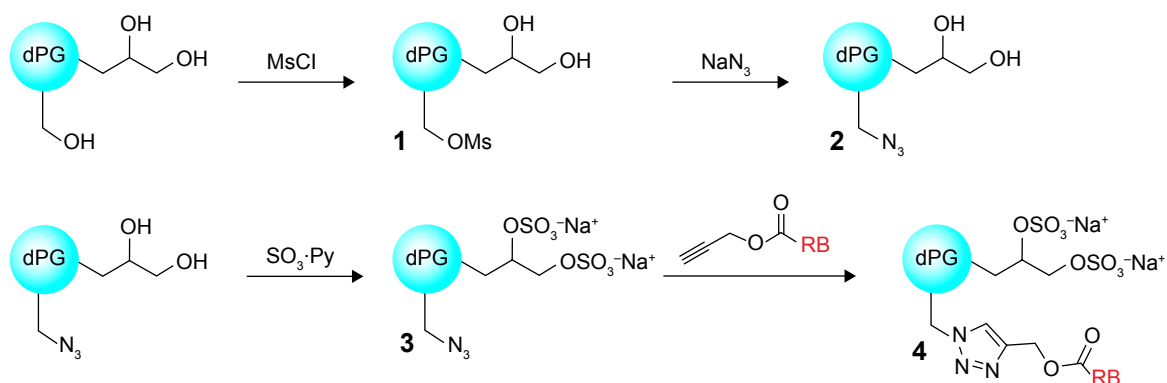

Figure S2 Schematic illustration of the synthesis of rhodamine-B-labeled dendritic polyglycerol sulfate (dPGS-RB).

Notes: The synthesis through partial mesylation (1), azidation (2), sulfation (3), and click coupling of alkyne functionalized rhodamine B (4) is described in detail elsewhere.[1] A solution of dPGOH (9.87 g, 1.65 mmol, 133.2 mmol OH groups) in anhydrous pyridine was cooled to 0°C and mesyl chloride (1.78 mL, 2.63 g, 22.96 mmol, 0.17 eq. per OH group) was added dropwise over 30 min and later stirred for 24 h at room temperature (RT). The solvent was evaporated and the residue submitted to dialysis in methanol for 24 h. Then, the solvent was stirred in anhydrous DMF at RT, and sodium azide was added. The solution was heated (75°C) and stirred for 3 days. After cooling to RT, the mixture was filtered, and the solvent was evaporated. The residue was redissolved in methanol and filtered over celite. Later, the residue was dialyzed in methanol for 2 days. After evaporating the solvent, azide functionalized dendritic polyglycerol was dissolved in anhydrous DMF (7 mL) and heated to 60°C. Over a period of 2 h SO₃ pyridine complex in anhydrous DMF (3 mL) was added, the mixture was stirred for 2 h at 60°C and later for 2 days at RT. The pH was adjusted immediately to 8 by adding NaOH. The solvent was evaporated and the residue was subjected to ultrafiltration in water for 1 day. Evaporation of the solvent produced the title compound as a solid yield (degree of sulfation was 86%). For rhodamine-B-labeling azide, functionalized dPGS was dissolved in water and a solution (pH 8 adjusted) of copper sulfate (5 mg, 31.3 µmol), sodium ascorbate (25 mg, 126.67 µmol), and alkyne functionalized rhodamine B (4.1 mg, 7.93 mmol) was added. The solution was stirred for 3 days at RT. The crude product was ultrafiltrated in a saturated EDTA solution, followed by water. Size exclusion chromatography with Sephadex™ G-25 SEC in water and freeze-drying yielded the compound. Average number of dye molecule incorporation (2.4) per polymer was determined by UV-Vis-spectroscopy.

Abbreviations: DMF, dimethylformamide; EDTA, ethylenediaminetetraacetic acid; UV, ultraviolet.

Table S1 Characterization of the rhodamine-B-labeled NPs dPGOH-RB and dPGS-RB

| Polymer	$M_n{}^a$ (g/mol)	NF[b]	dF[c]	PDI[d]	$d_h \pm SD^e$ (nm)	ζ-Potential ± SD[f] (mV)
dPGOH-RB	6,000	81	–	0.31	5.1±0.5	–
dPGS-RB	12,100	54	67	0.25	6.7±0.9	−26.7±2.9

Notes: [a]Number average molecular weight calculated from the dF. [b]Number of functional groups per polymer. [c]Degree of functionalization determined by ^{1}H-NMR or elemental analysis. [d]Polydispersity index (DLS). [e]Hydrodynamic diameter (mean ± SD) by DLS in PBS (pH 7.4) from the size distribution by volume. [f]ζ-Potential (mean ± SD) in PBS (pH 7.4). The zeta potential of dPGOH-RB was not measured since the potential should be neutral.
Abbreviations: dF, degree of functionalization; ^{1}H-NMR, hydrogen-1 nuclear magnetic resonance; DLS, dynamic light scattering; SD, standard deviation; PBS, phosphate buffered saline.
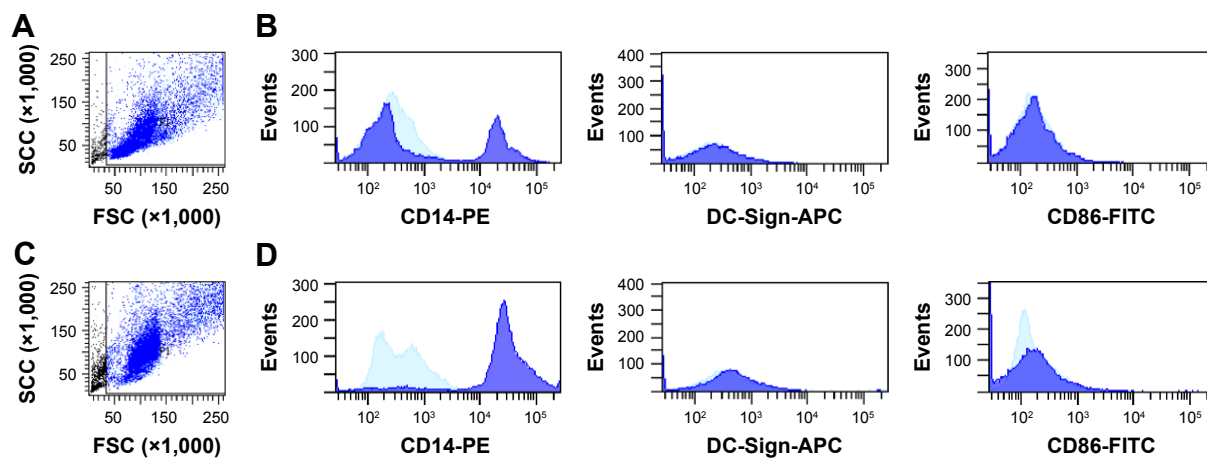
Figure S3 Quality control for the selection of CD14^{+} monocytes through MicroBeads.
Notes: For analysis, 1×10^{5} cells (PBMC or CD14^{+} monocytes) were stained with a monocyte-specific antibody, a-CD14-PE (TÜK4) or with dendritic cell-specific antibodies, a-DC-Sign-APC (DCN47.5) or with an activation marker, a-CD86-FITC (FM95). Samples were measured using the BD FACSAria III with Diva 6.0 software (BD Biosciences, Heidelberg, Germany). The measurements before (**A** and **B**) and after (**C** and **D**) using CD14 MicroBeads are depicted. It is clearly visible (**D**, panel CD14-PE) that the usage of CD14 MicroBeads leads to a specific increase in the amount of CD14^{+} monocytes. No DCs are present and cells are not activated.
Abbreviations: PBMC, peripheral blood mononuclear cell; CD, cluster of differentiation; DC, dendritic cell.
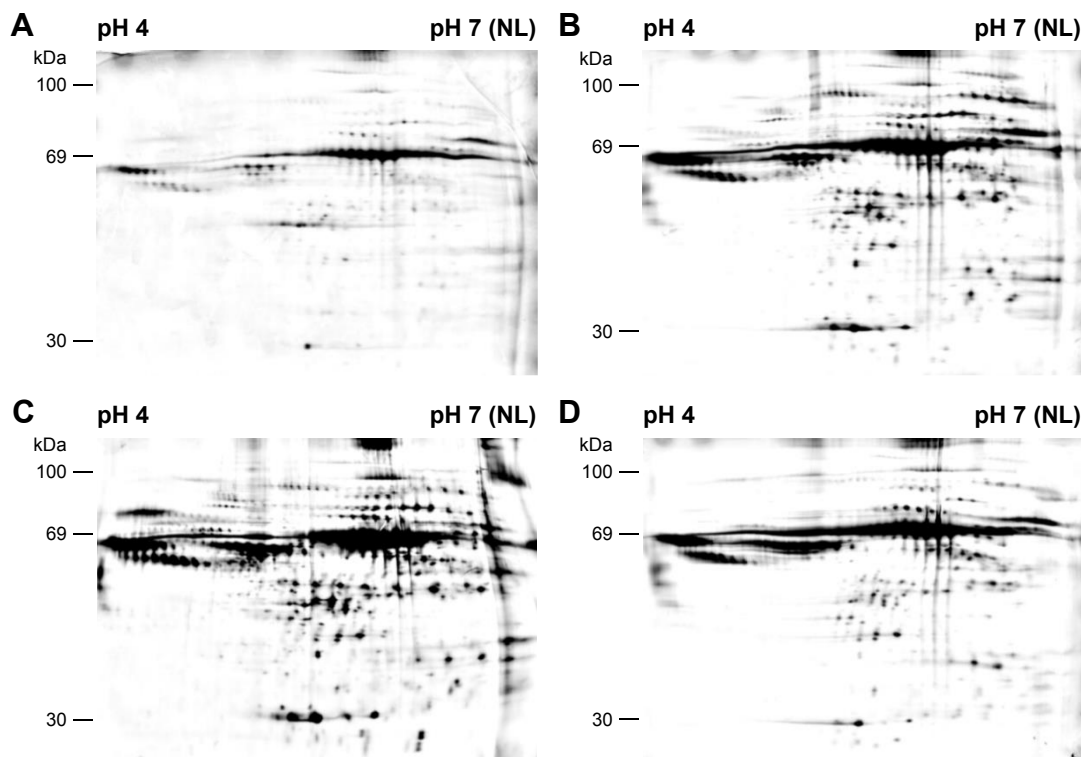
Figure S4 Analysis of the protein corona of dendritic polyglycerols by two dimensional (2D) gel electrophoresis.
Note: A typical 2D gel for control samples, that is, without nanoparticles (**A**), for dPGS-Au20 (**B**), dPGS-Au50 (**C**), and dPGOH-Au50 (**D**).
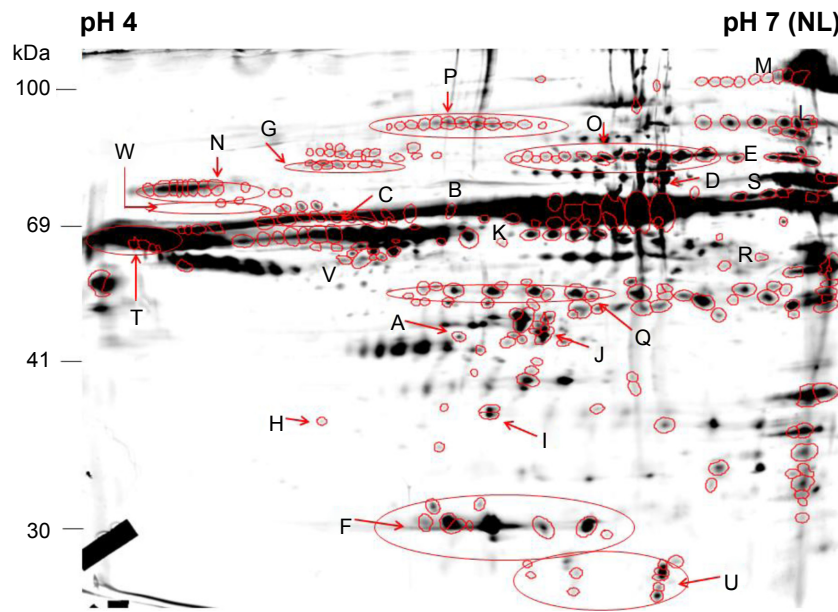
Figure S5 Analysis of the protein corona of dendritic polyglycerols by 2D gel electrophoresis.
Notes: A fusion gel, which is created by Delta2D software (DECODON, Germany) by merging all individual gel pictures, is depicted. This allows for visualization of all interesting protein spots, which are labeled with capital letters. All labeled spots have been further analyzed by MALDI-TOF/TOF.
Abbreviations: MALDI, matrix-assisted laser desorption ionization; TOF, time of flight.

Figure S6 Confocal microscopic images of dPGS-RB-treated CD14^{+} monocytes are depicted.
Notes: NPs (20 μg/mL) were pre-incubated with BSA (3 mg/mL), complete cell culture medium (CCM; RPMI-1640 with FBS [10%]), or serum-free medium (no serum) for 2 h. Cells were incubated for 6 h with NPs, washed (2 times PBS, 300 g, 5 min, RT) and stained with Hoechst (100 ng/mL for 5 min).
Abbreviations: NP, nanoparticle; BSA, bovine serum albumin; CCM, complete cell culture medium; FBS, fetal bovine serum; PBS, phosphate-buffered saline; RT, room temperature.

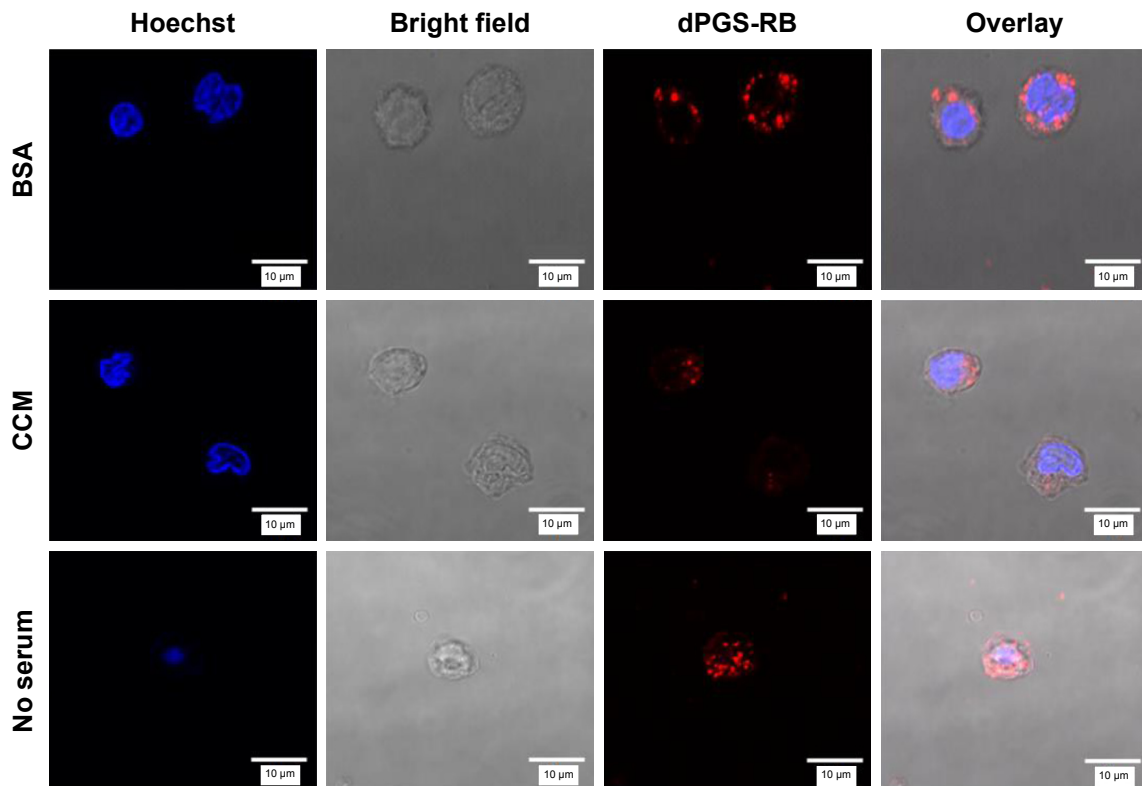|	Hoechst	Bright field	dPGOH-RB	Overlay

Figure S7 Confocal microscopic images of dPGOH-RB-treated CD14^{+} monocytes are depicted.
Notes: NPs (20 μg/mL) were pre-incubated with BSA (3 mg/mL), complete cell culture medium (CCM; RPMI-1640 with FBS [10%]), and serum-free medium (no serum) for 2 h. Cells were incubated for 6 h with NPs, washed (2 times PBS, 300 g, 5 min, RT), and stained with Hoechst (100 ng/mL for 5 min).
Abbreviations: NP, nanoparticle; BSA, bovine serum albumin; CCM, complete cell culture medium; FBS, fetal bovine serum; PBS, phosphate-buffered saline; RT, room temperature.
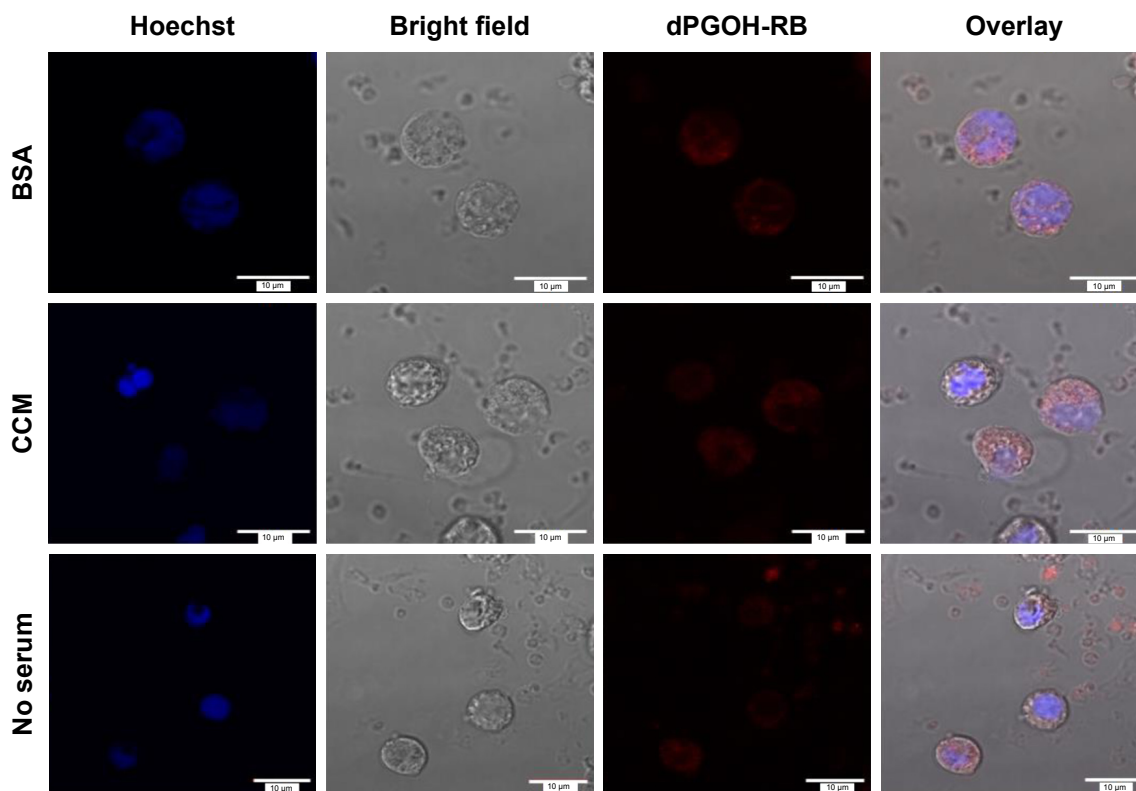
Table S2 Overview of all identified membrane proteins in the pull-down experiment using dPGS-Au50 NPs

Protein	Accession	MW (kDa)	MS	UP
60 kDa heat shock protein, mitochondrial	CH60_HUMAN	61.0	488.4	8
Amyloid-like protein 1	APLP1_HUMAN	72.1	22.0	1
ATP synthase subunit alpha, mitochondrial	ATPA_HUMAN	59.7	95.5	11
ATP synthase subunit beta, mitochondrial	ATPB_HUMAN	56.5	529.8	9
Basigin	BASI_HUMAN	42.2	134.0	2
Calcium-binding protein 1	CABP1_HUMAN	39.8	18.0	1
Carboxypeptidase M	CBPM_HUMAN	50.5	86.7	1
Cathepsin G	CATG_HUMAN	40.9	433.1	7
Heat shock cognate 71 kDa protein	HSP7C_HUMAN	70.9	107.1	2
HLA class I histocompatibility antigen, A-2 alpha chain	1A02_HUMAN	40.9	433.1	7
HLA class I histocompatibility antigen, A-24 alpha chain	1A24_HUMAN	40.7	52.9	2
HLA class I histocompatibility antigen, A-3 alpha chain	1A03_HUMAN	40.8	354	5
HLA class I histocompatibility antigen, B-57 alpha chain	1B57_HUMAN	40.2	314.6	5
Integrin β-II	ITB2_HUMAN	84.7	30	1
Interleukin-23 receptor	IL23R_HUMAN	71.1	15.1	1
Leukocyte immunoglobulin-like receptor subfamily B member 4	LIRB4_HUMAN	49.3	24.8	1
Myeloid cell surface antigen CD33	CD33_HUMAN	39.8	74.2	1
Protein disulfide-isomerase	PDIA1_HUMAN	57.1	53.4	1
Signal-regulatory protein beta-1 isoform 3	SIRBL_HUMAN	43.3	48.0	1
Sodium/potassium-transporting ATPase subunit beta-3	AT1B3_HUMAN	31.5	23.9	1
Transferrin receptor protein 1	TFR1_HUMAN	84.8	224.4	5
Vinculin	VINC_HUMAN	123.7	16.0	1

Notes: The dPGS-Au50 NPs were first pre-incubated with complete RPMI-1640 medium (containing 10% FBS) and then incubated with isolated MPs. Proteins were eluted, separated through SDS-PAGE and analyzed by using LC-MS/MS.
Abbreviations: NPs, nanoparticles; MPs, membrane proteins; MW, molecule weight; MP, membrane protein; MS, Mascot score; UP, unique peptides.

Reference

1. Groger D, Kerschnitzki M, Weinhart M, et al. Selectivity in bone targeting with multivalent dendritic polyanion dye conjugates. *Adv Healthcare Mater*. 2014;3(3):375–385.

Annex II

Supplementary information

Title:

Amphiphilic nanogels: influence of surface hydrophobicity on protein corona, biocompatibility and cellular uptake

Authors:

Tony Bewersdorff, Alexandra Gruber, Murat Eravci, Malti Dumbani, Daniel Klinger, Andrea Haase

Journal:

International Journal of Nanomedicine Volume 2019:14 Pages 7861—7878

DOI: 10.2147/IJN.S215935

Link: https://doi.org/10.2147/IJN.S215935

Supplementary materials

Table of contents

Supplementary Table 1 Parameters for post-modification reaction of PPFPMA precursor particles

Nanogels		HPA			Hydrophobic group			
Type	Sample	eq	n [mmol]	m [mg]	hydrophobic group	eq	n [mmol]	m [mg]
hydrophilic	**PHPMA**	3	4.76	358	-	-	-	-
moderate hydrophobic	**BENZA-20**	2.4	3.81	286	hexylamine (HEXA)	0.6	0.95	102
	HEXA-20	2.4	3.81	286	benzylamine (BENZA)	0.6	0.95	96
hydrophobic	**CHOLA-20**	2.4	3.81	286	dodecylamine (DODA)	0.6	0.95	450
	DODA-20	2.4	3.81	286	cholesteryl (CHOLA)	0.6	0.95	176

Notes: Post-modification of reactive precursor particles was carried out on dispersed PPFPMA particles (400 mg, 1.59 mmol w.r.t monomer units of PPFPMA particles, 1.0 eq) in DMF by adding different molar ratios of amine functionalized moieties (3.0 eq w.r.t. monomer units) and TEA (660 µL, 4.77 mmol, 3.0 eq w.r.t. monomer units), as summarized. The reaction was allowed to proceed at 50 °C for 24 h. Afterwards the particles were purified by extensive dialysis first against DMF (1 week) and subsequently against DI water (1 week) and MQ (1 week).

Abbreviations: DMF, dimethylformamide; TEA, triethylamine.

Supplementary Table 2 Parameters for post-modification reaction of PPFPMA precursor FITC-particles

Nanogels		HPA			Hydrophobic group			
Type	Sample	eq	n [mmol]	m [mg]	hydrophobic group	eq	n [mmol]	m [mg]
hydrophilic	**PHPMA**	3	1.78	134	-	-	-	-
moderate hydrophobic	**BENZA-20**	2.4	1.43	107	hexylamine (HEXA)	0.6	0.36	38
	HEXA-20	2.4	1.43	107	benzylamine (BENZA)	0.6	0.36	36
hydrophobic	**CHOLA-20**	2.4	1.43	107	dodecylamine (DODA)	0.6	0.36	169
	DODA-20	2.4	1.43	107	cholesteryl (CHOLA)	0.6	0.36	66

Notes: The synthesis of the fluorescence labelled NGs was carried out analogue to the post-modification of the unlabelled NGs but in a two-step approach. Briefly, freeze-dried PPFPMA particles (2.00 g, 7.93 mmol w.r.t monomer units of PPFPMA particles, 1.0 eq) were dispersed in 400 ml DMF by short treatment in a sonication bath (Elmasonic P30 H, Elma, Germany). The particles were swollen overnight in DMF before FITCA (71 mg, 0.16 mmol, 0.02 eq w.r.t monomer units) and TEA (3.3 ml, 23.8 mmol, 3 eq w.r.t. monomer units) were added and heated to 50 °C. After 24 h, 30 ml of the dispersion (150 mg PPFPMA-FITC particles) were reacted for another 24 h with different ratios of amine functionalized moieties (3.0 eq w.r.t. monomer units). Afterwards the NGs were purified by extensive dialysis against DMF and subsequently against DI water and MQ.

Abbreviations: NGs, nanogels; DMF, dimethylformamide; FITCA, amine functionalized fluorescein; TEA; triethylamine; DI water, deionized water; MQ, ultrapure water.

Supplementary Table 3 Quantification of NG protein coronas as measured *via* LC-MS/MS

Protein names	BENZA-20		HEXA-20		CHOLA-20		DODA-20	
Serum albumin	o	19.76	o	23.28	o	9.68	o	8.75
Apolipoprotein A-I	o	23.76	-	7.05	-	7.86	-	10.06
Hemoglobin subunit alpha	o	12.11	o	7.63	o	6.24	o	12.05
Complement factor B (Fragment)	o	5.12	o	5.76	+	10.36	o	7.27
Complement C3	-	2.99	o	7.11	-	2.63	o	6.44
Apolipoprotein A-II	o	7.93	-	1.74	-	3.88	-	2.08
Pigment epithelium-derived factor	+	1.00	+	4.60	+	5.51	+	7.76
Vitronectin	o	1.12	+	5.78	+	4.53	+	3.07
Pentraxin	+	1.92	+	2.56	+	6.26	+	4.35
Inter-alpha-trypsin inhibitor heavy chain H2	o	1.12	o	3.19	+	4.41	+	4.33
Hemoglobin fetal subunit beta	o	2.81	o	2.22	+	4.12	o	3.18
Complement factor I	o	0.88	o	2.01	+	6.41	+	3.14
Complement component C9	-	1.59	o	2.01	o	2.31	o	3.90
Hemoglobin subunit beta	o	1.86	-	0.94	o	2.47	o	1.85
Prothrombin	o	1.45	+	3.93	o	0.96	o	1.04
C-X-C motif chemokine	+	3.09	-	0.54	-	0.20	-	0.44
Serum amyloid A-4 protein	o	0.85	o	1.10	o	0.83	-	0.64
Apolipoprotein E	o	0.99	+	2.75	-	0.10	-	0.32
Complement C4	-	0.08	+	1.44	+	1.25	+	1.07
Protein AMBP	x	0.00	x	0.00	+	1.42	+	1.12
Plasma serine protease inhibitor	o	0.41	o	0.56	+	1.24	o	0.73
Gelsolin	+	0.52	+	0.94	+	0.73	+	0.71
Complement C8 beta chain	-	0.17	o	0.66	+	1.19	o	0.73

Haptoglobin (Zonulin)	o	0.49	o	0.62	o	0.70	o	0.92
Immunoglobulin J chain	-	0.35	o	0.49	o	1.19	-	0.36
Lipocalin 2	+	0.14	+	1.16	+	0.84	+	0.48
Paraoxonase 1	o	0.77	o	0.32	o	0.68	o	0.70
Thrombospondin-1	-	0.06	-	0.06	+	1.29	o	0.67
Alpha-2-macroglobulin	o	0.32	+	0.49	+	1.11	+	0.63
Serum amyloid A protein	+	0.94	-	0.21	o	0.35	o	0.54
Apolipoprotein B	o	0.35	-	0.30	o	0.61	o	0.62
Uncharacterized protein	+	0.41	+	0.76	+	0.53	+	0.42
Apolipoprotein A-IV	o	0.40	-	0.17	o	0.41	-	0.31
Lipopolysaccharide-binding protein	o	0.18	+	0.24	o	0.15	+	1.09
Alpha-2-HS-glycoprotein	x	0.00	x	0.00	x	0.00	+	0.35
Proteoglycan 4	+	0.01	+	0.55	x	0.00	+	0.46
Histidine-rich glycoprotein	+	0.09	+	0.16	+	0.54	+	0.49
Serum amyloid A protein	+	0.38	+	0.15	x	0.00	x	0.00
Coagulation factor V	-	0.05	+	0.43	o	0.18	+	0.37
Golgin B1	x	0.00	+	0.22	x	0.00	+	0.25
Complement factor H	x	0.00	+	0.32	+	0.15	+	0.23
Complement C8 alpha chain	-	0.03	o	0.24	o	0.29	o	0.30
Alpha-1-antiproteinase	-	0.10	-	0.08	o	0.17	+	0.46
Alpha-fetoprotein	+	0.32	o	0.24	-	0.08	o	0.17
Alpha-1B-glycoprotein	o	0.14	o	0.14	+	0.39	o	0.18
Protein HP-20 homolog	o	0.15	+	0.25	o	0.19	o	0.21
Primary amine oxidase, liver isozyme	-	0.16	-	0.07	o	0.29	-	0.07
Spleen trypsin inhibitor I	o	0.19	o	0.10	o	0.14	+	0.31
ApoN protein	+	0.33	+	0.18	o	0.14	o	0.10
Antithrombin-III	x	0.00	+	0.02	+	0.21	+	0.29

SERPIND1 protein	+	0.15	+	0.20	+	0.22	+	0.18
Hepatocyte growth factor-like protein	o	0.09	o	0.14	+	0.35	o	0.13
Sulfhydryl oxidase	+	0.04	+	0.31	+	0.05	+	0.21
Uncharacterized protein	x	0.00	+	0.20	x	0.00	+	0.11
Actin, cytoplasmic 2	-	0.07	-	0.10	o	0.19	-	0.13
Beta-2-glycoprotein 1 (Apo-H)	-	0.08	x	0.00	o	0.14	o	0.14
Tetranectin	x	0.00	x	0.00	+	0.08	+	0.18
Apolipoprotein C-III	x	0.00	x	0.00	x	0.00	+	0.12
Uncharacterized protein	+	0.06	+	0.13	+	0.16	+	0.21
Serpin H1	o	0.06	+	0.11	+	0.26	o	0.07
Uncharacterized protein	x	0.00	x	0.00	+	0.27	+	0.06
Lactotransferrin	+	0.09	+	0.23	+	0.12	+	0.10
Coagulation factor XIII B chain	o	0.07	+	0.22	o	0.10	o	0.07
Carboxypeptidase B2	+	0.15	+	0.17	+	0.09	+	0.09
L-lactate dehydrogenase B chain	o	0.09	o	0.09	+	0.18	o	0.07
Uncharacterized protein	x	0.00	+	0.11	+	0.10	+	0.10
Hemopexin	o	0.08	-	0.01	o	0.16	o	0.12
Thrombospondin-4	o	0.07	-	0.03	+	0.25	-	0.03
Alpha-1-acid glycoprotein	x	0.00	+	0.06	+	0.12	x	0.00
C8G protein	o	0.03	+	0.07	x	0.00	+	0.17
Cartilage oligomeric matrix protein	x	0.00	x	0.00	+	0.08	x	0.00
Phosphatidylinositol-glycan-specific phospholipase D	o	0.05	o	0.08	+	0.12	x	0.00
Collagen alpha-1(I) chain	x	0.00	o	0.08	x	0.00	o	0.08
Cumulus cell-specific fibronectin 1 transcript variant (Fibronectin)	-	0.00	+	0.18	+	0.07	+	0.11
Coagulation factor XII	+	0.03	+	0.01	+	0.19	+	0.07

Apolipoprotein C-IV	o	0.09	o	0.09	o	0.05	o	0.06
Serpin A3-1	o	0.06	o	0.07	o	0.09	o	0.07
ECM1 protein	+	0.15	+	0.07	+	0.03	+	0.02
Complement C5a anaphylatoxin	o	0.04	+	0.09	+	0.07	+	0.10
Clusterin (GpIII)	-	0.02	x	0.00	o	0.12	-	0.04
Pyruvate kinase	x	0.00	+	0.10	+	0.03	x	0.00
Coagulation factor X	x	0.00	-	0.04	x	0.00	x	0.00
C-X-C motif chemokine	x	0.00	+	0.06	+	0.04	+	0.07
Serotransferrin	-	0.04	-	0.04	-	0.02	o	0.09
Procollagen C-endopeptidase enhancer	x	0.00	-	0.02	o	0.08	x	0.00
Plasma kallikrein	+	0.02	+	0.11	+	0.03	+	0.06
Complement component C6	+	0.01	+	0.09	+	0.06	+	0.07
Angiotensinogen	+	0.04	+	0.07	+	0.05	+	0.06
Complement component C7	o	0.03	o	0.06	o	0.06	o	0.06
Transthyretin (Prealbumin)	x	0.00	-	0.01	o	0.04	+	0.11
Alpha-enolase	x	0.00	x	0.00	+	0.05	x	0.00
Histone H2A.J (H2a/j)	x	0.00	+	0.05	x	0.00	x	0.00
Apolipoprotein M	+	0.12	o	0.03	-	0.02	o	0.04
Uncharacterized protein	o	0.04	o	0.05	+	0.05	+	0.07
L-lactate dehydrogenase A chain (LDH-A)	+	0.02	+	0.08	x	0.00	+	0.03
121 kDa protein	x	0.00	+	0.03	+	0.06	+	0.04
Fetuin-B	o	0.04	-	0.02	o	0.05	o	0.05
Leucine-rich alpha-2-glycoprotein 1	x	0.00	o	0.03	+	0.06	x	0.00
Periostin	x	0.00	+	0.04	x	0.00	+	0.03
Inter-alpha-trypsin inhibitor heavy	-	0.02	o	0.03	o	0.03	o	0.03

chain H3								
Retinol-binding protein 4	x	0.00	+	0.02	+	0.05	+	0.03
Adipocyte plasma membrane-associated protein	+	0.03	x	0.00	x	0.00	x	0.00
Chondroadherin	x	0.00	+	0.03	x	0.00	+	0.03
Histone H1.2 (CTL-1)	o	0.02	+	0.04	x	0.00	o	0.03
MGAT1 protein	x	0.00	x	0.00	o	0.03	x	0.00
Insulin-like growth factor-binding protein 3	x	0.00	+	0.03	+	0.04	+	0.03
Kininogen-2	x	0.00	+	0.03	x	0.00	+	0.02
Complement C1s subcomponent	+	0.01	x	0.00	+	0.04	x	0.00
Complement component 1, r subcomponent	x	0.00	x	0.00	+	0.03	x	0.00
Coagulation factor XIII A chain	+	0.02	+	0.03	x	0.00	x	0.00
Azurocidin 1	x	0.00	x	0.00	x	0.00	+	0.02
Alpha-2-antiplasmin (Alpha-2-AP)	+	0.02	+	0.04	+	0.02	+	0.02
Fructose-bisphosphate aldolase	-	0.01	o	0.04	-	0.01	o	0.03
78 kDa glucose-regulated protein	x	0.00	x	0.00	+	0.03	x	0.00
GLI pathogenesis-related 2	x	0.00	+	0.03	+	0.03	+	0.02
Fibulin-1 (FIBL-1)	-	0.01	x	0.00	x	0.00	x	0.00
C1QC protein	x	0.00	+	0.03	+	0.02	+	0.01
Phosphoglycerate kinase 1	x	0.00	+	0.02	+	0.02	+	0.02
Transketolase	+	0.02	+	0.01	+	0.03	x	0.00
SERPINA10 protein	+	0.02	x	0.00	+	0.02	x	0.00
Vitamin D-binding protein	x	0.00	-	0.01	x	0.00	+	0.03
Serum amyloid P-component (SAP)	x	0.00	x	0.00	+	0.01	x	0.00
C1QTNF3 protein	+	0.01	+	0.01	+	0.02	x	0.00

Vinculin	x	0.00	+	0.01	x	0.00	x	0.00
Collagen type VI alpha 3 chain	x	0.00	+	0.01	+	0.00	+	0.02
Elongation factor 1-alpha 1	x	0.00	x	0.00	x	0.00	+	0.01
Heat shock 70 kDa protein 1A	x	0.00	+	0.01	x	0.00	x	0.00
Moesin	x	0.00	+	0.01	x	0.00	+	0.01
Talin 1	x	0.00	+	0.01	x	0.00	x	0.00
Collagen type XVIII alpha 1 chain	+	0.00	+	0.01	x	0.00	x	0.00

Notes: Bound proteins were analysed using LC-MS/MS, protein quantities were calculated using the TOP 3 approach and relative quantities were obtained by comparison to the reference particle PHPMA. A particular protein in a NG corona can be increased (ie quantity at least 1.5-fold higher, indicated by +), decreased (ie values are 0.5 or lower, indicated by -) or similar in amount (indicated by o) compared to the reference particle PHPMA. If a particular protein was not measured in a specific corona this protein is marked with an "x".

Abbreviations: NGs, nanogels; LC-MS/MS, liquid chromatography-tandem mass spectrometry; NG, nanogel.

Supplementary Table 4 Characterization of the FITC labelled NGs

Nanogels		Precursor particle diameter d_h [nm] in DI water	Particlediameter d_h [nm] in DI water
Type	Sample		
hydrophilic	PHPMA-FITC		160 ± 30
moderate	BENZA-20-FITC		175 ± 45
hydrophobic	HEXA-20-FITC	150 ± 40	165 ± 40
hydrophobic	CHOLA-20-FITC		165 ± 20
	DODA-20-FITC		170 ± 40

Notes: NGs-FITC were freshly dispersed in DI water and sonicated for 30 min at RT. Particle sizes are denoted as the hydrodynamic diameter and the respective standard deviation.

Abbreviations: DI water, deionized water.
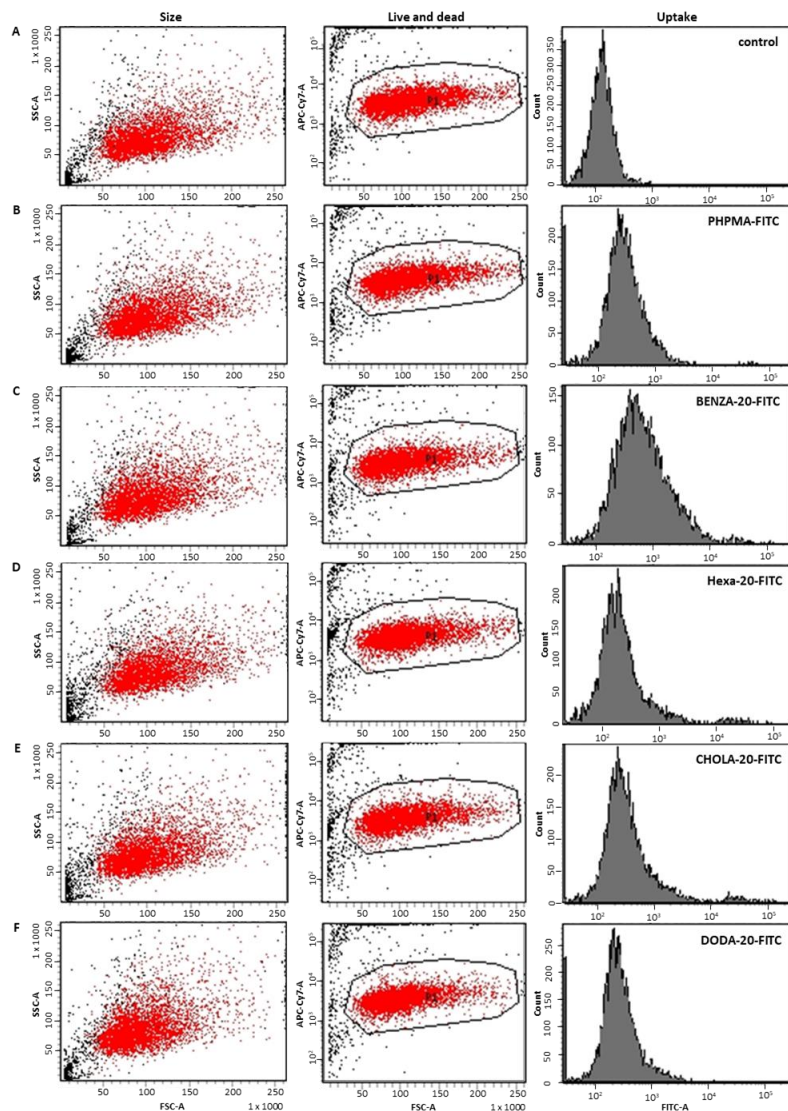
Supplementary Figure S1 Illustration of the differentiation steps used in the evaluation of the flow cytometry experiment using a well established method.[48]

Notes: The first channel (size) shows the size distribution to separate cell debris or cell aggregates. The second channel (living and dead) differentiates the dead from the living cells. The third channel (uptake) illustrates NG cell uptake using the FITC signal. Here we depict the three channels for THP-1 control cells (A) and cells treated with the NGs, B) PHPMA-FITC, C) BENZA-20-FITC, D) HEXA-20-FITC, E) CHOLA-20-FITC and F) DODA-20-FITC are illustrated. **Abbreviations:** SSC, sideward scatter; FSC, frontward scatter
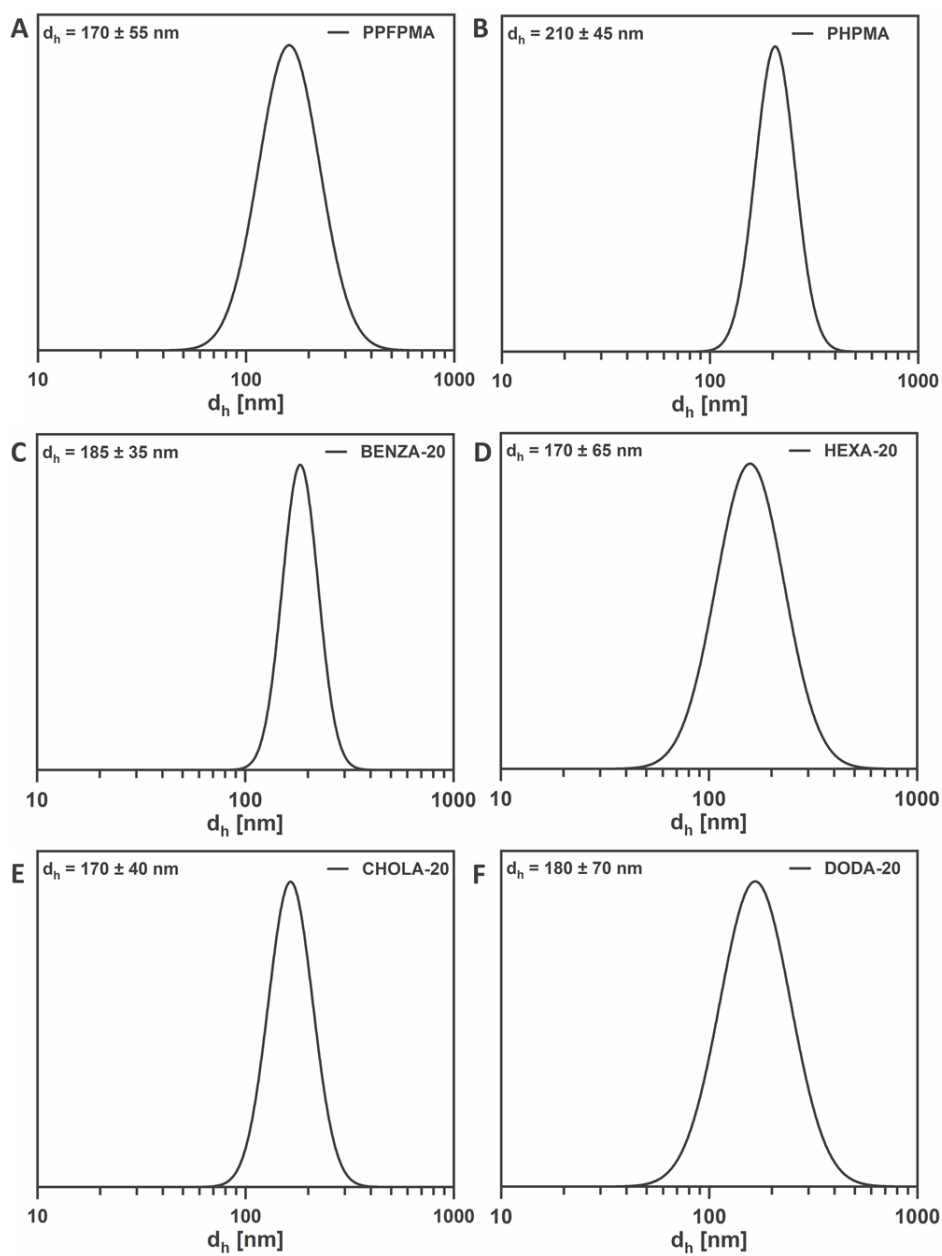
Supplementary Figure S2 DLS curves of amphiphilic NGs in DI water

Notes: Measurements are carried out at an angle of 173°. Depicted are the curves for

A) PPFPMA precursor particles, B) PHPMA NG, C) BENZA-20 NG, D) HEXA-20 NG,

E) CHOLA-20 NG and F) DODA-20 NG.

Abbreviations: NGs, nanogels; dh, hydrodynamic diameter.
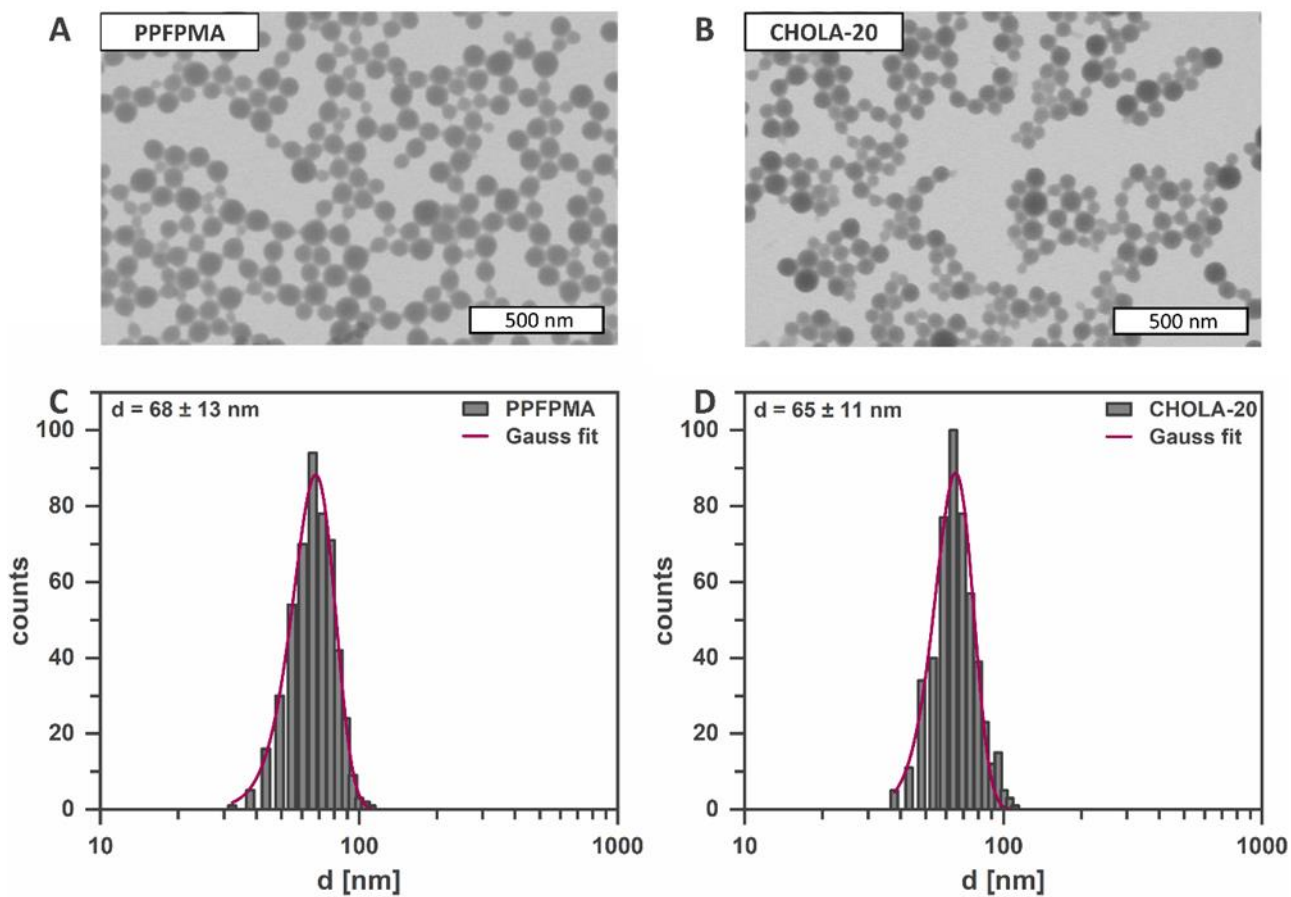
Supplementary Figure S3 TEM images and statistical evaluation of the particles size of

PPFPMA precursor particle and CHOLA 20 NG as representative sample of the amphiphilic NGs

Notes: Size and size distribution of the nanogels in the dried state were evaluated by determining

the diameter of 500 nanogels each sample with the software ImageJ. TEM images of A) PPFPMA

reactive precursor particle and B) CHOLA-20 NG as well as the respective statistical evaluation

C) PPFPMA and D) CHOLA-20 NG are depicted.

Abbreviations: NGs, nanogels; d, diameter; TEM, transmission electron microscopy

Supplementary Figure S4 Representative 2D gel images depicting the protein corona of all NGs

Notes: NGs (300 µg/ml) were incubated with CCM for 30 min. Bound proteins were eluted and

analysed using 2DE analysis. Depicted are the resulting 2D gels for A) PHPMA, B) BENZA-20,

C) HEXA-20, D) CHOLA-20 and E) DODA-20. All significant spots, ie spots with increased

intensities (> 1.5, $p < 0.05$, n=3), relative to the control (CCM without NGs) are labelled.

Abbreviations: NGs, nanogels; CCM, complete cell culture medium (RPMI 1640 containing 10%

FBS); FBS, fetal bovine serum; 2DE, two dimensional gel electrophoresis.

Annex III

Supplementary information

Title:

The influence of shape and charge on protein corona composition in common gold nanostructures

Authors:

Tony Bewersdorff, Emanuel A. Glitscher, Julian Bergueiro, Murat Eravci, Enrico Miceli, Andrea Haase, Marcelo Calderón

The influence of shape and charge on protein corona composition in common gold nanostructures

Tony Bewersdorff,[§a] Emanuel A. Glitscher,[§b] Julian Bergueiro,[c] Murat Eravci,[a] Enrico Miceli,[b] Andrea Haase*[a], Marcelo Calderón*[bde]

a German Federal Institute for Risk Assessment (BfR), Department of Chemical and Product Safety, Berlin, Germany.

b Freie Universität Berlin, Institute of Chemistry and Biochemistry, Takustrasse 3, 14195 Berlin, Germany.

c Centro Singular de Investigación en Química Biolóxica e Materiais Moleculares (CIQUS), Departamento de Química Orgánica, Universidade de Santiago de Compostela, Santiago de Compostela, Spain.

d POLYMAT and Applied Chemistry Department, Faculty of Chemistry, University of the Basque Country UPV/EHU, Paseo Manuel de Lardizabal 3, 20018Donostia-San Sebastián, Spain.

e IKERBASQUE, Basque Foundation for Science, 48013 Bilbao, Spain.

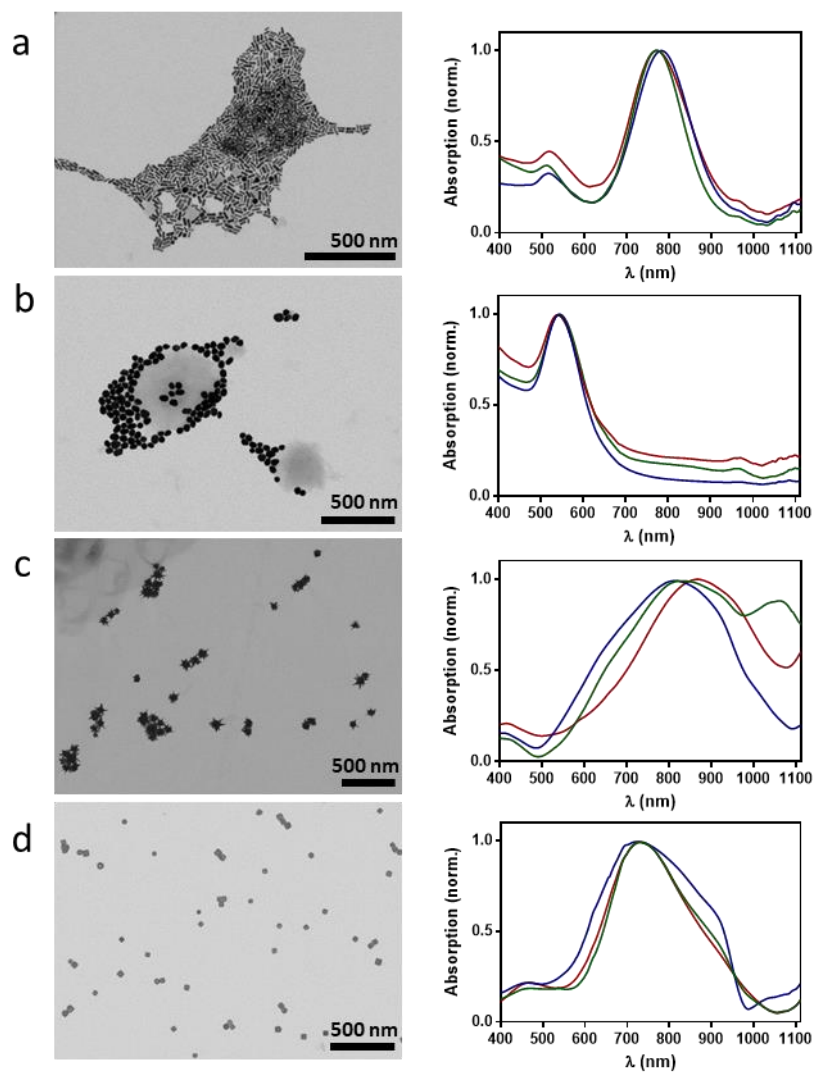§ The authors contributed equally to this work.

* Corresponding authors

Fig. S1 Additional TEM images of AuNPs and their absorption spectra for (a) spheres, (b) rods, (c) stars and (d) cages. The absorption spectra are color coded indicating different surface functionalization (green for OCH_3, blue for COOH, red for NH_2).
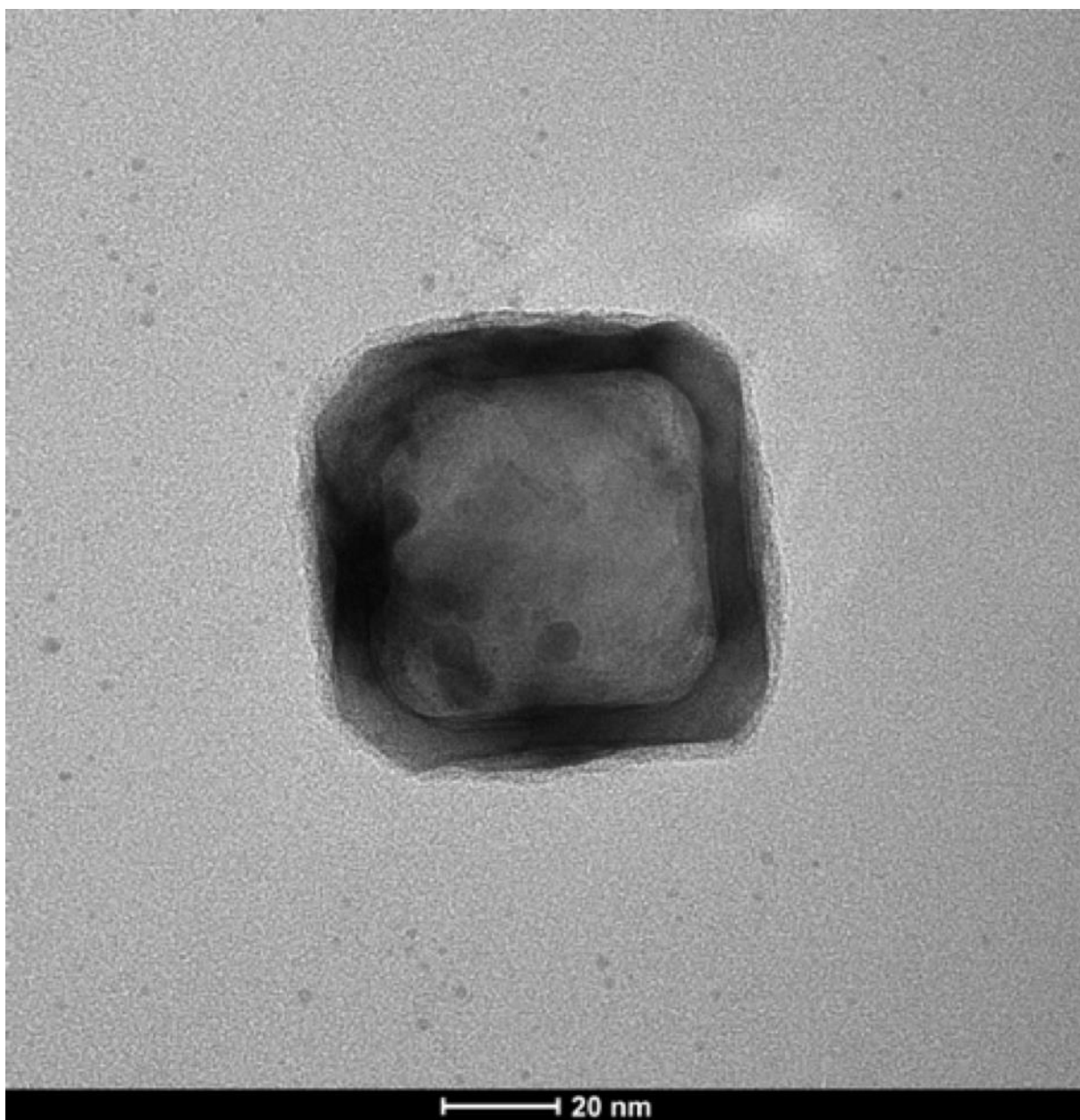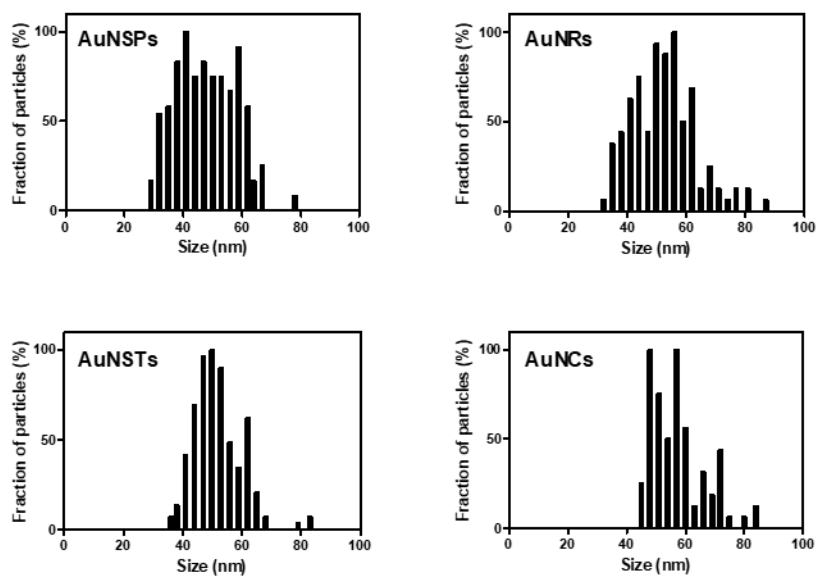
Fig. S2 High resolution TEM image of AuNC.

Fig. S3 TEM size distributions of all different AuNPs analyzed by ImageJ software with at least 150 particles counted for each variant.
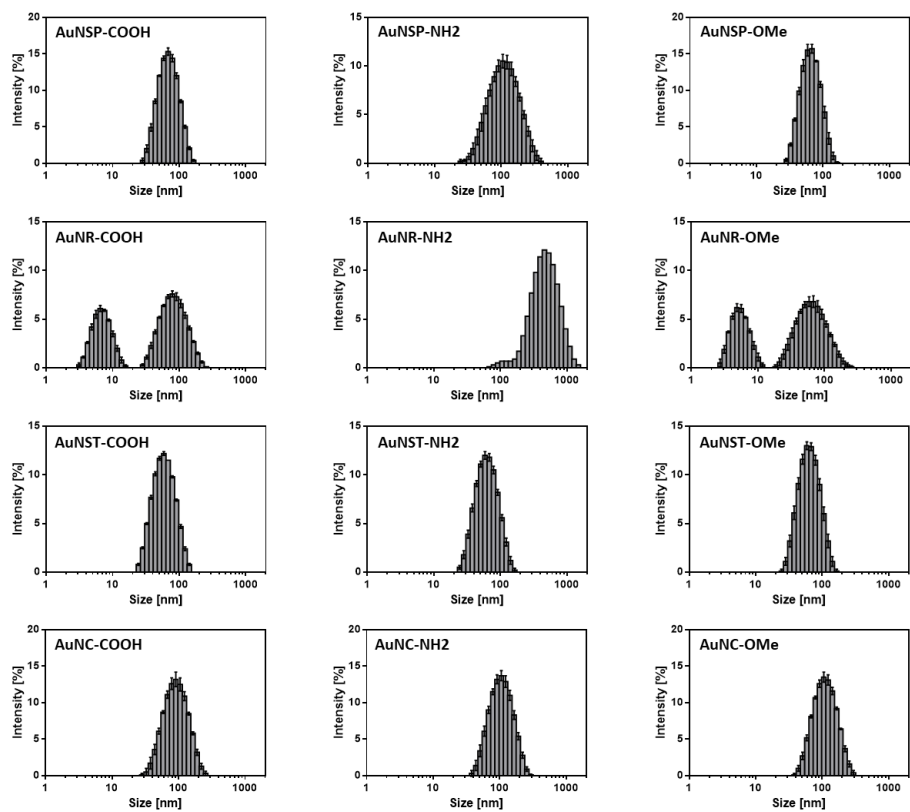
Fig. S4 DLS size distributions of all different AuNPs.
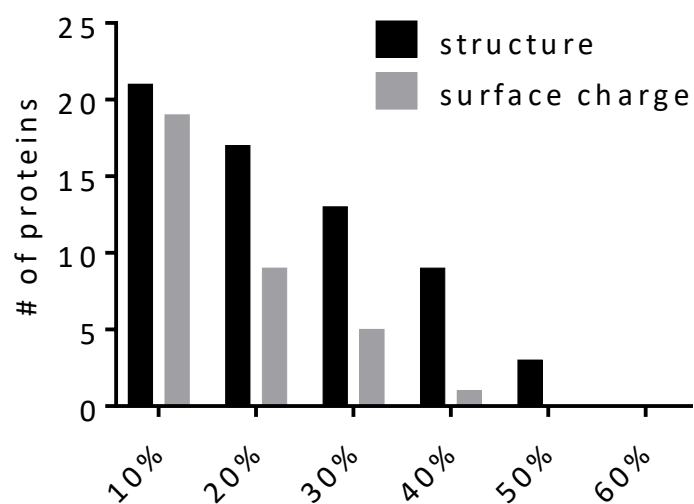
Fig. S5 Number of percentage differences within the analysis groups. The mean values of the corresponding properties were calculated and the standard deviations were determined. Percentages of the proteins were averaged over the AuNPs either with constant structure or unchanged surface charge. Subsequently, the standard deviations were counted with regard to their percentage deviation from the mean value.